STUDIES ON LASER INDUCED FLUORESCENCE IN SUBSONIC AND SUPERSONIC JET USING KETONE TRACERS

Thesis

Submitted in partial fulfillment of the requirements for the award of the degree of

DOCTOR OF PHILOSOPHY

By

SHELAR VIKAS M.

DEPARTMENT OF PHYSICS

NATIONAL INSTITUTE OF TECHNOLOGY KARNATAKA,

SURATHKAL, MANGALORE – 575025

March, 2014

D E C L A R A T I O N

by the Ph.D. Research Scholar

I hereby *declare* that the Research Thesis entitled **"Studies on Laser Induced Fluorescence in Subsonic and Supersonic Jet Using Ketone Tracers"** which is being submitted to the **National Institute of Technology Karnataka, Surathkal** in partial fulfillment of the requirements for the award of the Degree of **Doctor of Philosophy** in **Physics** is a *bonafide report of the research work carried out by me*. The material contained in this Research Thesis has not been submitted to any University or Institution for the award of any degree.

SHELAR VIKAS M.

Register No. –**080834PH08F03,**

Department of Physics

National Institute of Technology Karnataka, Surathkal, INDIA

Place: NITK-Surathkal

Date:

C E R T I F I C A T E

This is to *certify* that the Research Thesis entitled **"Studies on Laser Induced Fluorescence in Subsonic and Supersonic Jet Using Ketone Tracers"** submitted by **Shelar Vikas Manohar** (Register Number: 080834PH08F03) as the record of the research work carried out by him, is *accepted* as the *Research Thesis submission* in partial fulfillment of the requirements for the award of degree of **Doctor of Philosophy**.

Research Guide(s) **Prof. G. Umesh,** **Prof. G. Ramachandran**
(Name and Signature with Date)

Prof. N.K. Udayashankar
Professor & Head of the Department
Chairman – DRPC
(Signature with Date and Seal)

Acknowledgements

I thank my advisor, Prof. G. Umesh, for his advice and guidance in my research. Without his guidance and support, none of this would have been possible. I would like to thank my co-advisor Prof. G. Ramachandran, for his invaluable support and direction. I must thank Dr. G. M. Hegde, CeNSE, IISc, Bangalore and Dr. M. N. Satyanarayan, Dept. of Physics, NITK for providing valuable guidance through their roles in the interdisciplinary PLIF. I am grateful to Prof. K. P. J. Reddy and Prof. G. Jagadeesh for granting me to make use of LHSR laboratory at IISc, Bangalore. I would like to thank Prof. N. K. Udayashankar, HOD, Dept. of Physics, RPAC members Prof. M. B. Saidatta, and Prof. G. K. Shivakumar, Dept. of Physics and DRPC committee members for their guidance and suggestions.

I thank all the research students at LHSR, IISc, for their extensive experimental support and for many helpful discussions. I thank all of the support staff at the LHSR, Aerospace Engineering Dept., IISc, Bangalore for their help during experiments at LHSR. I am also grateful to Prof. R. V. Ravikrishna, Saurabha Markandeya and S. Krishna, Department of Mechanical Engineering, IISc, Bangalore for helping in supersonic jet imaging.

The support received from the faculty members, the non-teaching staff and the research scholars of the Physics department at NITK is gratefully acknowledged.

I would like to thank my parents Manohar and Shashikala, for their love and generosity. They are the source of inspiration, and without them this could not have been possible. I acknowledge my loving wife, Sujata, for her patience, perseverance, and support. My brother Vilas continues to inspire me throughout my research work. My aunt Prema, have been a great support to me over the years. They have helped to mold me into the person I am today, and I am grateful for it. Finally I would like to thank God for giving strength to pursue my degree.

Dedicated to my parents

Abstract

The present work focuses on the study of LIF from ketone based tracers for gas flow visualization. For all these studies a frequency quadrupled, Q switched, Nd:YAG laser (266 nm) was used as an excitation source. The quenching effect of oxygen on LIF of acetone, Methyl Ethyl Ketone (MEK) and 3-pentanone was studied quantitatively at low pressures (~700 torr) with oxygen partial pressures upto 450 torr. Nitrogen was used as a bath gas into which these molecular tracers were added in different quantities according to their vapor pressure at room temperature. Further Smoluchowski theory was used to calculate the quenching parameters and compared with the experimental results.

The molecular density distribution measurement in turbulent nitrogen jet ($Re \approx 3X10^3$), using acetone and MEK tracers was demonstrated. Emitted fluorescence images of subsonic jet flow field were recorded on CMOS camera. The dependence of PLIF intensity on acetone vapor density was used to convert PLIF image of nitrogen jet into the density image on pixel by pixel basis. Instantaneous quantitative density image of nitrogen jet, seeded with acetone was obtained. Arrow head shaped coherent turbulent structures were observed in our experiments. PLIF imaging was used for supersonic jet, using acetone as molecular tracer. For supersonic jet, the fluorescence images were recorded on ICCD camera. Significant decrease in the PLIF intensity due to the presence of oxygen was clearly observed. The dependence of PLIF intensity on binning of images and air pressure was studied. It was demonstrated that even with the presence of the condensation of acetone, one can obtain good quality PLIF images. It was also shown that binning and Gaussian image processing of steady state jet PLIF images can further improve the image quality for quantitative analysis.

Keywords: PLIF; Fluorescence quenching; Oxygen; Ketones; Coherent structures; Supersonic jet;

Contents

List of Figures……....iv

List of Tables……vii

Nomenclature……...viii

1. INTRODUCTION TO LIF AND SOME BASIC THEORETICAL CONCEPTS OF FLUORESCENCE……....1

    1.1. Introduction……....1

    1.2. Electromagnetic radiation as quantized field…….…..3

    1.3. On energy shell transition matrix element for fluorescence…….…...5

    1.4. Density matrix formalism…….…..7

    1.5. Scope and objective of the present work…….…...8

    1.6. Overview of thethesis……8

2. LITERATURE REVIEW……....11

    2.1. Introduction to PLIF……..11

    2.2. Fluorescence spectroscopy……...11

    2.3. Absorption and emission spectrum……...13

    2.4. PLIF technique…….……13

    2.5. Current state-of-art……15

        2.5.1. LIF tracers…….……..15

        2.5.2. Atoms and diatomic molecules……...16

        2.5.3. Polyatomic organic molecules…….……...17

2.5.4. PLIF measurements……23

2.6 Conclusions……...24

3. EFFECT OF OXYGEN ON LIF OF KETONES IN STATIC CONDITIONS……..25

3.1. Fluorescence quenching……25

3.1.1 Mechanism of quenching…...……...25

3.2. Oxygen quenching effect on LIF……..……27

3.3. Theory of fluorescence quenching……28

3.4. Quenching rate constant (k_q)……29

3.5. Experimental details used to study the LIF quenching in gas phase……....31

3.6. Results and discussion on gas cell experiments……33

3.7. Conclusions……..42

4. SUBSONIC JET FLOW VISUALIZATION USING PLIF……....45

4.1. Introduction……...45

4.2. Structure of subsonic axisymmetric jet……47

4.3. Theoretical consideration for image conversion……...48

4.4. Experimental technique……49

4.4.1. PLIF experimental set up……...49

4.5. Acetone seeded jet……....54

4.6. MEK seeded jet……58

4.7. Effect of oxygen on acetone PLIF...……62

4.8. Conclusions……...64

5. SUPERSONIC JET FLOW VISUALIZATION USING PLIF……67

5.1. Introduction……..67

5.2. Supersonic flow from Convergent-divergent (C-D) nozzle……68

5.3. Structure of supersonic jet……69

5.4. Supersonic jet and Schlieren optical setup……...70

5.5. Comparison of PLIF with Schlieren and CFD simulations……..74

5.6. Effect of oxygen in supersonic jets……...78

5.7. Conclusions……..81

6. CONCLUSIONS AND FUTURE DIRECTIONS……..83

6.1. Summary……...83

6.2. Main conclusions of the thesis……..84

6.3. Future directions……...86

APPENDIX I……87

APPENDIX II……..…..97

REFERANCES……...101

PUBLICATIONS..……111

BIO-DATA……113

List of figures

Figure 1.1 Energy level diagram for fluorescence emission from an atom.

Figure 1.2 Fluorescence geometry in the laboratory co-ordinate system.

Figure 2.1 Jablonski diagram showing transition between the molecular energy levels.

Figure 2.2 Optimized molecular structure of acetone and MEK.

Figure 3.1 Fluorescence collisional quenching process.

Figure 3.2 Fluorescence resonance energy transfer [FRET].

Figure 3.3 Schematic of LIF experimental setup used for gas flow diagnostics.

Figure 3.4 Photograph of the experimental setup (monochromator and the gas chamber).

Figure 3.5 The laser energy dependency on the gas phase LIF of acetone at nitrogen bath gas pressure of one bar. Other tracers used in our experiments also show similar behavior.

Figure 3.6 Stern-Volmer plot for acetone LIF in nitrogen bath gas at 700 torr pressure.

Figure 3.7 Stern-Volmer plot for MEK LIF in nitrogen bath gas at 700 torr pressure.

Figure 3.8 Stern-Volmer plot for 3-Pentanone LIF in nitrogen bath gas at 700 torr pressure.

Figure 3.9 Comparison of experimentally determined and theoretically calculated (using Chapman-Enskog relation) values of SV coefficient (ksv) for all the three tracers.

Figure 3.10 Comparison of experimentally determined and theoretically calculated (using Chapman-Enskog relation) values of quenching rate (kq) for all the three tracers.

Figure 4.1 Schematic of free turbulent axisymmetric jet.

Figure 4.2 Schematic of PLIF experimental setup for gas flow visualization and mixing studies.

Figure 4.3 Normalized centerline exit velocity profile from the jet.

Figure 4.4 a) The Raw acetone PLIF image as obtained from the camera. b) Gray scale image of the flow processed using MATLAB code.

Figure 4.5 a) The Raw MEK PLIF image as obtained from the camera. b)Gray scale image of the flow processed using MATLAB code.

Figure 4.6 Gas phase acetone PLIF image for Re $\approx$ 2-3 X10^3.

Figure 4.7 a) Gas Cell with filling pressure range from 0 to 20 bar. b) PLIF image for acetone partial pressure of 160 torr inside the chamber.

Figure 4.8 Gray scale PLIF intensity, averaged over the image area, as a function of acetone partial pressure in the gas cell.

Figure 4.9 Image of nitrogen gas jet seeded with acetone, showing (a) partial pressure and (b) molecular number density ($x10^{24}$ m^{-3}).

Figure 4.10The acetone number density contour image of the jet shown in Fig. 4.9.

Figure 4.11 The gas phase MEK PLIF gray scale image of nitrogen jet purged through liquid MEK.

Figure 4.12 Gray scale LIF intensity averaged over image area as a function of MEK partial pressure.

Figure 4.13 The MEK molecular number density ($x10^{24}$ m^{-3}) image in nitrogen jet.

Figure 4.14 The cross section images of the nitrogen jet at various x/D by assuming axisymmetric gas jet.

Figure 4.15 The convergent axisymmetric nozzle.

Figure 4.16PLIF image of acetone seeded in nitrogen jet released into ambient atmosphere.

Figure 4.17PLIF image of acetone seeded in air jet released into ambient atmosphere.

Figure 4.18 LIF gray scale image intensity in nitrogen and air jet over the jet cross section one diameter away from the nozzle.

Figure 5.1Gas flow in a converging and diverging passage.

Figure 5.2Converging and diverging nozzle for obtaining supersonic gas flows.

Figure 5.3Shock cell structure in the plume of an over-expanded jet.

Figure 5.4 Experimental arrangement for PLIF visualization of supersonic gas flows.

Figure 5.5 Intensified gated CCD camera and convergent-divergent (C-D) nozzle.

Figure 5.6 Schematic of Schlieren set up with concave mirrors of diameter 150 mm and focal length of 3000 mm.

Figure 5.7 PLIF image of over-expanded nitrogen jet for gas tank pressure of a) 18 bar b) 16 bar c) 14 bar d) 12 bar.

Figure 5.8 Effect of averaging on PLIF imaging of supersonic jet.

Figure 5.9 a) Schlieren image b) comparison between Schlieren and PLIF images of the supersonic jet at 18 bar stagnation pressure.

Figure 5.10 Simulated image using CFD for tank pressure of 16 bar.

Figure 5.11 Comparison between CFD simulated density image (top) and PLIF density image (bottom) for tank pressure of 16 bar.

Figure 5.12Comparison between PLIF images of over-expanded Supersonic jets in a) air and b) nitrogen for tank pressures of i) 18 bar ii) 16 bar iii) 14 bar iv) 12 bar respectively.

Figure 5.13 Location of cross sections chosen for image intensity observation in nitrogen supersonic jet at 18 bar tank pressure.

Figure 5.14 Gray scale intensity in nitrogen and air jets at (a) middle of the shock cell and at (b) the center of the mach disk as indicated in figure 5.13.

Figure 5.15 Effect of stagnation pressure on PLIF image intensity in air supersonic jets.

Figure A.1Co-ordinate system for analysis of light polarization.

Figure A.2 Representation of linear polarization states in X-Y plane.

Figure A.3 Vector $\vec{A}(\vec{r}, t)$ with its components $A_1$and A_2.

Figure A.4 Polarization representation on the Poincare's sphere.

List of Tables

Table 2.1 The properties of the tracers relevant to LIF and PLIF experiments.

Table 3.1 SV coefficients and oxygen quenching rate constants for the ketones under the study.

Table 3.2 Experimental results and theoretically calculated SV coefficients and oxygen quenching rate constants.

Table 4.1 The properties of acetone and MEK tracers relevant to PLIF.

Nomenclature

Symbols

E	laser energy ((J/cm^2)
c	speed of light
h	Plank's constant
k_q	collisional quenching rate
n_{abs}	total number density
n_i	number density of colliding species i
M	Mach number
A	cross section area of the nozzle
P	total pressure (torr)
Pi	partial pressure of species i (Pa)
Re	Reynolds number
U	exit velocity
S_0	Singlet ground state
S_1	Singlet 1stelectronic excited state
S_2	Singlet 2ndelectronic excited state
S_f	fluorescence signal
Sc	Schmidt number
T	temperature (K)
	energy-shell transition matrix
Cp	specific heat capacity
k	Boltzmann constant
h	Plank's constant
F	fluorescence intensity in the presence of quencher
F_0	fluorescence intensity in the absence of quencher
k_{SV}	Stern-Volmer quenching constant
[Q]	number density of quencher
k_f	rate fluorescence intensity
k_{total}	total rate of deactivation
k_q	bimolecular quenching rate constant
k_d	diffusional rate constant

f_Q	quenching efficiency
N_A	Avogadro's number
D	mutual diffusional coefficient
M	molecular mass of tracer/quencher
$\vec{E}$	electric field of electromagnetic radiation
$\vec{H}$	magnetic field of electromagnetic radiation
$\vec{A}$	vector potential
a	amplitude of electromagnetic wave
A_{ni}	amplitude for absorption of radiation by atom
$\mathcal{E}_{fn}$	amplitude for emission of radiation from atom
$Y_{l,m}$	spherical harmonic function
L	total angular momentum

Greek

η_{opt}	collection optics collection efficiency
λ	wavelength (nm)
ν	kinematic viscosity
	wave number (cm^{-1})
σ	absorption cross-section
	Lenard-Jones potential parameter
ϕ	fluorescence quantum yield
χ_{abs}	mole fraction
Ω_D	collisional integral
ρ	gas density
	density matrix
$\hat{\varepsilon}$	state of polarization
φ_n	profile function

Subscripts

i	designates species i
	designates initial energy state
f	designates final energy state
	designates fluorescence signal

t	designates tracer
q	designates quencher
$\vec{k}$	designates momentum of photon
p	designates polarization of photon
RC	designates right circularly polarized
LC	designates left circularly polarized

Acronyms

LIF	Laser Induced Fluorescence
SV	Stern-Volmer
LJ	Lennard-Jones
PLIF	Planar Laser Induced Fluorescence
ICCD	Intensified Charge Coupled Device
CCD	Charge Coupled Device
CMOS	Complementary Metal Oxide Semiconductor
MEK	Methyl Ethyl Ketone
FRET	Fluorescence resonance energy transfer
C-D	Convergent Divergent
CFD	Computational Fluid Dynamics
FVM	Finite Volume Method
DNS	Direct Numerical Simulations

CHAPTER 1

INTRODUCTION TO LIF AND SOME BASIC THEORETICAL CONCEPTS OF FLUORESCENCE

1.1 Introduction

Recent advances in the field of aerodynamics have become possible due to the emphasis on quantitative estimation of fluid flow parameters such as density, pressure, velocity and temperature. Researchers have developed variety of techniques for this purpose over the past several decades. Flow visualization provides, measurement tool for most of these estimations in the entire flow field (Restic, S. et al. 2006).

Planar Laser Induced Fluorescence (PLIF) is a non intrusive optical technique used in the flow diagnostics, which is based on the measurement of fluorescence emitted by tracer molecules excited by a laser. Excitation is usually achieved by the use of light in the UV-visible wavelength range. Tracer molecules are either seeded in to the flow or naturally present in the flow. PLIF technique involves interaction of electromagnetic radiation with atomic or molecular systems. Therefore, quantum theory for interaction of electromagnetic radiation with atomic system provides the theoretical framework for understanding PLIF. Along with the electromagnetic intensity, state of polarization of light is also an important aspect. State of polarization is related to the electric field of the electromagnetic wave. In this chapter we discuss density matrix formalism to understand the estimation of the state of polarization of the emitted fluorescence.

Simply stated, the basic concept of fluorescence involves the interaction of polarized electric field $\hat{\varepsilon}_i$ having frequency ν_i and wave vector $\vec{k}_i$ incident on an atom which is in an eigen state of energy E_i with spin and parity J_i, π_i. After absorbing the radiation, the atom gets in to an excited state of energy E_n with spin and parity J_n, π_n

which decays subsequently into a state of energy $E_f > E_i$ with spin parity J_f, π_f emitting radiation with frequency ν_f and wave vector $\vec{k}_f$ as shown in the figure 1.1.

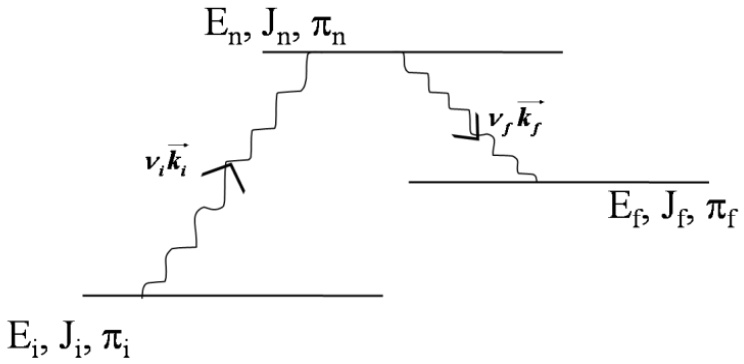

Figure 1.1 Energy level diagram for fluorescence emission from an atom.

We therefore outline here a simple quantum field theoretical approach to the phenomenon of fluorescence from atoms, which can be applied to discuss the polarization effects associated with the phenomenon. Let us consider polarized radiation with frequency ν_i and wave vector $\vec{k}_i$ which may be chosen to be along the z-axis in the laboratory incident on an atom located at the origin **O** of a right handed Cartesian co-ordinate system. The material emits radiation with frequency $\nu_f < \nu_i$ and along $\vec{k}_f$ with polar angles (θ,ϕ) as shown in the figure 1.2.We wish to determine the state of polarization of the emitted radiation.

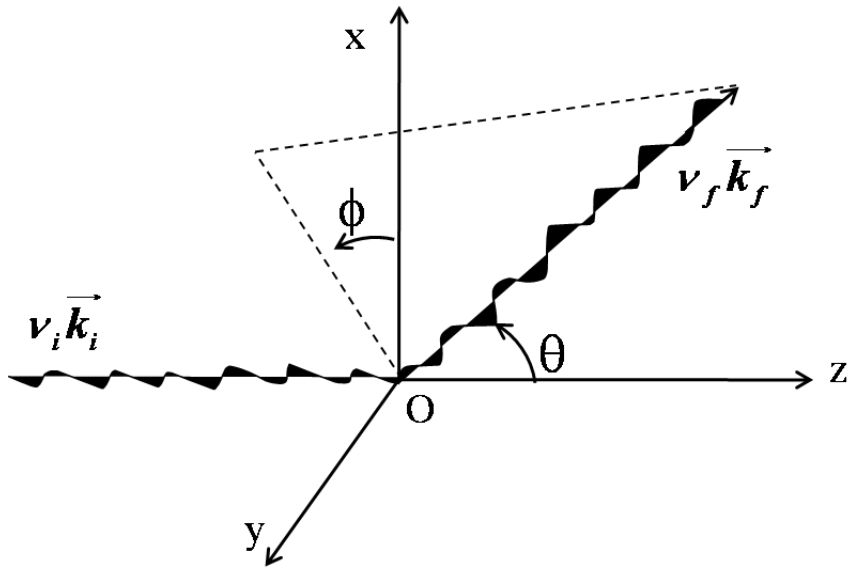

Figure 1.2 Fluorescence geometry in the laboratory co-ordinate system.

1.2 Electromagnetic radiation as quantized field

It is well known that electromagnetic radiation of all frequencies ranging from radio waves to ultraviolet and gamma rays is described by the famous equations of Maxwell. They are transverse waves with the electric and magnetic fields $\vec{E}$ and $\vec{H}$ vibrating perpendicular to the direction of propagation. Using natural units ħ=1, c=1 and the Coulomb gauge (Jackson et al. 2001, Jackson, J.D., 1962), $\vec{E}(\vec{r},t)$ and $\vec{H}(\vec{r},t)$ may be expressed in terms of the vector potential $\vec{A}(\vec{r},t)$ through

$$\vec{E} = -\frac{\partial \vec{A}}{\partial t}, \vec{H} = \vec{\nabla} \times \vec{A} \qquad (1.1)$$

The vector field $\vec{A}(\vec{r},t)$ satisfies the Maxwell equations

$$(\nabla^2 - \frac{\partial^2}{\partial t^2})\vec{A} = 0 \qquad (1.2)$$

$$\vec{\nabla} \cdot \vec{A} = 0 \qquad (1.3)$$

Usually in the literature the polarization $\hat{\varepsilon}$ is associated with the electric field $\vec{E}(\vec{r},t)$ and as such can be associated with the vector potential itself, since $\vec{E}(\vec{r},t)$and $\vec{A}(\vec{r},t)$ are related through (1.1). The polarization of incident radiation may conveniently be

chosen to be either $\hat{\varepsilon}_x$ which represents linear polarization along the x-axis or $\hat{\varepsilon}_y$ which represents linear polarization along y-axis.

Electromagnetic field is essentially a quantum field and it is this aspect which comes into play in phenomena involving absorption and emission of radiation. Therefore it is worthwhile to examine fluorescence from this stand point and focus attention on polarization.

Any general solution for (1.2) satisfying (1.3) may be written in the form

$$\vec{A}(\vec{r},t) = \frac{1}{L^{3/2}} \sum_{\vec{k},p=1,2} \hat{\varepsilon}_p \left[a_{\vec{k},p} e^{i(\vec{k}\cdot\vec{r}-\omega t)} + a^*_{\vec{k},p} e^{-i(\vec{k}\cdot\vec{r}-\omega t)} \right] \quad (1.4)$$

where $\omega = h\nu = c|\vec{k}|$, the summation over $\vec{k}$ is with respect to the integers n_x, n_y, n_z using the box normalization i. e.,

$$k_x = \frac{2\pi n_x}{L}, k_y = \frac{2\pi n_y}{L}, k_z = \frac{2\pi n_z}{L}, \quad (1.5)$$

where L denotes the length of a side of the cubic box and summation over p is with respect to two linearly independent states of polarization (which are orthogonal to $\vec{k}$). The field quantity $\vec{A}(\vec{r},t)$ given by (4) is real valued.

So long as the amplitudes $a_{\vec{k},p}$ and $a^*_{\vec{k},p}$ are considered as complex numbers conjugate to each other, the vector $\vec{A}(\vec{r},t)$ represents a classical field. This is also referred to as c-number theory. On the other hand, if $a_{\vec{k},p}$ and $a^*_{\vec{k},p}$ are replaced by operators $a_{\vec{k},p}$ and $a^\dagger_{\vec{k},p}$ satisfying the commutation relations

$$\left[a_{\vec{k},p}, a^\dagger_{\vec{k}',p'} \right] = \delta_{\vec{k},\vec{k}'} \delta_{p,p'}, \quad (1.6a)$$

$$\left[a_{\vec{k},p}, a_{\vec{k}',p'} \right] = 0, \quad (1.6b)$$

$$\left[a^\dagger_{\vec{k},p}, a^\dagger_{\vec{k}',p'} \right] = 0, \quad (1.6c)$$

the Maxwell field becomes a quantized field and the theory is referred to as q-number theory or second quantized field theory.

The operator

$$N_{\vec{k},p} = a^\dagger_{\vec{k},p} a_{\vec{k},p} \quad (1.7)$$

is referred to as a number operator which is obviously Hermitian i.e. $N_{\vec{k},p} = N^{\dagger}_{\vec{k},p}$ and has real eigen values $n_{\vec{k},p}$ which are integers. We may write

$$N_{\vec{k},p}\left|n_{\vec{k},p}\right\rangle = n_{\vec{k},p}\left|n_{\vec{k},p}\right\rangle \quad (1.8)$$

with $n_{\vec{k},p} = 0,1,2 \ldots$ which represent number of photons with momentum $\vec{k}$ and polarization p in the quantized field. The operators $a_{\vec{k},p}$ and $a^{\dagger}_{\vec{k},p}$ are respectively referred to as annihilation and creation operators. The lowest state with $n_{\vec{k},p} = 0$ for all $\vec{k}$ and p is referred to as the vacuum state of the field and denoted by $|\ \rangle_0$. In other words, the vacuum state $|\ \rangle_0$ is such that

$$a_{\vec{k},p}|\ \rangle_0 = 0 \text{for all } \vec{k}\ , p \quad (1.9)$$

It then follows that

$$\left|n_{\vec{k},p}\right\rangle = \frac{1}{\sqrt{n\ !}}\ \ (a^{\dagger}_{\vec{k},p})^{n}|\ \ \rangle_0 \quad (1.10)$$

In particular, if a single photon, with polarization $\hat{\varepsilon}_x$ or $\hat{\varepsilon}_y$and travellingalong the z axis is incident on the fluorescing material, it may be represented by $a^{\dagger}_{\vec{k},p}|\ \ \rangle_0$ with p=1 corresponding to $\hat{\varepsilon}_x$ and p=2 corresponding to $\hat{\varepsilon}_y$.

1.3 On energy shell transition matrix element for fluorescence

Following essentially the formalism developed by Oo et al. (2007), the transition matrix element on the energy shell for fluorescence may be written as

$$\langle \vec{k}_f p_f | T | \vec{k}_i p_i \rangle = \sum_n \mathcal{E}_{fn}\left(\vec{k}_f p_f\right)\varphi_n A_{ni}(\vec{k}_i p_i) \quad (1.11)$$

with $E_i+\omega_i = E_f+\omega_f$. Here p_i and $p_f$take values ± 1. The symbols $\hat{\varepsilon}_{\pm 1}$are related to the circular polarization states (see Appendix). The photon is a particle with spin 1. The spin $|1,\pm 1\rangle$ states are identified as polarized state $\hat{\varepsilon}_p, p = \pm 1$ which are related to the circular polarization states through

$$|1,+1\rangle = \hat{\varepsilon}_{+1} = -\hat{\varepsilon}_{RC}; |1,-1\rangle = \hat{\varepsilon}_{-1} = \hat{\varepsilon}_{LC} \quad (1.12)$$

The ± 1 projections of spin 1 is with respect to the direction of propagation i. e. $\vec{k}_i$ in the initial state and $\vec{k}_f$in the final state. The symbol $A_{ni}(\vec{k}_i p_f)$ denotes the amplitude

for absorption of radiation by the atom and $\mathcal{E}_{fn}(\vec{k}_f p_f)$ denotes the amplitude for emission of the radiation, while φ_n is a profile function (Stenflo et al. 1998). If $E_i+\omega_i= E_n$ the process is said to be resonance fluorescence.

When radiation is absorbed or emitted by an atom, angular momentum and parity are conserved. Therefore the photon which is emitted or absorbed is also characterized by well defined angular momentum quantum number L and parity. Without going into the details, we may point out that the Maxwell equation (1.2) admits spherical harmonics $Y_{l,m}(\theta,\phi)$also as solutions, since ∇^2 may be written as

$$\nabla^2 = \frac{1}{r^2}\left[\frac{\partial}{\partial r}\left(r^2\frac{\partial}{\partial r}\right)+\frac{1}{\sin\theta}\frac{\partial}{\partial\theta}\left(\sin\theta\frac{\partial}{\partial\theta}\right)+\sin\theta^2\frac{\partial^2}{\partial\varphi^2}\right] \quad (1.13)$$

in terms of spherical polar coordinates. As such l is referred to as orbital angular momentum of the photon. Clearly $Y_{l,m}$ are characterized by parity $(-1)^l$. Since the photon has spin 1, the total angular momentum L can take values (l -1) (if l> 0), l, (l +1). Conversely l can take values L-1, L, L+1 for given total angular momentum L. Clearly the l=L±1 states are of same parity which is opposite to the parity of the state with l=L. It transpires that the state with L=l satisfies the transversality condition and is referred to as the 2^L magnetic multipole state. It is denoted as $\vec{A}^{(m)}_{L,M}$ with the projection M of angular momentum L along the direction of propagation taking values L, L-1,… -L. On the other hand, the solutions with l=L+1 or l=L-1 do not individually satisfy the transversality condition, but it is possible to find an appropriate linear combination of these two solutions which satisfies the transversality condition. This combination is referred to as 2^L electric multipole state and denoted as $\vec{A}^{(e)}_{L,M}$ with M taking values L, L-1… -L. Both are eigen states of the square of total angular momentum with eigen value L (L+1), but are of opposite parity. These are referred to as the multipole field solutions of the Maxwell equations (Oo et al. 2004).

Thus, we may write

$$\mathcal{E}_{fn}(\vec{k}_f p_f) = \sum_{L_f} C\left(J_f, L_f, J_n; m_f, M_f, m_n\right) D^{L_f}_{M_f p_f}(\phi,\theta,0)^*\left(ip_f\right)^{g_+(L_f)} I_{L_f}(\omega_f) \quad (1.14)$$

$$A_{ni}(\vec{k}_i p_i) = \sum_{L_i} C\left(J_i, L_i, J_n; m_i, p_i, m_n\right)(ip_i)^{g_+(L_i)} I_{L_i}(\omega_i) \quad (1.15)$$

in equation (1.11) for fluorescence as depicted in figure 1.2. In equations (1.14) and (1.15) the notation used for the Clebsch-Gordan coefficients (C-G coefficients) and the rotation matrix D follows Rose (1957). The transition strengths $I_L(\omega)$are of the form

$$I_L(\omega) = I_L^{(m)}(\omega)g_-(L) + I_L^{(e)}(\omega)g_+(L) \tag{1.16}$$

where $I_L^{(m)}$ denotes the strength for the magnetic multipole transition and $I_L^{(e)}$denotes the strength of electric multipole transition. The projection operators $g_\pm$ are

$$g_\pm(L_f) = \tfrac{1}{2}\left[1 \pm (-1)^{L_f}\pi_n\pi_f\right] \tag{1.17}$$

in (1.14), while

$$g_\pm(L_i) = \tfrac{1}{2}\left[1 \pm (-1)^{L_i}\pi_n\pi_i\right] \tag{1.18}$$

in (1.15).

1.4 Density matrix formalism

Let us for example consider the incident radiation on the material to be polarized along the x-axis. Such initial state of polarization is $\hat{\varepsilon}_x$, may be represented by 2×2 density matrix

$$\rho^i = \tfrac{1}{2}\begin{bmatrix} 1 & -1 \\ -1 & 1 \end{bmatrix} \tag{1.19}$$

with respect to $\hat{\varepsilon}_{p_i}$, $p_i = \pm 1$ states. We now address the theoretical problem of determining the 2×2 density matrix ρ^f of the emitted radiation along $\vec{k}_f$, using the on energy-shell transition matrix T for the phenomenon of fluorescence. We have

$$\rho^f = T\rho^i T^\dagger \tag{1.20}$$

Explicitly, the elements of ρ^f are given by

$$\rho^f_{p_f p_f'} = \sum_{p_i p_i'} T_{p_f p_i}\, \rho^i_{p_i p_i'} (T^\dagger)_{p_i' p_f'} \tag{1.21}$$

$$= \sum_{p_i, p_i'} T_{p_f p_i}\, \rho^i_{p_i p_i'} T^*_{p_f' p_i'} \tag{1.22}$$

where

$$T_{p_f p_i} = \left\langle \vec{k}_f p_f \middle| \mathrm{T} \middle| \vec{k}_i p_i \right\rangle \tag{1.23}$$

1.5 Scope and objective of the present work

Fluorescence and phosphorescence signal depends on concentration, pressure, excitation wavelength and temperature in a characteristic way. For quantitative analysis, tracer signal dependence on these parameters must be well understood. The objective of the present work was to study the fluorescence from flowing gases seeded with ketone tracers and to measure the concentration profiles of the tracer molecules.

The main research objectives were:

1. To study the effect of oxygen on fluorescence and, consequently, on the image quality in gas flow visualization.
2. Identify different fluorescent tracers for the gas flow at ambient temperature based on the previous literature.
3. Investigate the dependence of LIF signal from these tracers on the gas flow parameters.
4. To study the application of PLIF for high speed gas flow.
5. Measure the concentration profiles from PLIF images.
6. To study the PLIF in supersonic jet taking acetone as the tracer.

1.6 Overview of the thesis

The work presented in the thesis is divided into six chapters. Detailed results of experimental investigations of LIF quenching by oxygen, comparison with the calculated results based on the collision theory, PLIF imaging of subsonic and supersonic jet using acetone and MEK tracer are presented.

Chapter 1 presents an introduction to the interaction of electromagnetic radiation with atom and subsequent fluorescence. Quantum mechanical formalism for state of polarization of fluorescence emission from an atom is presented. The scope and objectives of the present work are mentioned at the end of this chapter.

Chapter 2 presents detailed literature survey on the recent status of the research work on LIF and PLIF.

Chapter 3 mainly focuses on the effect of oxygen on laser induced fluorescence of acetone, MEK and 3-pentanone in static cell with nitrogen as a bath gas. By varying oxygen partial pressure, LIF signal was recorded from acetone seeded nitrogen at constant pressure in a static chamber. Stern-Volmer (SV) coefficients and quenching rate constants were calculated using SV plots. SV plots are found to be linear for all the tracers.

Further Smoluchowski theory was used to calculate the quenching rate and compared with the experimental results. It is found that the estimation of quenching rate by using Stokes Einstein diffusion relation deviates from the experimental result. This is due to the under estimation of diffusion coefficient. The results obtained by using diffusion coefficient from Chapman and Enskog relation are comparable with the experimental quenching rates.

Chapter 4 reports the PLIF imaging in subsonic jet using acetone and MEK as tracers. The analysis of PLIF images for the Reynolds number 2-3x10^3 shows that arrow head shaped coherent turbulent structures are present even at low Reynolds number.

These coherent structures are found to be non-overlapping with separate boundaries. Coherent structures are responsible for the transformation to the turbulence at downstream of the jet. There is a clear distinction between laminar region and turbulence with coherent structures and incoherent instabilities. These PLIF intensity images were converted to acetone density and pressure images by using intensity dependence on these parameters. To study the effect of oxygen in acetone PLIF images at subsonic velocities, jet flow images of air and nitrogen jet are compared.

Chapter 5 reports the PLIF imaging in supersonic jet using acetone as tracers in nitrogen bath gas. The main challenges in implementing acetone PLIF in supersonic flow are discussed. Acetone tracer and high speed ICCD camera was used for supersonic jet flow visualization at Mach 2.5. PLIF image of supersonic jet is compared with the Schlieren and CFD modeling for the same tank pressures. Image processing was used to improve the quality of the obtained PLIF image. Further to study the effect of oxygen in real time flow, air was used as bath gas and the results were compared with that for nitrogen as bath gas for four different tank pressures.

Chapter 6 summarizes all the results and conclusions of the research work. Suggestions for further research on this topic are also mentioned.

CHAPTER 2

LITERATURE REVIEW

2.1 Introduction to PLIF

Investigation of the physical properties of gases flowing at both sub-sonic and super-sonic speeds is of broad interest in fluid mechanics, aeronautics and combustion science. Parameters that are monitored in such studies include temperature, species concentration, pressure and flow velocity (Hiller, B. et al. 1988). Among the various techniques employed Laser induced Fluorescence (LIF) and Planar Laser induced Fluorescence (PLIF) have attracted more attention in recent years (Schulz, C. and Sick, V. 2005, Löffler, M. et al. 2010). LIF is based on the observation of fluorescence from the fluorophore through the excitation of electronic energy levels that are usually populated by absorption of photons in the UV-visible range. This allows qualitative and quantitative determination of concentration, pressure and temperature. Before doing quantitative measurement by LIF, the influence of preponderant parameters (concentration of tracer and oxygen, pressure, temperature, laser power, combination of tracer and excitation wavelength etc.) on the fluorescence or phosphorescence signal must be characterized (Guibert, P. et al. 2006).

2.2 Fluorescence Spectroscopy (Jablonski diagram)

Spectroscopy is the study of emission of electromagnetic radiation, its interaction and exchange with matter. Fluorescence spectroscopy is one of the most sensitive techniques capable of detecting even a single molecule (Moerner, W. E. and Fromm, D. P. 2003, Tani, T. et al. 2006).

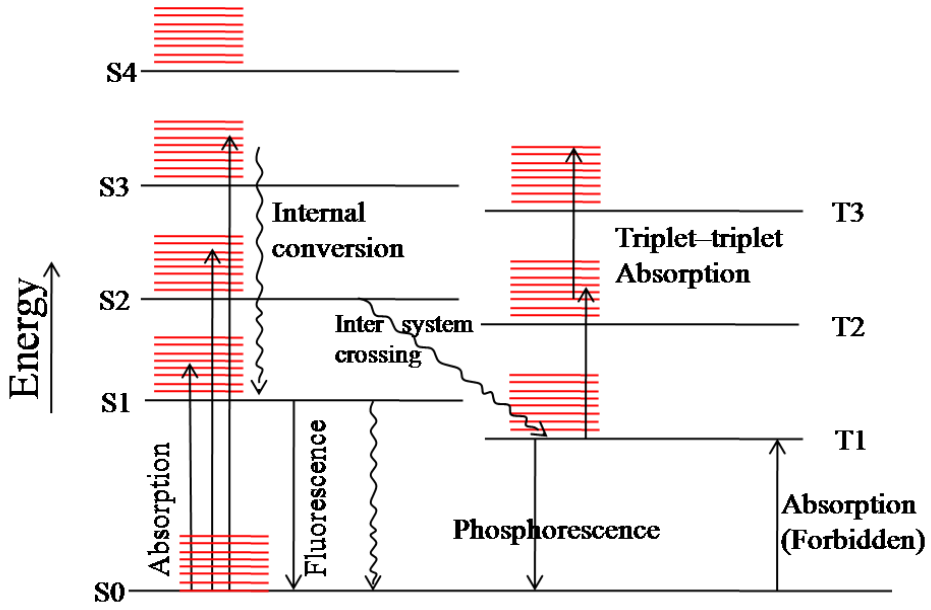

Figure 2.1 Jablonski diagram showing transition between the molecular energy levels.

A well known Jablonski diagram as shown in the figure 2.1 is used to explain all the various possible pathways during the interaction between a photon and the molecule. Emission of light from the molecules by transition between the electronic energy levels is called luminescence. Electronic states of the molecules can be divided into singlet and triplet states. A singlet state is one in which all of the electrons in the molecule have their spins paired. Triplet states are those in which one set of electron spin remains unpaired. A triplet state will always lie lower in energy than its corresponding singlet state.

De-excitation of a molecule from any of the excited states S_1, S_2… may occur through pathways such as internal conversion, intersystem crossing, fluorescence and phosphorescence. Internal conversion is the nonradiative vibrational relaxation towards lowest level of electronic state. This process occurs within timescale of 10^{-13}-10^{-11} s. Fluorescence is a radiative transition between the energy levels with the singlet states S_1 and S_0, in the timescales of 10^{-10}-10^{-7} s. One more nonradiative deactivation pathway is intersystem crossing. In this process (10^{-10}-10^{-8} s) transition takes place between one of the vibrational levels of singlet state and isoenrgitic

vibrational level of the triplet state. Another important radiative transition from lowest triplet state to the ground state is phosphorescence. This is a long process occurring over a timescales of the order of 10^{-4}-10s (Valeur 2001).

2.3 Absorption and Emission Spectrum

Absorption is an excitation of electron from lower energy to the higher energy level by the interaction of the molecule with the photon. Absorption spectrum is the plot of absorbance (A) as function of wavelength. Emission spectrum is a measure of emitted intensity as a function of wavelength. In order to get fluorescence emission, wavelength of the excitation light should be within the band of the absorption spectrum of the molecule. Lasers within UV region of the spectrum are ideal excitation sources for most of the molecules (Mycek M. A. and Pogue B. W. 2003).

2.4 PLIF technique

PLIF is a two dimensional (2D) LIF imaging technique, which makes use of laser light sheet created by using proper optics. LIF or PLIF has been widely investigated and used in fluids for estimating species concentration (Lozano, A. et al. 1992, Thurber, M. C. and Hanson, R. K. 2001) pressure (Yuen, L. S. et al.1997, Lachney, E. R. and Clemens, N. T. 1998, Thurber, M. C. et al. 1999, Rossmann, T. et al. 2003) and temperature measurements (Thurber, M. C. et al. 1997,Lachney,E. R. and Clemens, N. T. 1998, Koch, J. D. and Hanson, R. K. 2003, Löffler, M. et al.2010). In several applications, such as fuel concentration measurement by LIF, the tracer molecule should have satisfactory spectroscopic and thermodynamic properties similar to that of the fuel (Smith, J. D. and Sick, V. 2007).

The strength of fluorescence signal not only depends on concentration but also on pressure, temperature and excitation wavelength in its own characteristic way. Hence for quantitative analysis tracer signal dependencies on these quantities must be well understood.

For the molecules with broadband absorption, fluorescence triggered by laser excitation can be modeled as in equation (2.1). For weak excitation (linear excitation

regime) the fluorescence intensity, S_f, is given by (Thurber, M. C. et al. 1999, Koch, J. D. and Hanson, R.K. 2003, Modica, V. et al.2007)

$$S_f = \eta_{opt} \frac{E}{hc/\lambda} n_{abs}(P,T)\sigma(\lambda,T)\Phi(\lambda,T,p_i) \qquad (2.1)$$

where

η_{opt} is the efficiency of the collection optics,

E is the incident laser fluence (J/cm^2),

hc/λ is energy of photons (J) at excitation wavelength (λ),

n_{abs} is the number density of exciting species (cm^{-3}),

σ is the molecular absorption cross section of exciting species(cm^2/molecule),

Φ is the fluorescence quantum yield (number of photons emitted per absorbed photon),

P is the total Pressure (Pa),

p_i is the partial pressure of exciting species,

T is the temperature in Kelvin.

Number density (n_{abs}) of the absorbing species can be written in terms of mole fraction (χ_{abs}) as follows

$$n_{abs} = \frac{\chi_{abs} P}{kT} \qquad (2.2)$$

where k is Boltzmann constant (1.381×10^{-23} J/K), P is the total pressure and T is the temperature of the exciting species. Equation (2.1) is the basic relation used for the quantitative measurement of PLIF in terms of flow parameters like concentration, temperature and pressure. Due to the non uniform laser fluence, finite dimensions of the laser sheet and limited collection efficiency of the optical lens system, it is difficult to determine absolute values of these parameters accurately. Hence relative measurements of these parameters are performed by using fluorescence intensity emitted by a gas with known properties for calibration purposes.

The objective of this study is to investigate the LIF signal dependence on the flow parameters, especially species concentration and pressure. It is proposed to measure the concentration profiles of selected species in gas flow field by PLIF.

2.5 Current state-of-art

Laser induced fluorescence and planar laser induced fluorescence has been frequently employed for investigations in fluid dynamics, combustion studies and internal combustion engine applications. For LIF studies, fluorescence tracer is often seeded in to the gas flow stream.

2.5.1 LIF tracers

Tracers are added in the gas flow or fuels in case of combustion diagnostics for quantitative analysis. Ideally the tracer should behave similar to the bath fluid and it should yield strong fluorescence signal which should be proportional to the desired physical parameters. However, there is no single "best tracer" available which could be used for all possible applications (Schulz, C. and Sick, V. 2005). The most frequently used and best studied classes of tracers are aliphatic carbonyls (acetone (Thurber, M. C. et al. 1998, Loffler, M. et al.2010), 3-pentanone (Koch, J. D. and Hanson, R.K. 2003) and biacetyl (Guibert, P. et al. 2006)) and small aromatic compounds (toluene (Luong, M. et al. 2008)) in gas phase. Several molecules have been used as tracers based on the following criteria.

i. It should have high quantum yield,Φ so that low concentrations of tracers could yield a large LIF intensity.
ii. It should have sufficiently high vapor pressure at room temperature so that it can be seeded in higher concentrations.
iii. It should possess good absorption cross section for light emitted by commercially available high power lasers.
iv. The fluorescence lifetime of the tracer should be short enough to enable measurement of fast flows and gases having low collisional quenching or bath gas effects.
v. It should have low environmental toxicity.
vi. It should not be expensive, so that it can be used at high flow rates.

2.5.2 Atoms and diatomic molecules

Materials in atomic state are good candidates for fluorescence due to their high absorption cross sections in UV-visible range. However atomization requires higher temperatures and usually strong absorption leads to saturation of the fluorescence signal. Thus atoms are not suitable tracers at room temperatures (Schulz, C. and Sick, V.2005).

Several diatomic molecules such as NO (Rossmann, T. et al. 2001, Hsu, A. et al. 2009), OH (Pitz, R. W. 2008), I_2 (Iida, N. and Ando, A.1994) and molecular oxygen are used as tracers in the flow field studies and combustion diagnostics. In spite of its toxicity NO is frequently used in the diagnostic application by exciting it with 226 nm laser light. This is due to its thermal stability, well characterized spectroscopy, strong absorption of light from tunable dye lasers and its natural presence in many flows of interest (Lee M. P. et al. 1993, Tseng, C. C. et al. 2009). The two line LIF technique was developed by McMillin, B. K. et al. (1993) to measure the temperature in supersonic flow field. In this method, fluorescence ratio from NO was obtained by sequentially exciting the two initial energy levels. The ratio was used to obtain the temperature dependence of the absorbing species. This method was used to minimize the signal dependence on number density, mole fraction and collisional quenching of fluorescent tracer. The technique generally requires two lasers and two cameras for measurements. The cameras are gated so that each camera integrates the fluorescence signal excited from only one of the lasers (McMillin, B. K. et al. 1993).

Diles et al. (2000) measured the rotational temperature with an error of 10% by LIF excitation and detection of NO emission from ro-vibrational levels. The main advantage of this method is that it is fast since small portion of the entire fluorescence spectrum of NO is used for the calculation temperature. The disadvantages are that it is applicable to only at low pressures, low temperature and steady flows with minimum densities $< 10^{14}$ cm^{-3} and we also require LIF spectrum at a reference temperature and pressure (Diles, G. et al. 2000).

OH radical was used in numerous combustion studies as the LIF tracer. Sick et al. (2004) used the Nd: YAG laser output, tuned to 266.188 nm by using an etalon, as the excitation source for exciting the A←X (2, 0) band of OH for their combustion studies. Fluorescence of OH radical in the range 265-325 nm was collected by a CCD camera.

2.5.3 Polyatomic organic molecules

Due to their high density of states compared to atomic and diatomic molecules, polyatomic molecules have broad band absorption spectrum and, hence, excitation is possible at several wavelengths. Aromatic compounds, such as benzene and toluene, have strong absorption cross sections and hence high fluorescence quantum yield. Structure dependant properties of this class of molecules can be suitably exploited. Since larger molecules have very low vapor pressure, seeding the gas flow at room temperature is a problem. One more drawback of the aromatic compounds is quenching of fluorescence signal by oxygen (Luong, M. etal.2008). Toxicity is yet another problem with this class of compounds. Organic dyes are frequently used for liquid phase flow diagnostics. These are highly fluorescent compounds and absorption usually lies in the visible range of electromagnetic spectrum (Sutton, J. A. et al. 2008, Crimaldi, J. P. 2008). However seeding of these molecules in gas flow is rather difficult because of their very low vapor pressure and tendency for molecular dissociation.

Saturated aliphatic compounds are non fluorescent and their absorption band lies in vacuum UV region. Excitation of such materials frequently leads to photo dissociation. Unsaturated molecules are usually unstable and tend to polymerize, whereas aliphatic compounds with chromophores have attractive spectroscopic properties. The combination of conjugated chromophores (diketones) usually shift absorption and fluorescence spectrum towards higher wavelengths. Such class of compounds includes ketones (R_2-CO), aldehydes (RCHO) and amines (R_3N). In the case of aldehydes formaldehyde tends to polymerize and hence it is difficult to handle in gas phase. Acetaldehyde has photo physical properties approximately similar to acetone, but is more toxic than acetone and, hence, acetaldehyde is usually not used.

Ketones are the most frequently used organic carbonyls as tracers. Among these acetone is a very popular tracer due to its high vapor pressure, low boiling point (56°c) and excellent fluorescent properties (Lozano, A. et al. 1992, Yuen, L. S. et al.1997, Thurber, M. C. and Hanson, R. K. (1999, 2001), Löffler, M. et al. 2010). This tracer was extensively studied and successfully used. Its absorption cross section extends from 225-320 nm. Thurber, M. C. (1999) under took extensive study of acetone LIF dependency on gas flow parameters. To explain the results, he developed a straight forward photo physical model which satisfactorily accounted for the observed complex behavior of acetone fluorescence signal. At the same time other researchers found that acetone is not the ideal tracer for certain diagnostic conditions (Thurber, M. C. and Hanson, R. K. 1999, Koch, J. D. 2005). Löffler et al. (2010) studied acetone LIF in internal combustion engine and reported the calibration data for quantitative measurement of temperature and pressure. It can be used for studies with 266 nm light from Nd: YAG laser. The physical properties of the some of the ketone tracers relevant to LIF and PLIF experiments are presented in the Table 2.1.

[$]**Table 2.1** The properties of the tracers relevant to LIF and PLIF experiments.

Tracers	**Chemical formula**	**Boiling point (^oC)**	**Vapour pressure at 20^oC (mm of Hg)**	**Absorption wavelength range (λ_{abs} in nm)**	**Fluorescence wavelength range (λ_{fl} in nm)**
Acetone	(CH_3 (CO) CH_3)	56.1	180	~225-320	~320-550
MEK*	(CH_3 (CO)CH_2CH_3)	80	100	~220-330	~350-550
3-Pentanone	(CH_3CH_2(CO)CH_2CH_3)	102	78	~230-320	~340-550 (peak 420)
Biacetyl	(CH3(CO)(CO)CH3)	88	52	~200-490	~440-510 ~510-600 (P)[@]

[$]Ref: Above data is compiled from the references mentioned at the end of the thesis.

*MEK-Methyl Ethyl Ketone or 2-Butanone,

[@]P-Phosphorescence.

Methyl Ethyl Ketone (MEK) has properties similar to that of acetone. This is due to the similarity between acetone and MEK as seen in figure 2.2. This molecule is used as a tracer to subsonic flow visualization, which is presented in detail in chapter 4.

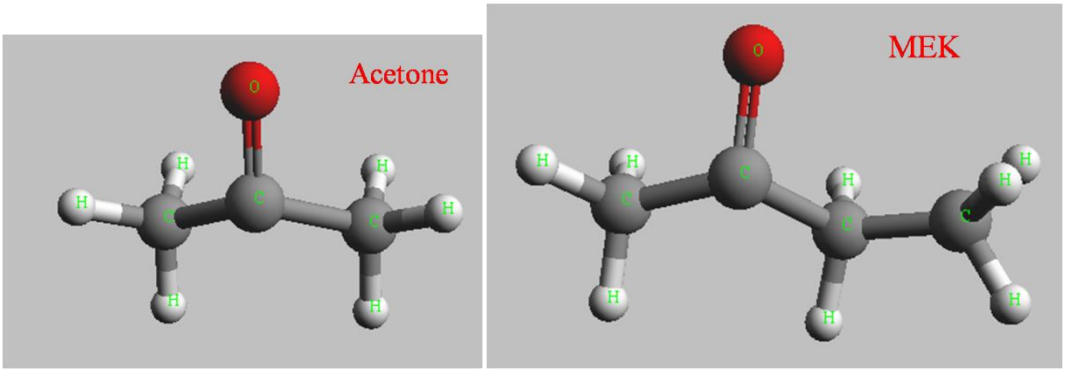

Figure 2.2 Molecular structures of acetone and MEK.

Similar to acetone, 3-pentanone (CH_3CH_2 (CO) CH_2CH_3) has broad absorption spectrum in the range 230-320 nm and fluorescence from 350-550 nm (peak-420 nm). Koch et al. (2003) studied the gas phase 3-pentanone absorption and fluorescence from 300-875 K in different bath gases such as nitrogen and air. In their experiments, nitrogen and air was passed through 3-pentanone liquid until it gets saturated. The exit temperature and pressure information is used to calculate the exact mole fraction of 3-pentanone since vapor pressure is known function of temperature. KrF (248 nm), XeCl (308 nm) excimer laser and Nd: YAG laser (266 nm) are used in these experiments.

Interestingly they found that for 3-pentanone, for excitation at wavelengths equal to 248 nm and 266 nm, the absorption cross section is insensitive to the temperature range of interest. For 308 nm laser, the cross section increases with temperature. This is due to the increase in the population of the excited vibrational levels of the ground electronic state. For all these excitation wavelengths, fluorescence quantum yield decreased with temperature. Similar to acetone this behavior is attributed to faster non radiative quenching at higher temperatures. They

also found that fluorescence ratio of 308 nm and 248 nm is more sensitive than in the case of acetone studied by Thurber et al. (2001). Based on these observations they suggested two line thermometry at longer excitation wavelength (Koch, J. D. and Hanson, R. K. 2003).

Modica et al. (2007) studied the temperature and pressure dependencies of LIF of gas phase 3-pentanone and compared their experimental results with the model which was previously developed by Thurber et al. (1998) for acetone and Koch et al.(2005) for 3-pentanone. The authors used 266 nm Laser beam from frequency quadrupled Nd: YAG Laser. The studied temperature and pressure ranges were 373-573 K and 0.1-4 MPa, respectively, in different bath gases such as nitrogen, air, carbon dioxide and pure oxygen. They found that fluorescence intensity increased with tracer mole fraction and reached saturation level and then decreased thereafter. This is due to high collision rates between the molecules which leads to re-absorption and auto quenching. In the absence of quencher, they found that LIF intensity increased at low pressures (0.1-1 MPa) and reached saturation at high pressures (1-4 MPa). This increase in fluorescence is attributed to the vibrational relaxation and, at high pressures, vibrational relaxation is faster than intersystem crossing. The quenching from oxygen was observed above 0.4 MPa. With increase in temperature the vibrational energy of the molecule increases as excited levels become more populated. Thus radiative intersystem crossing is more favored leading to decrease in fluorescence intensity which was observed to be 66% between the temperature ranges from 373-573K. Slight increase in fluorescence quantum yield at low temperatures (373K-473K) was observed which is due to an activation of intersystem crossing between triplets to singlet state. For bath gases N_2, air and CO_2 fluorescence per unit mole fraction increases linearly; this is not true for oxygen. This is due to energy transfer favored by exciplex formation. The correlation between their model and their experimental results was satisfactory (Modica, V. et al. 2007, Koch, J. D. and Hanson, R. K. 2003).

Biacetyl ($CH_3COCOCH_3$) is another frequently used molecule. The broad band absorption from 200 to 490 nm makes this compound interesting for 355 nm

excitation in LIF. Biacetyl can be excited with both 266 and 355 nm light from Nd: YAG laser. Its fluorescence spectrum ranges from 400-500 nm with lifetime of about 5 ns. It shows strong phosphorescence in the range of 500-600 nm with a lifetime of about 1.5 ms. Therefore, it is difficult to spectrally separate fluorescence from phosphorescence. In previous studies researchers have used nano second gated camera for separating both fluorescence and phosphorescence (Smith, J. D. and Sick, V. 2007).

LIF of biacetyl gas molecule was studied by Guibert, P. et al. (2006) using Ar-ion laser at wavelengths 333.3 nm to 363.8 nm for pressure range of 0.1-4 MPa and temperature range 373-573 K, respectively. They varied the biacetyl mole fraction in air and nitrogen bath gases in linear fluorescence regime. Linearity of the fluorescence was maintained by keeping laser energy well below the saturation level. They found that with increase in biacetyl mole fraction, fluorescence signal increases linearly and reaches saturation and decreases thereafter. This is due to re-absorption process and also self quenching at high mole fractions. Fluorescence intensity increased linearly with pressure. This is due to the collisional relaxation of the higher vibrational levels of excited states since the intersystem crossing is slower from this level. Similar to the previous studies fluorescence quenching due to oxygen was clearly observed. This is due to the formation of excited complex between oxygen and tracer molecule. Temperature effect was also studied by the authors and they found that fluorescence intensity increased initially and then decreased at higher temperatures. This was explained based on the biacetyl molecular energy levels in which both S_1 and T_1 are low lying energy levels and transition between S_1 to S_0 ($n \rightarrow \pi^*$) generates fluorescence. The lifetime of T_1 is long and, hence, due to intersystem crossing between T_1 to S_1 as temperature increases the fluorescence intensity increases. At higher temperatures the molecule acquires vibrational energy and reaches S_1 instead of T_1. This activates intersystem crossing between S_1 to T_2 which leads to decrease in fluorescence intensity (Guibert, P. et al. 2006).

In their previous work, Guibert et al. (2002) investigated the effect of pressure (0.1-0.65 MPa), temperature (360K-573K), flow velocity (2-30 m/s) and an

equivalence ratio (0.7-1.4) on the fluorescence signal and also their first order interactions. They found that the flow velocity has negligible effect on fluorescence, where as the other three parameters (temperature, pressure and equivalence ratio) and their first order interactions have significant effect. Using inversion quadratic model they have calculated equivalence ratio with an error less than 2.2%.

The effect of gas phase oxygen quenching on LIF of toluene between 300-650 K in nitrogen and oxygen were studied by Koban et al.(2005a) for bath gas pressure of 1 bar and oxygen partial pressures up to 400 mbar. Nd: YAG laser (266 nm) and KrF excimer laser (248 nm) were used as excitation sources. It was found that oxygen quenching of toluene fluorescence at higher temperatures and at 266 nm wavelength is very significant. Interestingly at 248 nm excitation and at higher temperatures, fluorescence quenching was not observed. These results were obtained using the Stern-Volmer (SV) plots. This unusual result is due to the collisional quenching dominated by fast intra molecular decay at higher temperatures and lower excitation wavelengths. The experimental results were explained by a model based on this assumption.

For the instantaneous measurement of concentration distribution in gas jets, Iida et al.(1994) used second harmonic (532 nm) light from Nd: YAG laser as an excitation source and iodine as the fluorescent seeder in bath gases of He, N_2 and CO_2. Fluorescence signal dependence on the concentration of tracer and on temperature was studied. They observed a linear variation of the fluorescence intensity with the seeder concentration for all the bath gases. In their study, laser energy was kept well below the saturation level. Their result shows that the fluorescence intensity distribution of a jet contains information of both concentration and temperature distribution. Instantaneous concentration distribution measurement of gas jet was obtained using the LIF method. Based on the Beer Lambert's law, they found that the absorption of fluorescence light has less influence than that of excitation light (Iida, N. and Ando, A. 1994).

2.5.4 PLIF measurements

Numerous studies were performed using PLIF technique for instantaneous quantitative measurements of gas flows, combustion diagnostics and aerospace applications. The strength of PLIF is in its ability to provide non intrusive instantaneous image of the flow field. This image must be related to flow field parameters and converted into an image of flow parameters of interest. The choice of PLIF tracer depends on the desired quantity, application and availability of excitation wavelength and detecting system. Early works, including Cruyningen et al. (1990), used biacetyl as a tracer to study the mixing of turbulent jets. Lozano et al. (1992) used acetone and biacetyl in their study and found that acetone is suitable as a tracer due to low toxicity and consistent signal level throughout the flow.

A quantitative planar measurement of mixed fluid states is very important to study the turbulent mixing processes. King et al. (1997) presented instantaneous quantitative planar measurements in mixed fluid at a molecular level using dual tracer PLIF technique. They used nitrogen from pressurized cylinders seeded with small amount of NO tracer as jet flow and, additionally, air from compressed air tank seeded with acetone (4.6 % by mass) was used as co-flow. By simultaneous imaging of LIF from NO and acetone, King et al. (1997) demonstrated the ability of PLIF to quantify mixed jet fluid in the mixing process of gas phase shear layers. Jets with Reynolds numbers ranging from 1000 to 50000 were investigated. To avoid the burden of instrumentation and experimental setup in dual laser and dual tracer techniques, Hu et al. (2002) developed a novel method. This method is based on the fluorescence emission and quenching of phosphorescence using single laser and single tracer. This technique was demonstrated for the molecular mixing of acetone seeded nitrogen jet in air by imaging mixed jet fluid fraction and mixing efficiency.

Tseng et al. (2009) investigated the transient injection and mixing of nitrogen and helium at high Reynolds number. The mixing of two helium streams in previously established nitrogen flow was studied. Nitrogen is seeded with NO which is excited with a 226 nm laser. Results show that the structure and mixing of the two streams is

highly irregular and unsteady (King, G. F.et al.1997, Hu, H. and Koochesfahani, M. M. 2002, Tseng, C. C. et al. 2009).

Liquid phase quantitative mixing in impinging jet was studied using PLIF by Unger et al. (1999). Rhodamine B is used as tracer in water, which is excited with 532 nm laser beam from Nd: YAG laser. Instantaneous quantitative imaging of jet with different Reynolds number ranging from 150-600 was performed. Pioneering experiments on PLIF in liquid phase, in three dimension (3D) was done by Tian et al. (2003) to study the buoyant jet flows of waste water using rhodamine 6G as tracer. In this study, laser sheet is swept across the flow and images were captured with high speed synchronized CCD camera rated for 260 frames per second. This technique is limited to short duration and small volumes due to image storage requirements and camera sensitivity. Although 3D PLIF system can provide more data, extensive post image processing is required for the quantitative concentration determination. Deusch et al. (2001) carried out similar studies in turbulent jet of water seeded with disodium fluorescein dye which is excited with Ar-ion laser. In this study, different methods for laser sheet scanning across the flow were used and they found that the piezoelectric mirrors with cylindrical lens produced better results.

2.6 Conclusions

Fluorescence from polyatomic molecules is explained in detail using Jablonski diagram. Detailed literature survey on LIF and PLIF techniques is presented. Based on the past investigations, ketones are seen to be better tracers for PLIF imaging in gas phase subsonic and supersonic flow field.

CHAPTER 3

EFFECT OF OXYGEN ON LIF OF KETONES IN STATIC CONDITIONS

3.1 Fluorescence quenching

Fluorescence emission from a fluorophore gets altered due to the presence of other molecules (fluorescent or non fluorescent). The reduction in fluorescence intensity by various processes is called "fluorescence quenching" or simply "quenching". Fluorescence quenching can occur through any of the pathways such as collisional energy transfer, charge transfer reactions or excited state complex formation. Alternatively, the fluorophore itself can absorb the emitted light, such a process termed as "self quenching".

3.1.1 Mechanisms for quenching

One of the main mechanisms for quenching phenomenon is collisional quenching (also called dynamic quenching), which occurs when the fluorophore molecule, in the excited state, comes in contact with a quencher molecule in the ground state. A prominent collisional quencher is oxygen in either solution, as dissolved oxygen, or in gas phase. Thus, the presence of oxygen in many gas flow experiments makes LIF imaging quite a challenge. In our experiments this process is more significant and is discussed in detail in the present chapter.

Figure 3.1 illustrates the collisional quenching process. S_0 is the ground electronic singlet energy state, S_1 is the first excited singlet state and S_n is the n^{th} excited singlet state. During the gas flow, the excited fluorophore molecule may decay through the energy transfer by collision with the quencher, leaving the fluorophore chemically un-altered.

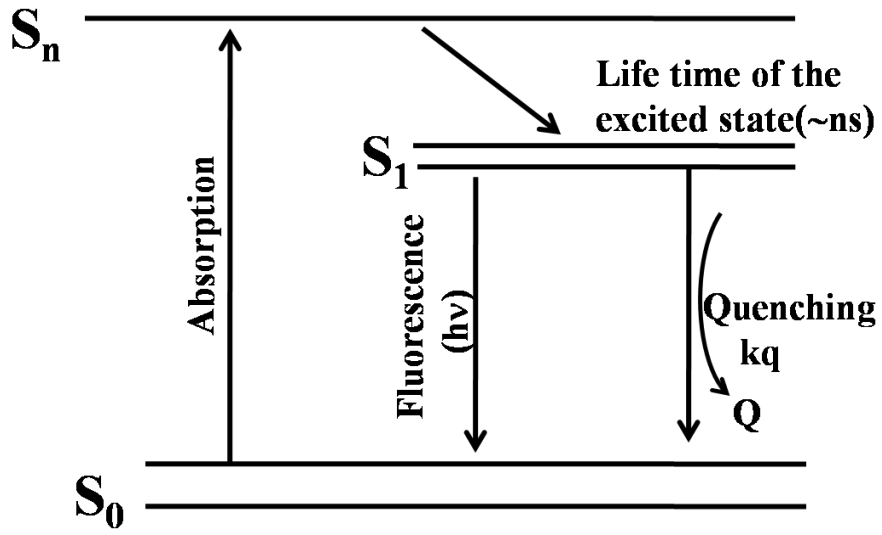

Figure 3.1 Fluorescence quenching by collisional process.

Fluorescence quenching may also occur due to other processes such as formation of non-fluorescent complex in the ground state or in the excited state of the fluorophore. This process is called static quenching, since it does not depend on the collision or the diffusion which are time dependent processes.

Static quenching occurs due to the formation of non fluorescent complex between the fluorophore, in the excited state, and the quencher. This complex returns to the ground state without emitting a photon as illustrated by the following equation

$$M^* + Q \rightleftharpoons (M \bullet Q)^* \xrightarrow{\substack{no-photon \\ emission}} M \bullet Q \qquad (3.1)$$

where M^* is the excited fluorophore and Q is the quencher molecule.

Another significant non-radiative pathway for decay of the excited fluorophore is the resonance energy transfer (RET) or fluorescence resonance energy transfer (FRET). This process occurs in cases where there is an overlap of fluorescence and absorption spectrum of the fluorophore molecule as depicted in figure 3.2. The electronic energy of the fluorophore is transferred through non-radiative dipole-dipole coupling (Lakowiz, J. R. 2006). RET mainly depends on the degree of spectral overlap.

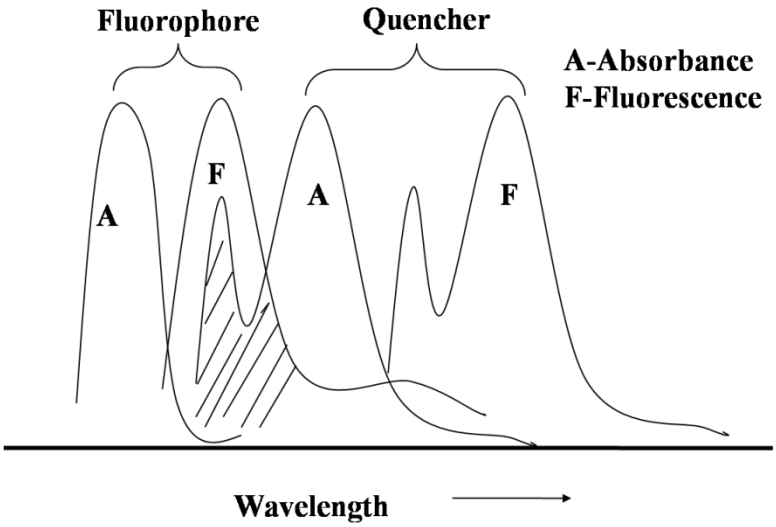

Figure 3.2 Fluorescence resonance energy transfer [FRET] (Valeur, B. 2001).

In the case of collisional quenching, decrease in the intensity of the fluorescence emission follows the Stern-Volmer model represented by the following equation (Stern et al. 1919, Lakowiz, J. R. 2006)

$$\frac{F_0}{F} = 1 + k_{SV} \times [Q] \tag{3.2}$$

where F and F_0 are the fluorescence intensities in the presence and absence, respectively of quencher. k_{SV} is the Stern-Volmer quenching constant, [Q] is number density of quencher molecule. This model was first used for analyzing dynamic quenching in the solution form by Vavilov (1929).

3.2 Oxygen quenching effect on LIF

Certain organic materials, such as ketones, have been used as tracer molecules in several gas flow visualization experiments (Lozano, A. et al. 1992, Thurber, M. C. and Hanson, R. K. (1999, 2001). Fluorescence quenching of organic molecules by oxygen is well known in solution as well as gas phases. For long time fluorescence quenching of ketones by molecular oxygen was not well understood. Nau and Scaiano (1996) have quantitatively investigated oxygen quenching of fluorescence from some ketones and diketones in the liquid phase. The quenching of LIF from toluene by

oxygen in the gas phase at elevated temperature (300-650 K) was carried out by Koban et al. (2005a). Based on the Stern-Volmer (SV) plots they found that the effect of oxygen quenching gets reduced with increase in the temperature. Koban et al. (2005b) also studied the effect of oxygen on LIF from 3-pentanone, used as a tracer, in nitrogen and air and concluded that quenching due to oxygen becomes predominant at higher pressures.

Oxygen quenching rate constants for ketones relevant to LIF in gas phase have not been quantified in the previous literature. In this thesis we have investigated oxygen quenching of LIF signal from acetone, methyl ethyl ketone (MEK) and 3-pentanone in nitrogen bath gas at low pressures (~700 torr) in order to understand the effect of oxygen quantitatively. Stern-Volmer plots were obtained for all the three tracers by varying oxygen concentrations. Further, oxygen quenching in ketones relevant to LIF are quantified and compared with the well established Smoluchowski theory (Reid, R. C. et al. 1987). Results presented here are very useful in LIF studies of high speed flows using ketones as tracers.

3.3 Theory of fluorescence quenching

For low excitation intensities (linear excitation regime), the fluorescence intensity F is directly proportional to the number density of the species n_{abs} (m^{-3}), absorption coefficient σ_a and fluorescence quantum yield Φ

$$F \propto n_{abs}(P,T)\sigma_a(\lambda,T)\Phi(\lambda,T,n_i) \tag{3.3}$$

where P and T are total pressure and temperature of the tracer, respectively and λ is the excitation wavelength. The effect of oxygen quenching depends on the fluorescence quantum yield Φ given by the following equation (Valeur, B. 2001)

$$\Phi = \frac{k_f}{k_{total} + k_{q\times} n_{o_2}} \tag{3.4}$$

where k_f (s^{-1}) is the rate fluorescence intensity, k_{total} (s^{-1}) is the total rate of deactivation including non-radiative decay, k_q (m^3s^{-1}) is bimolecular quenching rate constant and n_{o2} is number density of the quencher. Further, we may write

$$\frac{\Phi_0}{\Phi} = \frac{F_0}{F} = \frac{k_f}{k_{total}} \frac{k_{total} + k_q \times n_{o_2}}{k_f} = 1 + \frac{k_q}{k_{total}} \times n_{o_2} \tag{3.5}$$

where Φ_0 is the quantum yield in the absence of quencher and is given by the following relation

$$\Phi_0 = \frac{k_f}{k_{total}} \tag{3.6}$$

The effect of molecular quenching is expressed as Stern-Volmer (SV) coefficient (k_{sv}), which is given by the ratio of quenching rate coefficient to the total rate of deactivation. The SV coefficient is a measure of the efficiency of quenching. The quenching rate constant k_q is the measure of receptiveness and dynamics of the quenching processes. We may write

$$k_{SV} = \frac{k_q}{k_{total}} = k_q \tau_{eff} \tag{3.7}$$

where τ_{eff} is the effective life time of the excited state. The SV coefficient (k_{sv}) can be easily obtained from the slope of the SV plot using following equation

$$\frac{F_0}{F} - 1 = k_{SV} \times n_{o_2} \tag{3.8}$$

where F and F_0 are the LIF intensity in the presence and in the absence, respectively, of quencher (Koban, W. et al. 2005, Valeur, B. 2001).

3.4 Quenching rate constant (k_q)

Quenching rate constant or the bimolecular quenching rate constant (k_q) is the measure of quenching. For diffusion controlled quenching, reaction rate of quenching (k_q) is given by the following equation

$$k_q = f_Q k_d \tag{3.9}$$

where f_Q is the quenching efficiency and for oxygen it is found to be equal to unity. Thus, quenching rate constant is same as diffusional rate constant k_d.

According to Smoluchowski's simplified theory, the diffusion rate constant is given by the following equation

$$k_d = 4\pi N_A R_c D \tag{3.10}$$

where N_A is Avogadro's number, R_c is the closest distance between the molecules (Å), given by the sum of radii of the fluorescent tracer and the quencher. D is the mutual diffusion coefficient (m^2/s) expressed by the Stokes-Einstein relation

$$D = D_t + D_q = \frac{kT}{f\pi\eta}\left(\frac{1}{R_t} + \frac{1}{R_q}\right) \tag{3.11}$$

where D_t and D_q are the diffusion coefficients of the tracer and quencher molecule, respectively, η is the viscosity of the medium, f is coefficient for slip boundary conditions and is equal to 4 and it is 6 for stick or no-slip boundary conditions. Further, in equation 3.11, T is the absolute temperature and k is the Boltzmann's constant, R_t and R_q are the radii of tracer and quencher (Å) respectively. The radius of the tracer was calculated by adding atomic volume of the fluorophore molecule as given by Edward (1956) and that of the quencher molecule as given by Kuznicki et al (2001). Stokes Einstein diffusion equation is frequently used for modeling fluorescence quenching in fluids (Thipperudrappa, J. et al 2004, Arik, M. et al 2005, Biradar, D. S. et al 2007, Patil, N. R. et al 2012). For relatively small molecules the above equation underestimates the diffusion coefficient (Arik, M. et al 2005). This is because of the basic assumption of Stokes-Einstein relation which states that diffusing particle is much larger than the constituents of the medium, at infinite dilutions (Zangi, R. et al 2007). Thus in the present thesis, we have chosen to use the Chapman-Enskog relation which is based on thermodynamic and physical properties such as Lennard-Jones (L-J) parameters, temperature and pressure. The Chapman-Enskog relation for mutual diffusion coefficient is given by the following equation (Reid, R. C. et al 1987).

$$D = 0.001858T^{\frac{3}{2}}\sqrt{\frac{M_t + M_q}{M_t M_q}}\frac{f_D}{p\sigma_{tq}^2\Omega_D} \tag{3.12}$$

where M_t and M_q are the molecular mass of the tracer and the quencher molecules, f_D is the second order correction factor, usually between 1 and 1.03, in the present calculations and p is the total pressure of the gas mixture (in Pa), σ is the Lennard-Jones potential parameter. We have taken f_D=1 in our calculation the factor Ω_D is the collisional integral given by the following equation

$$\Omega_D = \frac{1.06036}{(T^*)^{0.15610}} + \frac{0.1930}{\exp(0.47635T^*)} + \frac{1.03587}{\exp(1.52996T^*)} + \frac{1.76474}{\exp(3.89411T^*)} \tag{3.13}$$

where $T^*=kT/\varepsilon_{tq}$, $\sigma_{tq}=1/2(\sigma_t+\sigma_q)$ *and* $\varepsilon_{tq}=(\varepsilon_t\varepsilon_q)^{1/2}$, subscripts *t* and *q* represent tracer and quencher, respectively. The symbols ε and σ are Lennard-Jones (L-J) parameters, which are the characteristic potential energy and the length of separation between the molecules where the potential is zero, in the well known L-J potential function. L-J potential (or 12-6 potential) is the physical model relating to the potential energy V_{LJ} between the two neutral molecules and the separation *r* between them.

$$V_{LJ} = 4\varepsilon\left[\left(\frac{\sigma}{r}\right)^{12} - \left(\frac{\sigma}{r}\right)^{6}\right] \tag{3.14}$$

L-J parameters were taken from earlier literature. Chapman and Enskog independently developed the theory by solving the Boltzmann equation (Reid, R. C. et al. 1987, Gross, J. et al. 2006).

3.5 Experimental details used to study the LIF quenching in gas phase

Our experimental setup was similar to the one used by Thurber et al. (1998) and Yuen et al. (1997). A Q-switched Nd: YAG Laser (model-LAB190 from Spectra

Physics Inc, Terra Bella Avenue, California, USA.) with a pulse width of 4 ns at 266 nm was used as excitation source. Princeton instruments Acton VM502 Grating monochromator (1200 g/mm), with wavelength resolution 0.1 nm and connected to a PMT, was used to record the LIF signal at specific wavelength. One of the major advantages of Nd: YAG laser for LIF studies is its high energy (few mJ) per pulse at fourth harmonic, which is sufficient to excite the molecules with very weak absorption cross section.

As shown in figure 3.3, a tracer was seeded into a nitrogen carrier gas by purging it through a bath of tracer liquid and directing the vapor mixture into the gas flow cell. The gas flow cell is a cylindrical mild steel chamber of diameter 10 cm and length 30 cm and has two quartz and two BK7 windows of 2.5 cm diameter at the middle of the chamber. The two diametrically opposite quartz windows are used for laser entry and exit.

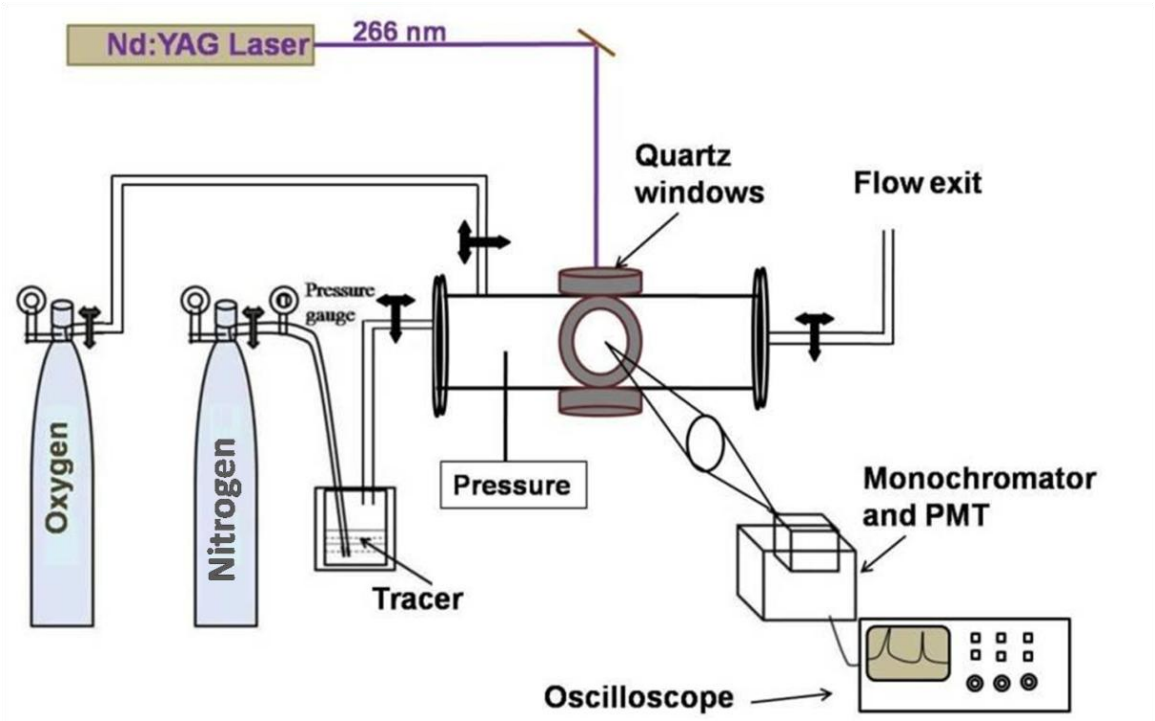

Figure 3.3 Schematic of LIF experimental setup used for gas flow diagnostics.

The other two diametrically opposite BK7 windows, with line-of-sight perpendicular to the laser beam path, were used for recording the LIF signal. Figure

3.4 shows the photograph of gas chamber connected to the monochromator and a pressure gauge.

Figure 3.4 Photograph of the experimental setup (monochromator and the gas chamber).

Digital pressure gauge having a measurement range of 0-2 bar (Huba control DAV-44V) was connected to the flow cell for pressure measurements inside the chamber. For oxygen quenching studies, a controlled amount of oxygen was added to the cell by monitoring the total pressure of the gas chamber.

3.6 Results and discussion on gas cell experiments

In order to study the quantitative effect of oxygen on LIF of ketones (tracer) in gas phase, the following experiments were performed. LIF signals of acetone, methyl ethyl ketone (MEK) and 3-pentanone were recorded at nitrogen bath pressures of 700 torr with varying oxygen partial pressures up to 450 torr. Nitrogen is used as a bath gas in which tracers are added in different quantities according to their vapor pressure at room temperature. The fluorescence emission from acetone and MEK tracers was collected at 435 nm (λ_{max}) (Lozano, A. et al. 1992), whereas, for 3-pentanone the monochromator was set to 420 nm (λ_{max}) (Modica, V.et al. 2007). To verify the linearity of LIF intensity with input laser energy, LIF intensity was plotted as a function of laser energy and the results are shown in figure 3.5. Linear fluorescence

regime was observed for all the three tracers. Therefore, the laser energy was kept at 30 mJ for all the experiments, which is well below the saturation level for LIF signal.

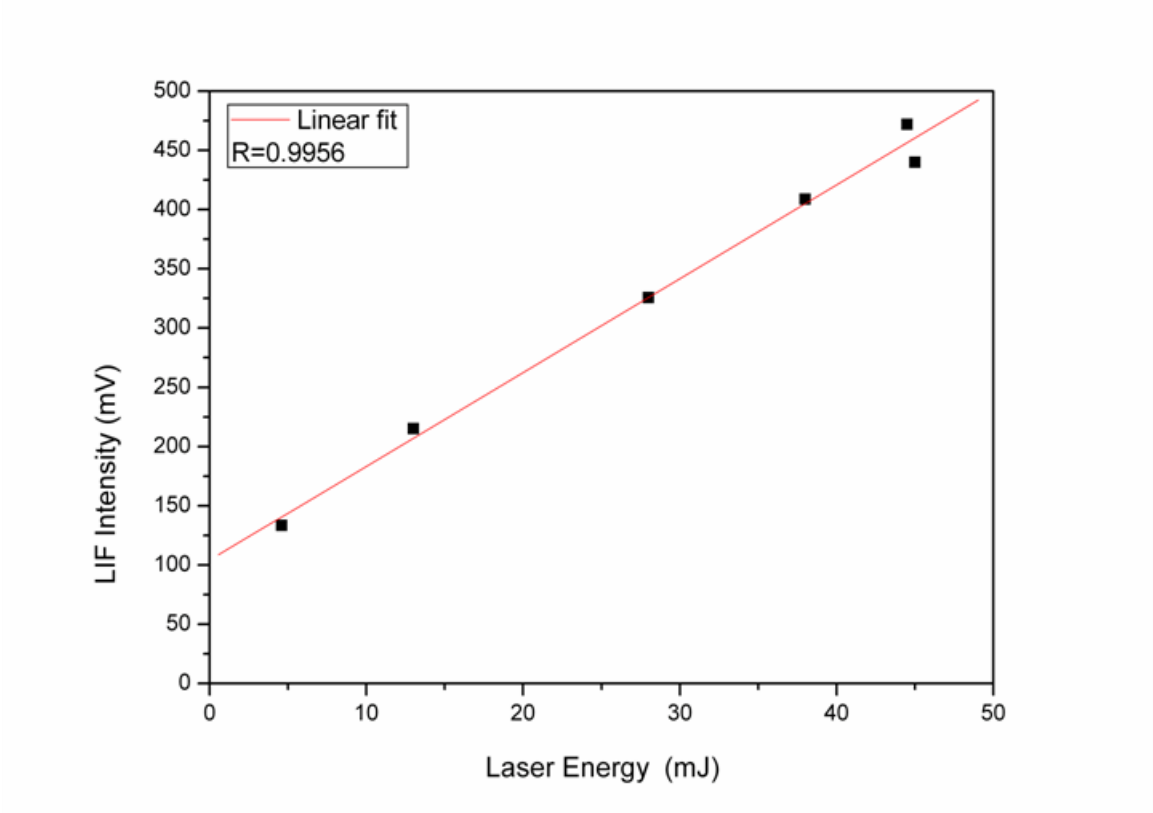

Figure 3.5 The laser energy dependency on the gas phase LIF of acetone at nitrogen bath gas pressure of one bar.

Other tracers used in our experiments also show similar behavior. Figures 3.6, 3.7 and 3.8 are the Stern-Volmer plots (SV plots) for acetone, MEK and 3-Pentanone in nitrogen bath gas, respectively. F and F_0 are the LIF intensity in the presence and in the absence of quencher respectively. The linearity of the SV plot suggests that quenching is collisional in nature and the fluorescence emission originates from the specific fluorophore used as tracer (Lakowiz, J. R. 2006). Any deviation from the linearity is an indication of contribution from other quenching processes, such as excimer or exciplex formation. Excimer is an excited dimer and exciplex is an excited complex formation with more than two species (Thipperudrappa J. et al. 2004). Oxygen quenching of LIF signal shows the linear SV plot for all the tracers.

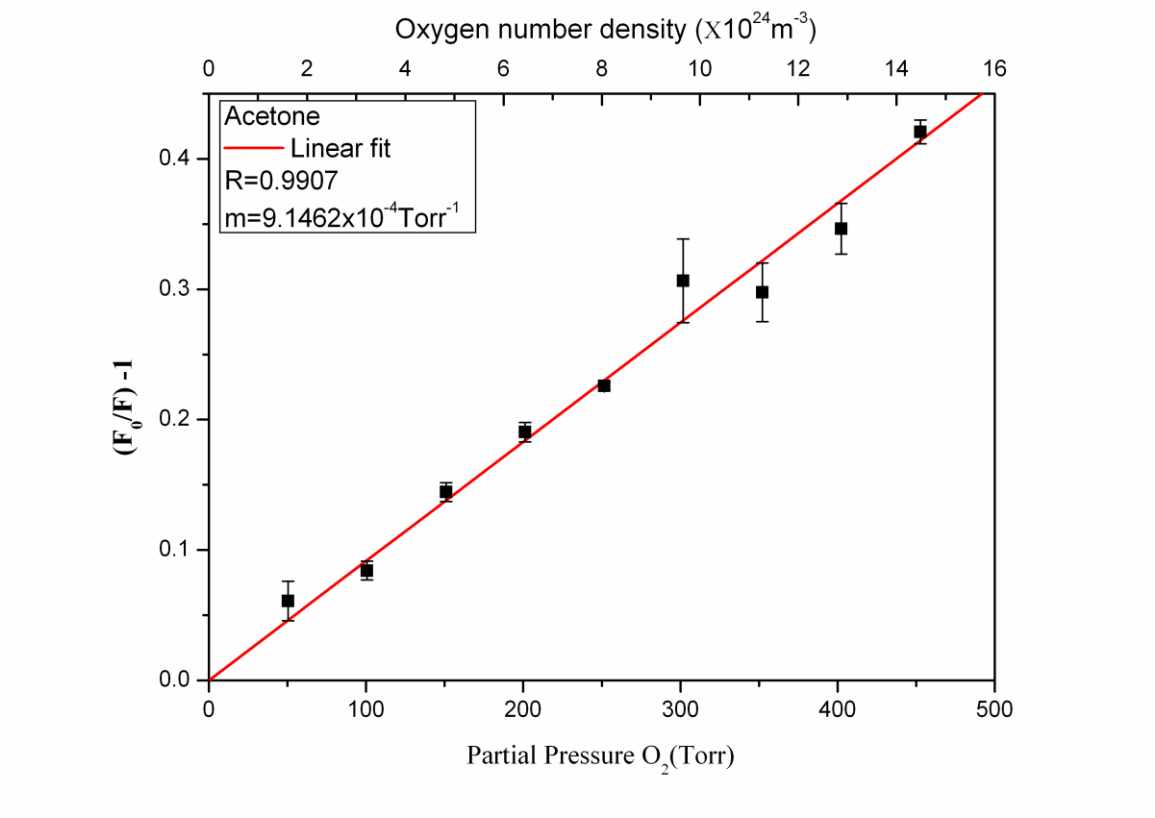

Figure 3.6 Stern-Volmer plot for acetone LIF in nitrogen bath gas at 700 torr pressure.

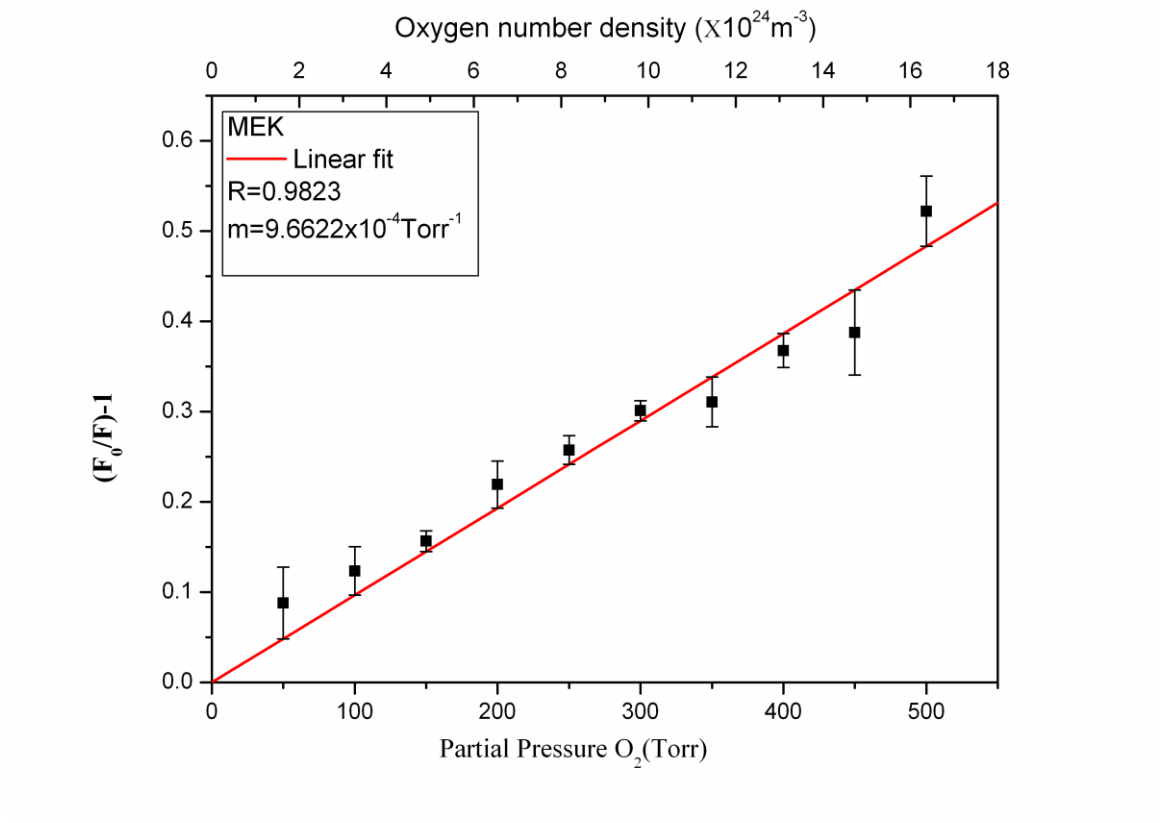

Figure 3.7 Stern-Volmer plot for MEK LIF in nitrogen bath gas at 700 torr pressure.

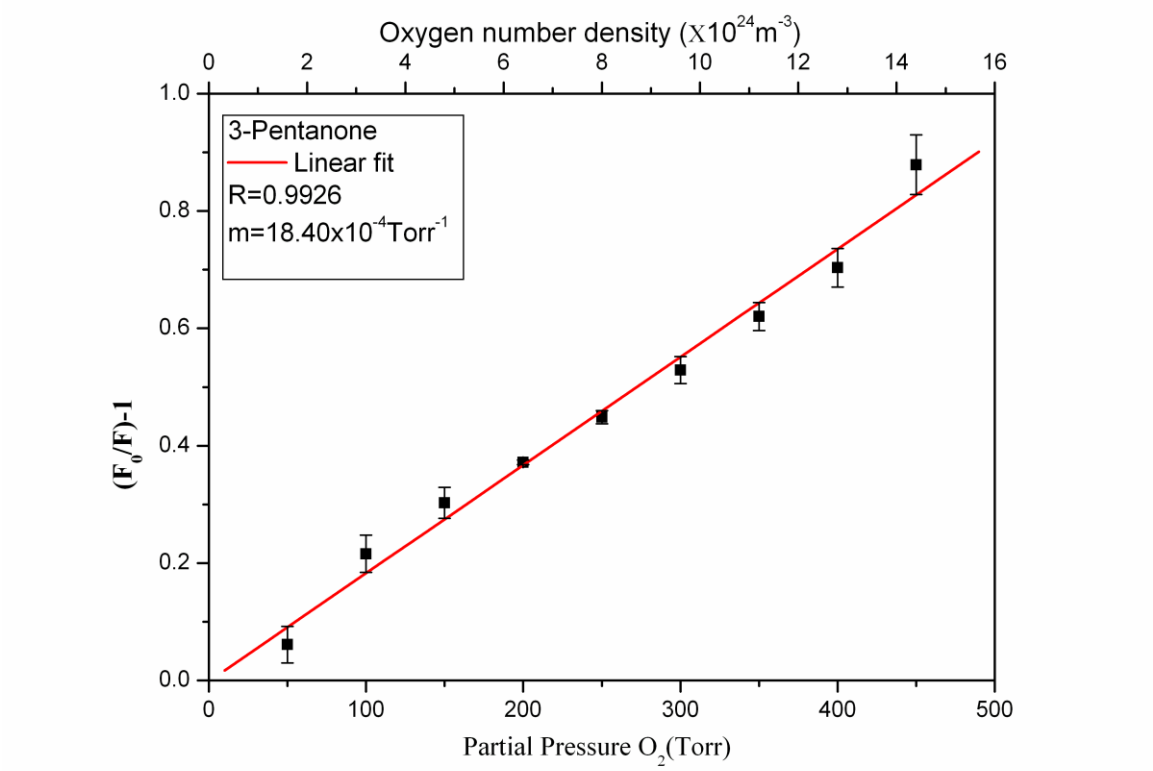

Figure 3.8 Stern-Volmer plot for 3-Pentanone LIF in nitrogen bath gas at 700 torr pressure.

From the Stern-Volmer plots SV coefficients k_{sv} and quenching rate constant k_q were calculated for the tracers under study and are given in Table 3.1. To calculate the quenching rate constant, the life time of the excited state was taken from previous literature (Nau, W. M. and Scaiano, J. C. 1996, O'Sullivan, M. and Testa, A. C. 1970).

Table 3.1 SV coefficients and oxygen quenching rate constants for the ketones under the study.

Tracers	Chemical formula	$k_{sv}(10^{-4}\text{Torr}^{-1})$	$k_{sv}(\text{Lmol}^{-1})$	τ(ns)	$k_q(10^9\text{LM}^{-1}\text{s}^{-1})$
Acetone	CH_3-CO-CH_3	9.1462	17.104	1.95[a]	8.7711
MEK	CH_3-CO-C_2H_5	9.6622	18.069	2.9[b]	6.2306
3-pentanone	C_2H_5-CO-C_2H_5	18.400	34.409	3.2[b]	10.753

[a]Reference Nau ,W. M. and Scaiano, J. C1996, [b]Reference O'Sullivan, M. and Testa, A. C. 1970;

Molecular oxygen is found to be an efficient fluorescence quencher due to its ground triplet state ($^3\Sigma_g^-$) and the two low lying singlet states ($^1\Delta_g$ and $^1\Sigma_g^+$). Oxygen quenching of fluorescence from organic molecules is possible by electronic transition from triplet ground state to any of these two low lying singlet states of oxygen. Electronic energy transfer equations between the excited molecule M* and the oxygen quencher can be written as (Schulz, C. and Sick, V. 2005, Valeur, B. 2001):

$$^1M^* + {}^3O_2(^3\Sigma_g^-) \rightarrow {}^1M + {}^1O_2(^1\Delta_g)$$

or (3.15)

$$^3M^* + {}^3O_2(^3\Sigma_g^-) \rightarrow {}^3M + {}^1O_2(^1\Delta_g)$$

Formation of excited state complex (exciplex, M^*O_2) may also influence the quenching. However, this requires that the energy difference between the singlet and triplet states of the tracer should be greater than 0.98 eV, the lowest singlet excitation energy of oxygen molecule. Hence, this process is less likely in the case of ketones than for aromatic molecules (Koch, J. D. et al. 2003). Thus, the influence of oxygen may be attributed to the collisional quenching. The quenching rate constants k_q [O_2] is the measure of the capability of oxygen to quench LIF. Our measurements yielded

quenching constant k_q of the order of 10^9 $Lmol^{-1}s^{-1}$. Similar results were observed in liquid phase by other researchers. Further, quenching rate constants for acetone and MEK were found to be low and comparable, whereas that for 3-pentanone was relatively high. This may be attributed to the photo physical similarity of acetone and MEK compared to 3-pentanone. Long lifetime of the excited state may also contribute to higher oxygen quenching sensitivity (Valeur, B. 2001).

Oxygen quenching observed here is collisional in nature and, hence, is controlled by diffusion process. Thus, the values of SV factors and quenching rate constants indicate that the effect of oxygen on LIF of acetone and MEK is expected to be relatively low (Koban, W. et al. 2005). This may be attributed to the faster vibrational relaxation as compared to intersystem crossing (Thurber, M. C. and Hanson, R. K. 1999). For diffusion controlled quenching, the theoretical approach explained in section 3.4 of this thesis is used to calculate the diffusion rate constant.

The experimentally determined values and the theoretically calculated values of SV coefficient and quenching rate are tabulated in Table 3.2.

Table 3.2 Experimental results and theoretically calculated SV coefficients and oxygen quenching rate constants.

	Experimental		Calculated from the model			
	k_{sv}	k_q	k_{sv}^a	k_q^a	k_{sv}^b	k_q^b
Tracers	(L mol^{-1})	(10^9LM^{-1}s^{-1})	(L mol^{-1})	(10^9LM^{-1}s^{-1})	(L mol^{-1})	(10^9LM^{-1}s^{-1})
Acetone	17.104	8.7711	1.1989	0.6148	14.939	7.6608
MEK	18.069	6.2306	1.8272	0.6300	21.743	7.4976
3-pentanone	34.409	10.753	2.0606	0.6439	23.900	7.4800

[a]Stokes-Einstein relation (equation 3.11), [b]Using Chapman and Enskog relation (equation 3.12);

Figure 3.9 and 3.10 show the correlation between the experimental and theoretical estimates of k_{sv} and k_q by using Chapman and Enskog relation. The estimates using Stokes-Einstein diffusion relation are seen to deviate significantly from the experimental values. This may be due to the underestimation of diffusion coefficient for small molecules as observed by other researchers (Arik, M. et al 2005).The k_q and k_{sv} values calculated using Chapman-Enskog relation are comparable with the experimentally estimated values. This may be due to the fact that Chapman-Enskog relation takes into account physical properties such as total pressure of the gas mixture.

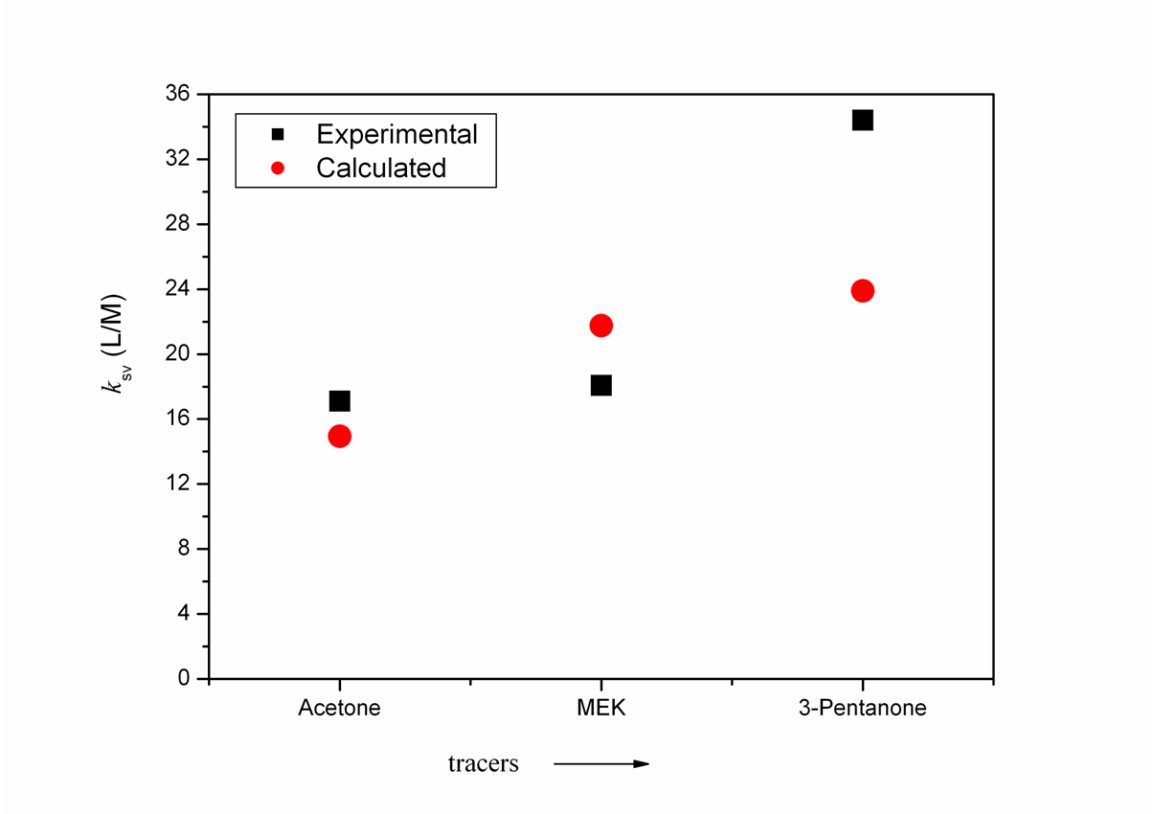

Figure 3.9 Comparison of experimentally determined and theoretically calculated (using Chapman-Enskog relation) values of SV coefficient (k_{sv}) for all the three tracers.

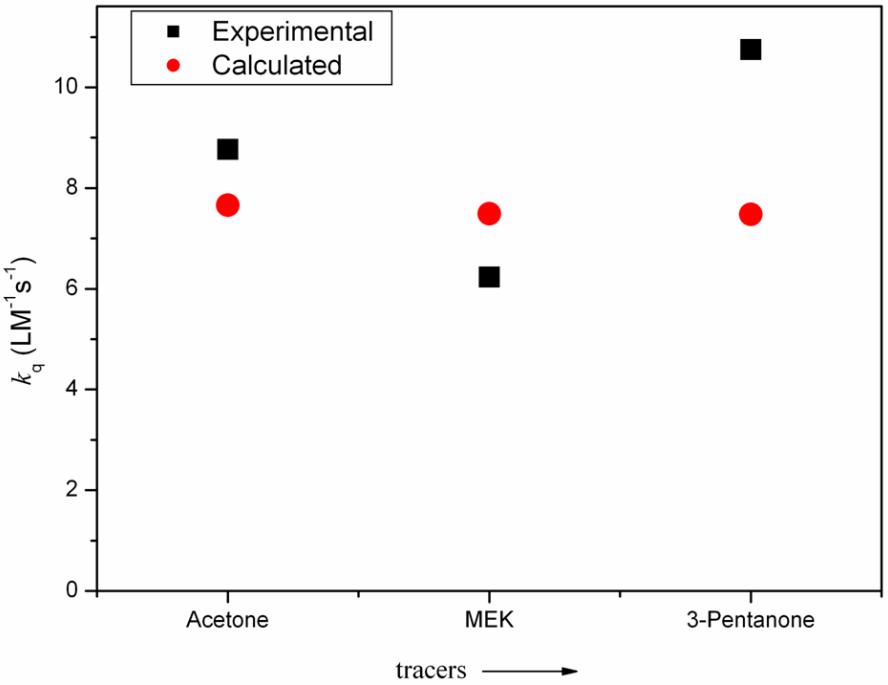

Figure 3.10 Comparison of experimentally determined and theoretically calculated (using Chapman-Enskog relation) values of quenching rate (k_q) for all the three tracers.

The correlations between experimental and theoretical values are observed to be quite good for the three tracers used in our experiments. The slightly larger deviation seen in the case of 3-pentanone is ascribed to its longer fluorescence lifetime compared to that of the other two tracers.

These results are published in "Spectroscopy Letters" (2013) 47(1), 12-18. (DOI:10.1080/00387010.2013.775463).

3.7 Conclusions

The quenching of LIF signal from the ketone tracers by molecular oxygen in nitrogen bath gas has been investigated for oxygen partial pressure varying from 0 to 450 torr. The fluorescence quenching is seen to be dominated by collisional process. From the SV coefficients and quenching rate constants, the effect of molecular oxygen was

found to be relatively low in case of acetone and MEK compared to 3-pentanone. This shows that, despite their low quantum yields compared to 3-pentanone these tracers can be effectively used for the gas flow studies which contain trace amount of oxygen at atmospheric pressures. Further, Smoluchowski theory was used to calculate the quenching rate and compared with the experimental results. It is found that the estimation of quenching rate by using Stokes - Einstein diffusion relation deviates significantly from the experimental results. This is due to the under estimation of diffusion coefficient. The results obtained by using Chapman-Enskog relation are seen to be comparable with the experimental quenching rates. The deviation in case of 3-pentanone is attributed to its long fluorescence life time. The present study on the effect of oxygen quenching on LIF intensity in the presence of tracers is very useful in understanding the chemistry of high speed flows generated in shock tunnels.

CHAPTER 4

SUBSONIC JET FLOW VISUALIZATION USING PLIF

4.1 Introduction

The most general application of planar laser induced fluorescence (PLIF) in aerodynamics is, for the measurement of spatial and temporal scalar structures in flowing gases at subsonic and supersonic velocities. PLIF images of short time-scale spatial structures can be obtained by ensuring that the image integration time is short compared to advective and straining timescales (Schulz et al. 2005). PLIF is widely used in such studies, due to its smaller time scales of the order of nanoseconds (Crimaldi, J. P. 2008). During the last century several major investigations were carried out to understand the turbulent flow field and fluid mixing. Quantitative planar imaging of density distribution in fluid flow is very important in understanding the physics of turbulent processes. In turn understanding of turbulent flow is of great importance due to its natural occurrence in many science and engineering applications. These applications include aerodynamics, fluid mixing, combustion, chemical reaction and jet noise generation in aerodynamics. Dimotakis, P. E. et al. (1983, 2005) studied turbulence in water jets employing PLIF of Rhodamine 6G and observed large scale vortices which are axisymmetric and spiral in nature. Based on these experimental results, the mixing and turbulence was explained. Similar structures were observed in the simulations of Siddhartha et al. (2000).

Gas jet flow visualization has several applications in fluid dynamics, such as design of civil and military aircrafts and combustion research. There are several methods used for visualization of low speed jets such as shadowgraphy, smoke flow visualization, LIF and absorption spectroscopy. Among various methods used for low speed jets, smoke flow visualization is very popular and frequently used due to its experimental simplicity. Only qualitative imaging is possible with the smoke flow visualization and shadowgraphy. A gas-jet is a highly dynamical system and hence has to be studied by fast visualization techniques providing high spatial and temporal

resolution. PLIF is a very attractive technique in such cases due to the fact that the fluorescence life time of the tracers discussed earlier (Chapter 3) lies in the order of nanoseconds (Acetone 2 ns). The major problem of tracer and fluid mixing in many flow visualization techniques such smoke flow visualization can be eliminated completely by PLIF technique, with the use of molecular tracers (Desevaux, P. 2001).

Among various tracers used, ketones are very popular organic carbonyls. Acetone is frequently used because of its high vapor pressure, low boiling point (56°c) and good fluorescence properties. Its absorption cross section extends from 225-320 nm. Acetone PLIF is well known in the literature for subsonic jets (Lozano, A. et al. 1992). Löffler et al. (2010) studied acetone LIF in internal combustion engine and reported the calibration data for quantitative measurement of temperature and pressure. Apart from structural similarity, Methyl ethyl ketone (MEK) possesses almost same physical and photo-physical properties as acetone. Table 4.1 shows the similarity between the acetone and MEK.

Table 4.1 The properties of acetone and MEK tracers relevant to PLIF.

Tracers	**Chemical formula**	**Boiling point (^oC)**	**Vapor pressure at 20^oC (mm of Hg)**	**Absorption wavelength (λ_{abs} /nm)**	**Fluorescence wavelength (λ_{fl}/nm)**
Acetone	$(CH_3(CO)CH_3)$	56.1	180	~225-320	~320-550
MEK	$(CH_3(CO)CH_2CH_3)$	80	100	~220-330	~350-550

In spite of these similarities of MEK with acetone relevant to PLIF, MEK is very rarely used in these experiments. This could be because of easy availability and relatively lower toxicity of acetone. In the present thesis, we have investigated fluorescence of MEK when excited by the fourth harmonic of Nd: YAG laser (266 nm).The dependence of PLIF intensity on MEK vapor density was used to obtain quantitative density profile in nitrogen jet. Coherent structures were observed in the

number density images of acetone seeded gas flow. Further, the effect of oxygen on acetone and MEK PLIF images were studied using 5 mm exit jet by using air as a bath gas instead of nitrogen and compared with it.

4.2 Structure of subsonic axisymmetric jet

In a recent review by Ball et al. (2012), turbulence from cylindrical free jetwas explained and several unanswered questions were also discussed. Most of the turbulent flow from jet contains both coherent structures and incoherent turbulence, but the former are more significant. It is well known that major contribution to mass, momentum and heat transfer is due to coherent structures. One of the reasons for the formation of these structures is localized instabilities in the flow. Understanding of these structures is also important to solve the major problem of aerodynamic noise generation (Fazle Hussein, A. K. M. 1986). Interaction among these coherent structures is not yet fully understood.

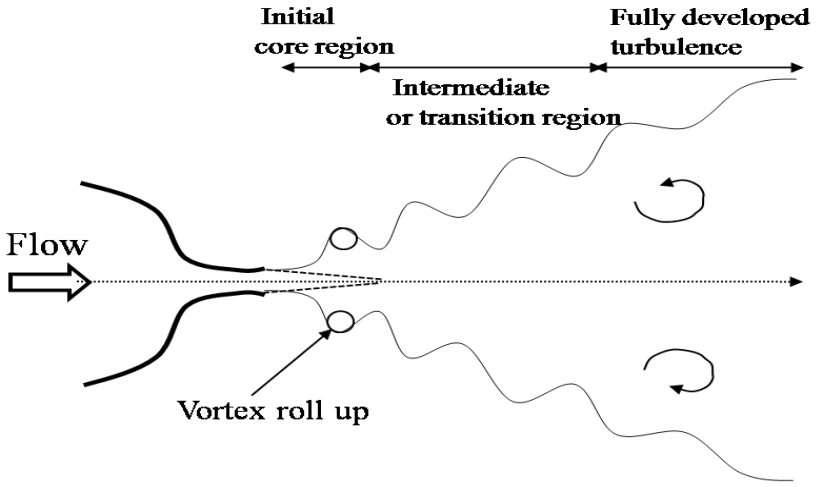

Figure 4.1 Schematic of free turbulent axisymmetric jet (Ball, C. G. et al. 2012).

Three regions in the turbulent cylindrical free jet were previously identified and those include near field region ($0 \leq x/D \leq 6$), intermediate ($6 \leq x/D \leq 30$) and far field region ($x/D \geq 30$) as shown in figure 4.1. Near field region or initial core region contains a potential core in which flow features are very similar to that at the exit of the nozzle. Both near and intermediate field regions are significant, since the growth

of these regions affects the entire characteristics in the downstream of the jet. Far field region is also called self-similarity region, and forms wholly developed turbulent region (Ball, C. G. et al. 2012). Agarwal and Prasad (2002) have found coherent structures even in self similarity regions. Thus, regions close to the intermediate field have to be understood completely for applications like turbulence control, mixing and entrainment. These regions are important in several engineering applications (Fiedler, H. E. 1998). Early studies on subsonic jet were mainly focused on far field region or self-similar turbulent region of the jet. However this trend has changed in recent years because of the advancement of the diagnostic tools in the investigation of subsonic flows.

4.3 Theoretical consideration for image conversion

The basis for number density measurement is linear dependency of LIF intensity on number density of the fluorescing tracer. For the molecules with broadband spectral absorption, fluorescence with laser excitation can be modeled as in Eq. (4.1). For excitation using low energy laser (linear excitation regime well below saturation) the fluorescence intensity S_f is given by the following equation

$$S_f \propto n_{abc}(P,T)\sigma(\lambda,T)\Phi(\lambda,T,n_i) \tag{4.1}$$

where n_{abs} is number density (cm^{-3}), σ is molecular absorption cross section of exciting species (cm^2/molecule), Φ is fluorescence quantum yield. Molecular absorption cross section is constant for the given excitation wavelength at ambient temperature. The fluorescence quantum yield is found to vary from 0.4 to 0.6 within the pressure range employed in the present study and also in investigations reported by previous researchers (Thurber, M. C. et al. 2001).

$$S_f = Cn_{abs}(P,T) \tag{4.2}$$

Equation 4.2 is the basis for the density imaging and C accounts for all the constants including laser energy and other experimental settings. Local Reynolds

number of the jet at the exit is given by the following equation (Dimotakis, P. E. 2000)

$$\mathrm{Re} = \frac{\rho U d}{\mu} = \frac{U d}{\upsilon} \tag{4.3}$$

where, $\rho$is the gas density (kg/m^3), $\mu$is absolute viscosity (Pa. S), $\nu=\mu/\rho$is kinematic viscosity (m^2/s) of the gas. U is the exit velocity (m/s) and d is the exit diameter (m) of the jet.

4.4 Experimental technique

4.4.1 PLIF experimental set up

PLIF measurement setup used is similar to the one used by Tseng et al. (2009), Pitz et al. (2008), Stevens et al. (2007) and Rossmann et al. (2001). Figure 4.2 shows experimental setup for PLIF imaging technique. In this setup, laser beam of 266 nm wavelength from Nd: YAG laser is transformed into a planar sheet using a cylindrical lens. Cylindrical plano-convex lens (width 2 cm, length 5 cm) of focal length 5 cm, in combination with a spherical plano-convex lens of focal length 70 cm can transform 4 mm diameter laser beam into a planar sheet of width 5 cm and thickness 15 μm. The resulting fluorescence image was captured on a Sony digital camera (Model-HDR-550XR) with CMOS sensor. In this case, a plane jet with exit diameter 2 mm was used to establish subsonic flow.

The normalized centerline velocity profile of the jet is shown in the figure4.3 as measured by the Pitot tube (with a maximum of 22.4 m/s) (Liepmann, H. W. and Roshko, A.1957). For LIF dependency studies and calibration, the gas cell described in section 3.6 was used. The two diametrically opposite quartz windows were used for entry and exit of laser sheet**.**

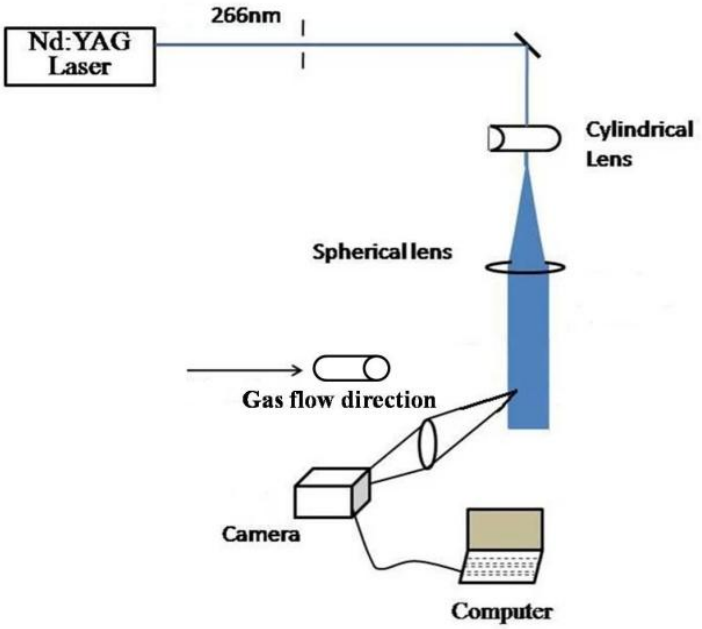

Figure 4.2 Schematic of PLIF experimental setup for gas flow visualization and mixing studies.

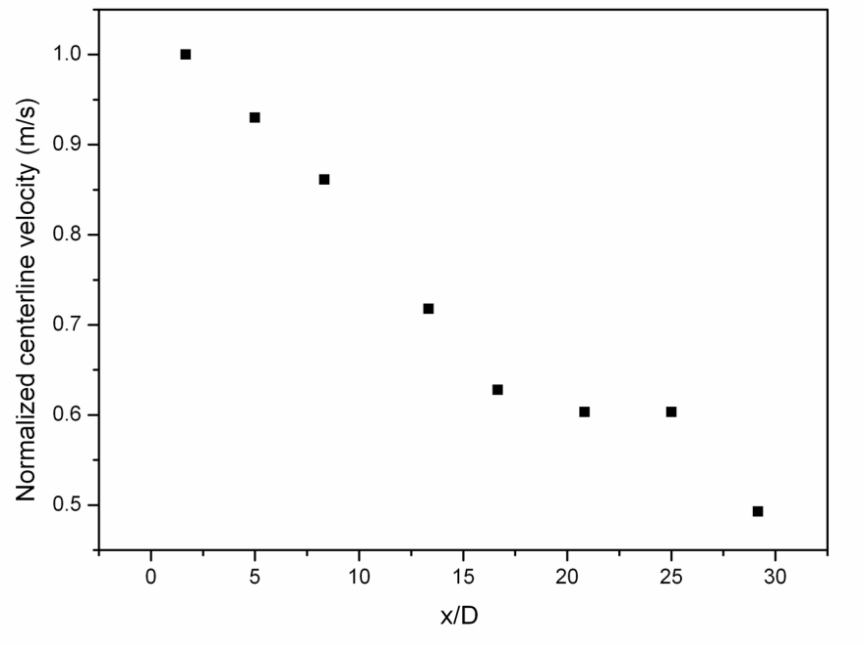

Figure 4.3 Normalized centerline exit velocity profile from the jet.

Typical PLIF images recorded are shown in figure 4.4 and 4.5. The PLIF raw images obtained on digital CCD/CMOS sensor usually have many imperfections in image acquisition systems, for example defective pixels, low light or uneven illumination etc. Thus there is need for image processing to correct for such a defects and increase the contrast of the image (Acharya, T. and Ray, R. K. 2005, Solomon, C. and Breckon, T. 2011). Figures 4.4(a) and 4.5(a) shows the PLIF images of acetone and MEK seeded jets, respectively, as captured by the camera. Several horizontal lines and defects are clearly observed in these images, this may be due to the uneven illumination. The processed images are shown in the following figures 4.4(b) and 4.5(b).

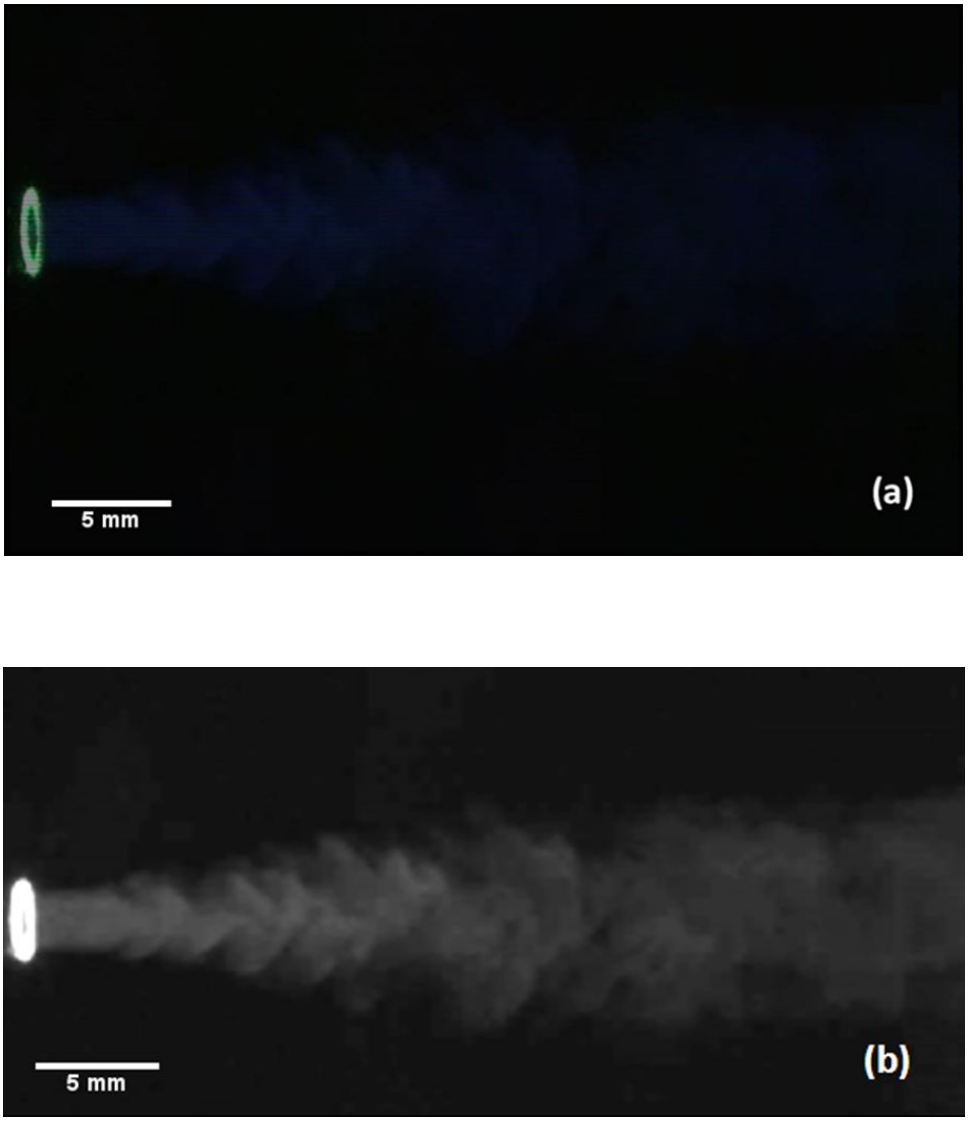

Figure 4.4 a) The Raw acetone PLIF image as obtained from the camera. b) Gray scale image of the flow processed using MATLAB code.

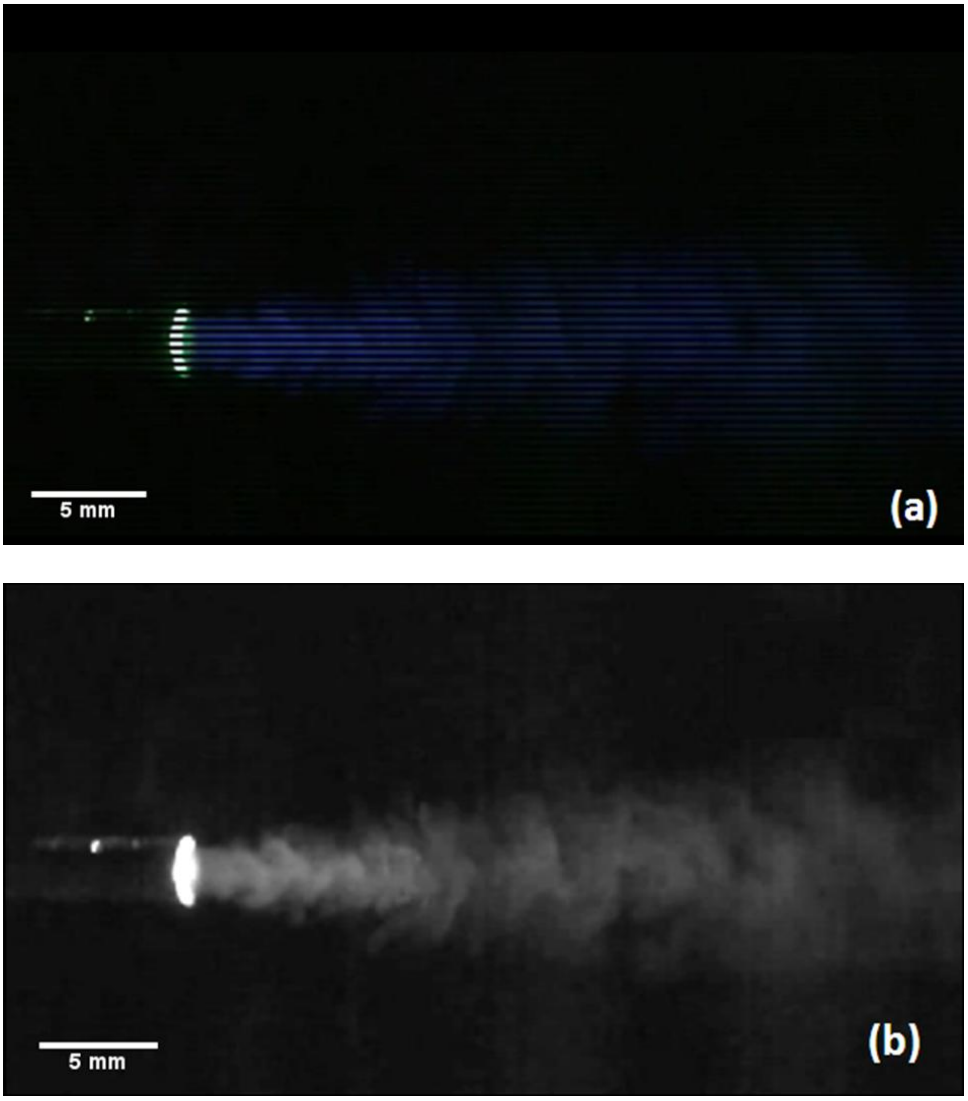

Figure 4.5 a) The Raw MEK PLIF image as obtained from the camera. b)Gray scale image of the flow processed using MATLAB code.

The image processing was carried out using MATLAB code given in Appendix II. Initially the defected pixel values were identified by sudden decrease in the intensity value and compensated by averaging. The next step involves smoothing the image by convolving with a Gaussian filter(Young, I. T. et al. 1995). The Gaussian filter in vertical and horizontal direction makes use of two dimensional Gaussian functions given by the following equation 4.4.

$$G(x, y) = \frac{1}{2\pi\sigma^2} e^{\frac{x^2+y^2}{2\sigma^2}} \qquad (4.4)$$

In this equation there are two free parameters which can be varied, namely the size of the discrete kernel and the value of σ, the standard deviation of the Gaussian function. The value of σ was varied from 0.1:0.1:1 and it was found that σ =1 and Kernel size 6X6 gives higher pixel intensity and better image quality. Thus Kernel size was taken as 6X6 and the value σ was kept 1 for the all processed images.

4.5 Acetone seeded jet

Analysis of acetone seeded PLIF image of the gas flow for Reynolds number Re equal to 2-3x10^3 shows arrow-head shaped coherent turbulent structures (Fig.4.6). These structures are present even at lower Reynolds number.

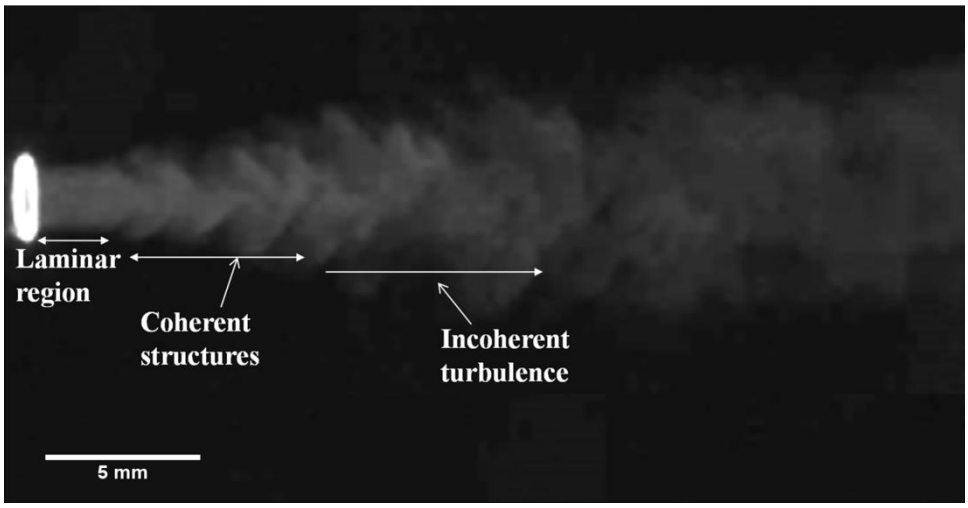

Figure 4.6 Gas phase acetone PLIF image for Re ≈ 2-3 X10^3.

The coherent structures are seen to be non-overlapping, with separate boundaries, as is evident from figure 4.6. Coherent structures are responsible for energy transfer in the turbulent downstream region of the jet. There is a clear distinction between laminar region, coherent structures and turbulent region within coherent instabilities. Similar coherent structures were observed in the Direct Numerical Solution (DNS) simulations reported by Siddhartha et al. (2000).

For Acetone LIF intensity calibration, the gas cell, described in the experimental section and shown in the figure 4.7(a), was used. Initially the gas cell was evacuated using a rotary pump and then acetone was leaked into it at the required partial pressure. The PLIF images were obtained for different partial pressures of acetone upto180 torr. A sample of the images recorded at 160 torr is shown in the

figure 4.7(b); such an image was used for calibration purposes. Figure 4.8 shows the calibration plot for converting gray scale intensity into density image.

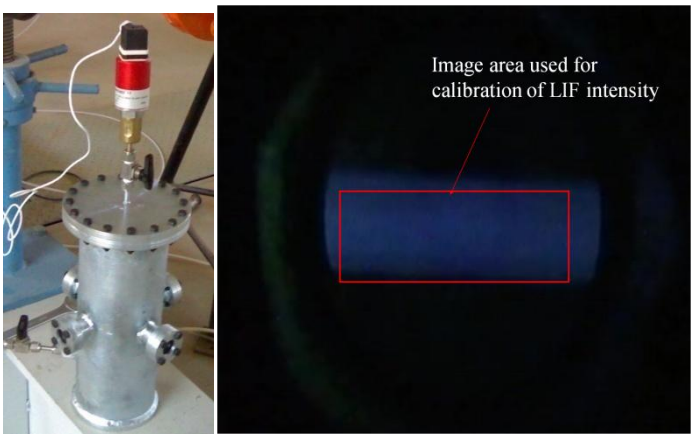

(a) **(b)**

Figure 4.7 a) Gas Cell with filling pressure range from 0 to 20 bar. b) PLIF image for acetone partial pressure of 160 torr inside the chamber.

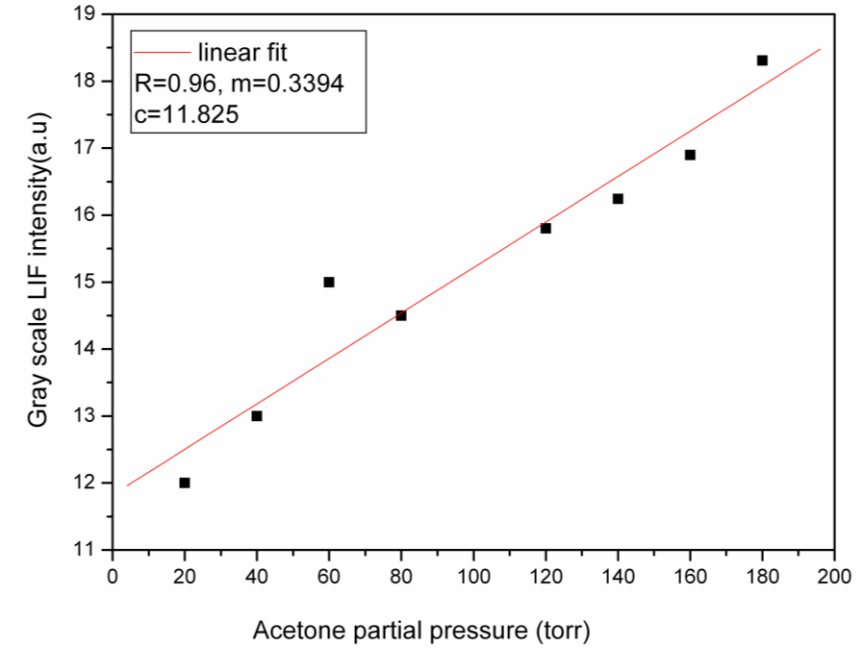

Figure 4.8 Gray scale PLIF intensity, averaged over the image area, as a function of acetone partial pressure in the gas cell.

Figure 4.9(a) and 4.9(b) show partial pressure and molecular number density images, respectively, for the intensity image shown in Fig.4.6. From these images it is clear that, acetone seeded in the flow behaves similar to the bath gas. The number density distribution and the main stream intensity images of the jet are alike. This method can be employed for understanding mixing of gases and boundary layer studies in subsonic jets. Further, analyzing these images, we observe that acetone molecular number density distribution varies in the cross section of the flow. The number density is large in the middle of the laminar region and gradually decreases towards the outer edge. On the other hand, in the coherent and incoherent turbulent regions, the distribution is more non uniform indicating the effect of centerline velocity. Velocity along the center of the jet is called centerline velocity. Near the nozzle exit and along the central portion of the jet, a region with an almost uniform mean velocity is called the potential core.

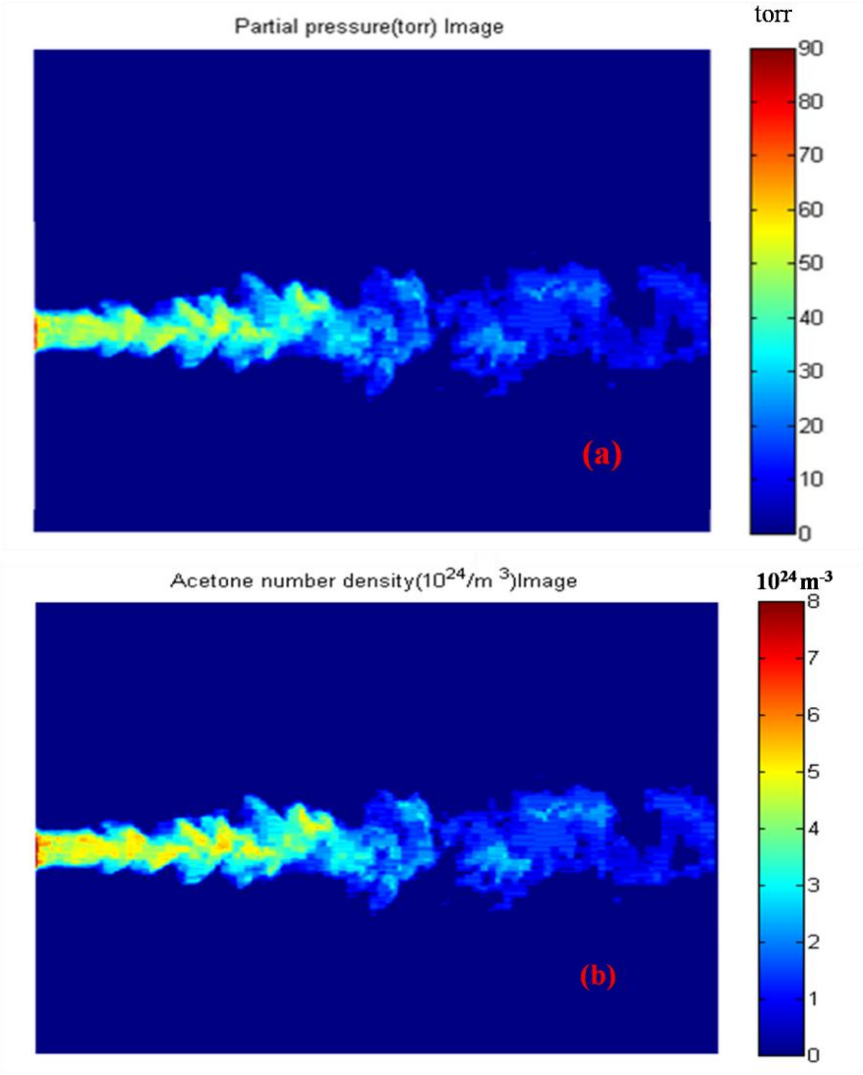

Figure 4.9 Image of nitrogen gas jet seeded with acetone, showing (a) partial pressure and (b) molecular number density (x10^{24} m^{-3}).

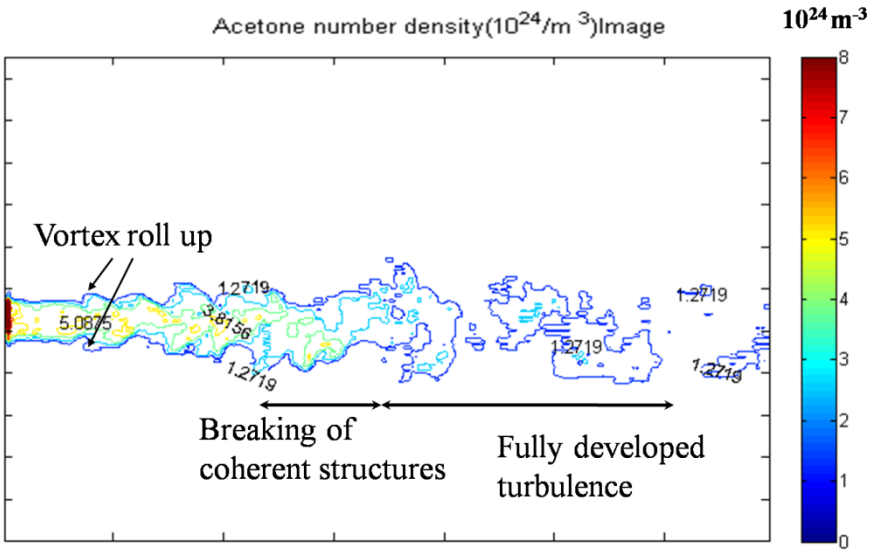

Figure 4.10 The acetone number density contour image of the jet shown in Fig. 4.9.

Figure 4.10 shows the number density contour map of the PLIF image shown in Fig. 4.9. We can clearly see the breaking of large coherent structures into incoherent structures. Initial vortex formation was clearly observed, whereas vortex pairing was not unambiguously observed in the images recorded. Coherent structures are seen to break-up and evolve into fully developed turbulence.

4.6 MEK seeded jet

As mentioned earlier, MEK has been used very rarely compared to acetone in PLIF experiments. For obtaining the molecular density imaging of MEK, the measurement of MEK fluorescence, excited by fourth harmonic of Nd:YAG laser, was used. A quantitative planar image of density distribution in fluid flow is important for a good understanding of the physics of turbulent processes.

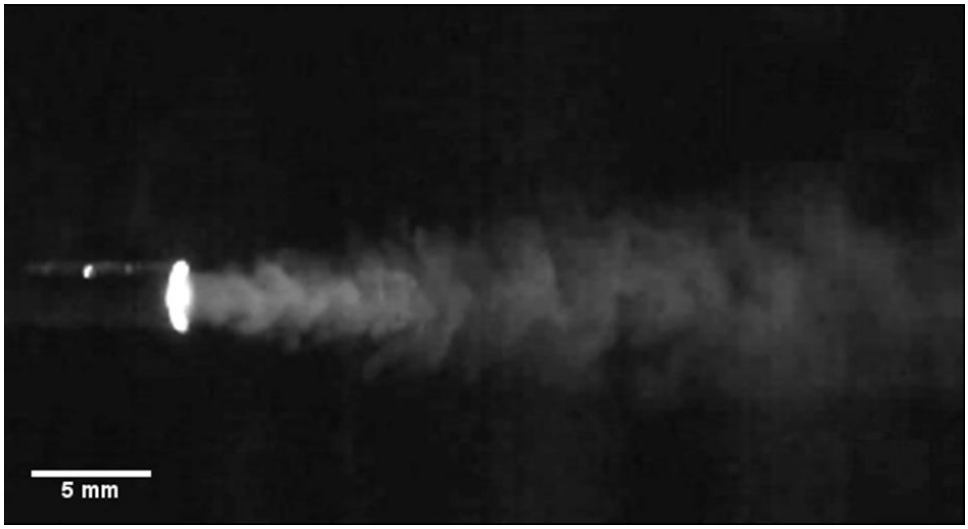

Figure 4.11 The gas phase MEK PLIF gray scale image of nitrogen jet purged through liquid MEK.

Initially the gas cell, described in the experimental section, was evacuated using rotary vacuum pump and MEK vapor was leaked into the gas cell at a vapor pressure ranging from 10 torr to 90 torr. The PLIF gray scale intensity image recorded is shown in Figure 4.11. Figure 4.12 shows the calibration plot used for converting gray scale intensity image into molecular number density image.

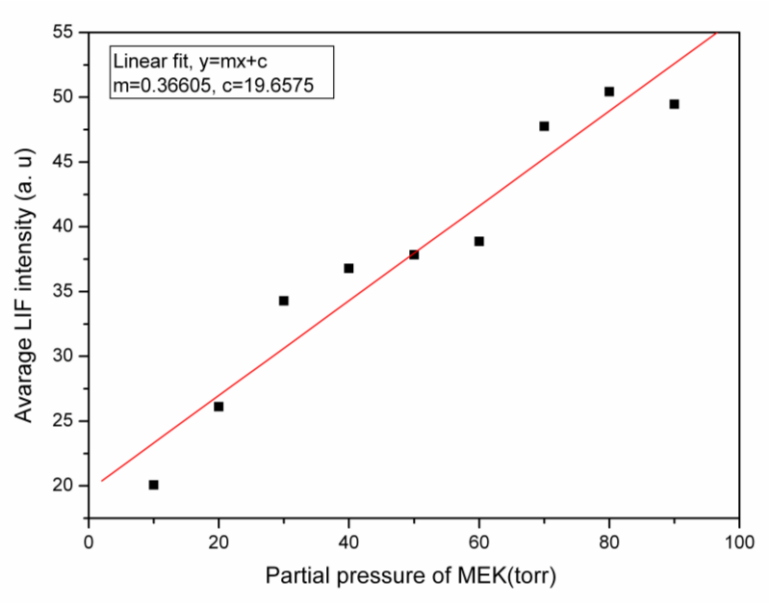

Figure 4.12 Gray scale LIF intensity averaged over image area as a function of MEK partial pressure.

Based on the linear dependence of the concentration on partial pressure, the PLIF intensity image was successfully converted to density image using equation 4.2. Figure 4.13 shows number density profile for the same intensity image as in figure 4.11.

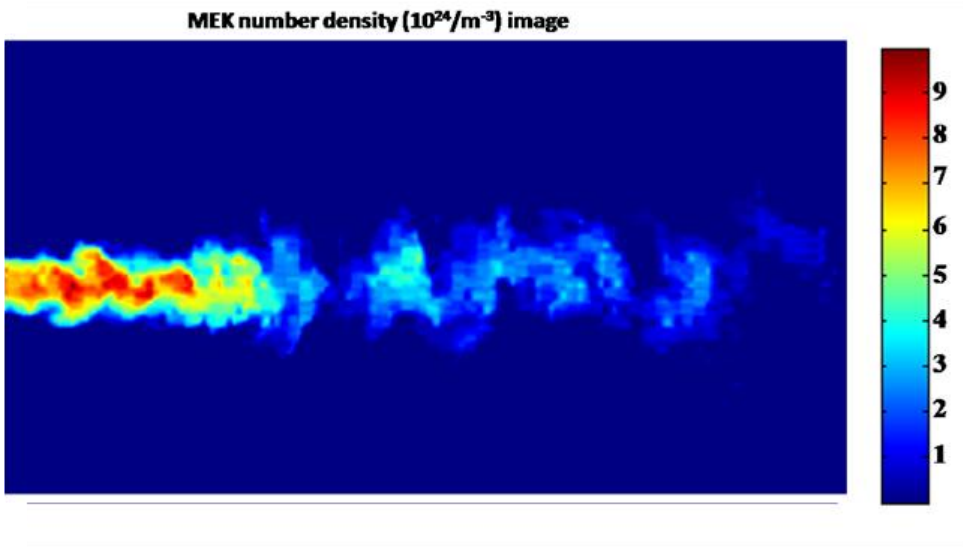

Figure 4.13 The MEK molecular number density (x10^{24} m^{-3}) image in nitrogen jet.

In this experiment we clearly observed the formation of large paired eddies. These coherent structures break up and form smaller eddies, which develop into turbulent structures of smaller length scales.

To understand the length scales of the coherent structures further downstream from the nozzle, cross sectional images were obtained and are displayed in Figure 4.14. These density images at various x/D values were obtained by assuming axisymmetric jet. Breaking of large scale vortices was clearly observed above four jet width. Analysis of the images shows that high intensity modes are present at x/D=1, 4, 7 confirming formation of coherent structures at definite spatial frequencies present in the flow at 3x/D ((FazleHussain, A.K.M. 1986,Abdel-Rahman, A. 2010, Agrawal, A. et al. 2002).

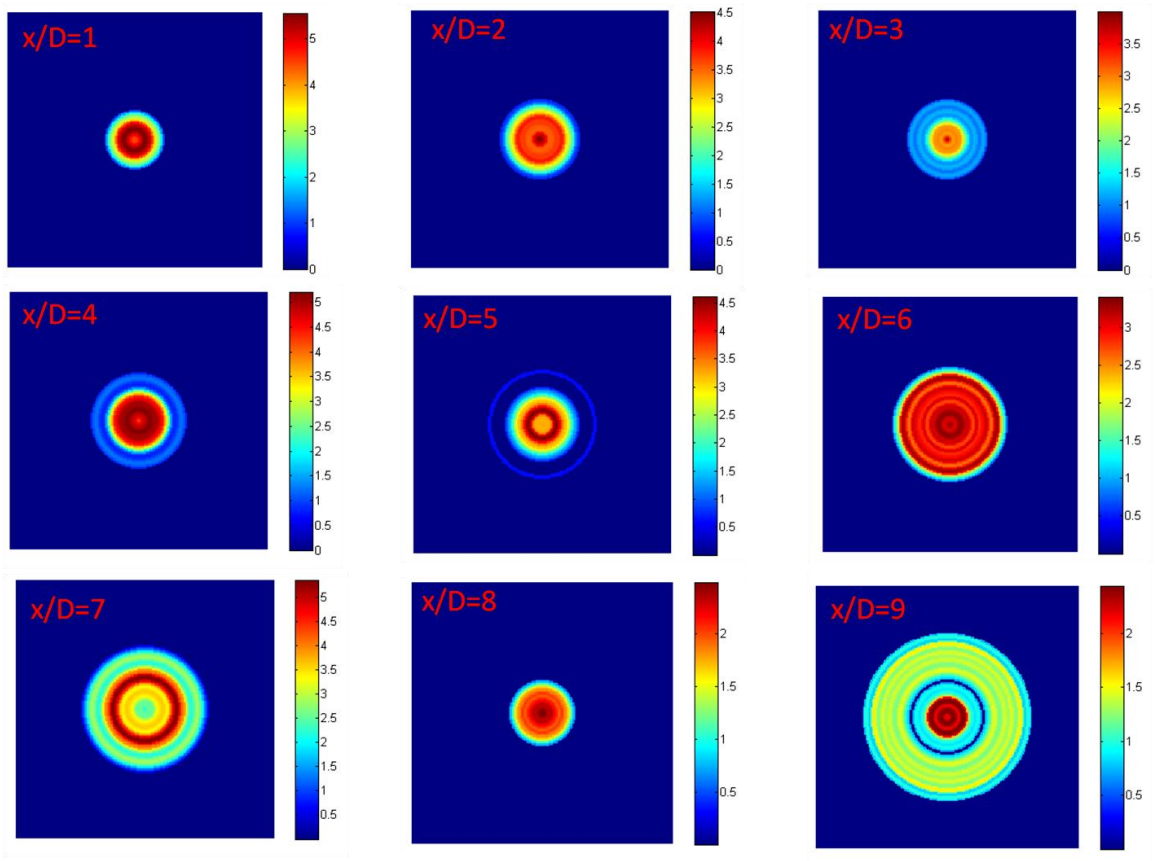

Figure 4.14 The cross section images of the nitrogen jet at various x/D by assuming axisymmetric gas jet.

4.7 Effect of oxygen on acetone PLIF

As mentioned in the previous chapter, the SV coefficient values indicate that quenching of the fluorescence emission is dominated by collisional processes. In order to examine the effect of oxygen for practical problems, the flow image recorded with nitrogen is compared with that with air as bath gases. For this purpose a convergent nozzle of exit diameter 5 mm, shown in the figure 4.15, was used. All other experimental parameters were kept the same as in the experiments described earlier in this chapter.

Figure 4.15 The convergent axisymmetric nozzle.

Initially acetone is seeded into nitrogen and then the gas is directed through the nozzle into ambient atmosphere. The gray scale image captured using the CMOS camera is shown in the figure 4.16. The image intensity is found to be much lower compared to 2 mm jet experiments. This is because of lower tracer concentration in this experiment.

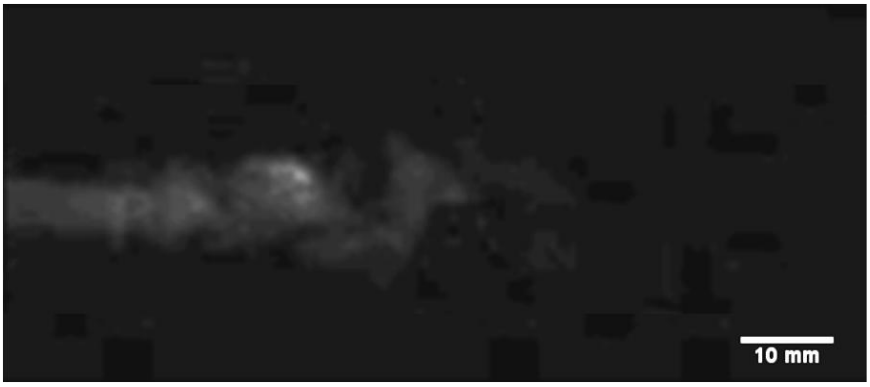

Figure 4.16 PLIF image of acetone seeded in nitrogen jet released into ambient atmosphere.

Further, to demonstrate the effect of oxygen, nitrogen is replaced by 99 % compressed air purged through liquid acetone and guided by the nozzle into the ambient atmosphere. In this case also the image intensity was very low as shown in the figure 4.17. Comparing both the images, it is seen that the gray scale intensity is almost same for both nitrogen and air jets.

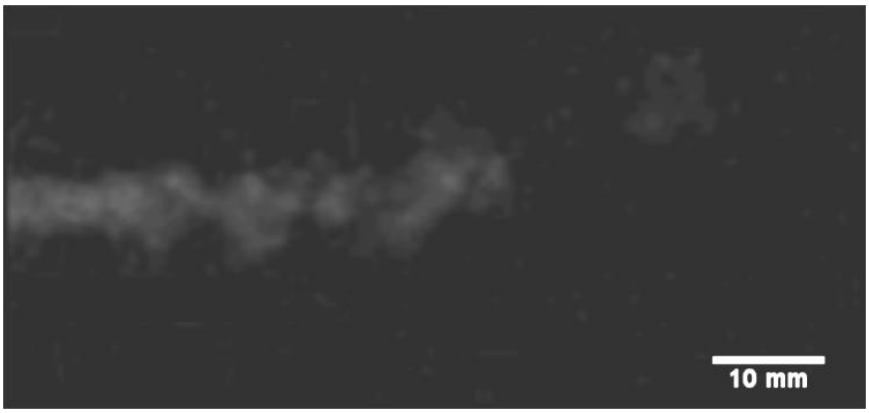

Figure 4.17 PLIF image of acetone seeded in air jet released into ambient atmosphere.

To compare the PLIF image from air and nitrogen jets, the image intensity was measured one diameter away from the nozzle. The Gray scale intensity from this PLIF image was collected using MATLAB software and plotted against the cross section of the jet. Figure 4.18 shows the comparison between nitrogen and air jet seeded with acetone as tracer.

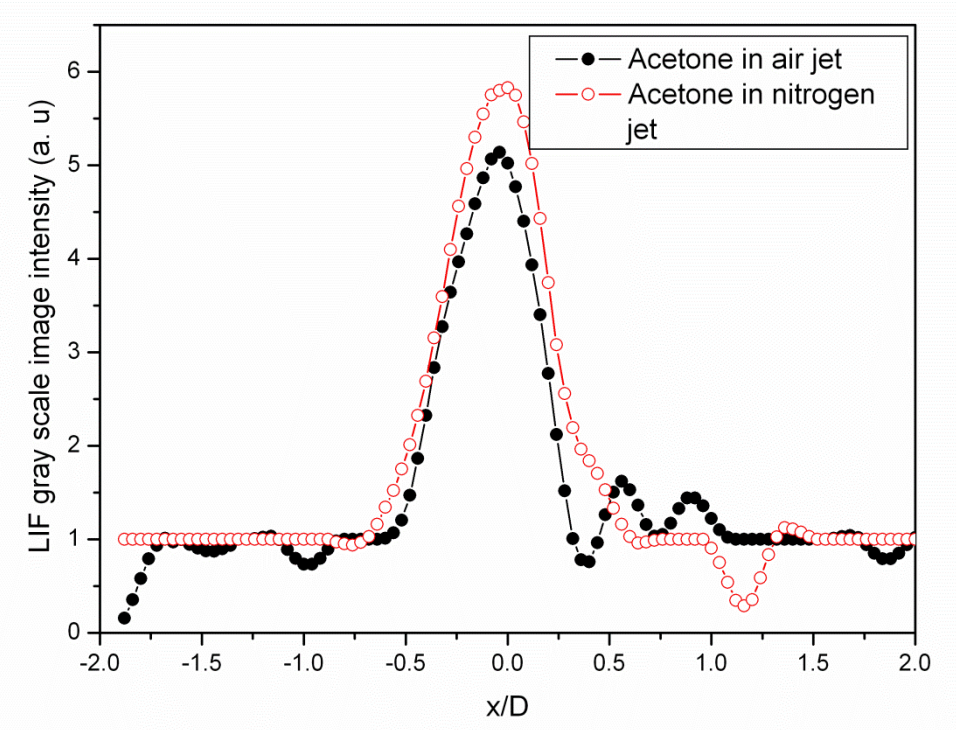

Figure 4.18 LIF gray scale image intensity in nitrogen and air jet over the jet cross section one diameter away from the nozzle.

From this graph, it is clear that LIF gray scale intensity of acetone in nitrogen is comparable with that in air. This may be attributed to the low velocities of the jet leading to less collisional quenching. Thus less collisional quenching in low speed jet, allows one to use PLIF of acetone flow visualization.

4.7 Conclusions

PLIF Experiments were carried out to study the gas flow diagnostics in subsonic flow regime. PLIF intensity images of acetone and MEK were converted into density images. Coherent vortices were observed in subsonic jets. These coherent structures were found to be non-overlapping with clear boundaries separating them. These structures were found to be more axisymmetric than spiral in nature. Coherent structures are responsible for energy transfer leading to turbulence in downstream of the jet. Breaking of coherent structures into turbulence was clearly observed. There is

a clear distinction between laminar region, coherent structures and turbulence with incoherent instabilities. The high intensity modes are observed to be present for x/D=1, 4, 7 which confirms that coherent structures occur at definite spatial frequencies present in the flow at 3x/D.

Further, the effect of oxygen on low speed jets was investigated. Acetone PLIF images of nitrogen and air jets released into ambient atmosphere were compared. Very low quenching was observed, because of the lower collision frequencies at low gas flow velocities. This was confirmed by investigations carried out on supersonic velocities and presented in the next chapter of this thesis.

Results described in this chapter have been published in Eur. Phys. J. Appl. Phys. (2013) 62, 31102.

CHAPTER 5

SUPERSONIC JET FLOW VISUALIZATION USING PLIF

5.1 Introduction

Better understanding of supersonic jets is necessary owing to its enormous applications in aerospace engineering such as, thrust generation for rockets, gas turbines, gas mixing and jet noise reduction. Extensive investigations have been carried out by several researchers to understand such phenomena (Mitchell et al. 2007, Leyko, M. et al. 2011, Morris P. J. et al. 2013). Supersonic jets are routinely created in the laboratory by allowing high pressure gas to escape through a convergent divergent (C-D) nozzle into a low pressure gas region. For studying such supersonic jets, optical flow visualization techniques are ideally suited. There are several optical techniques used for visualization of supersonic jet, such as shadowgraphy, Schlieren photography and laser based methods such as LIF and absorption spectroscopy. Among these methods, Schlieren photography is very popular and is frequently used due to its capability of directly recording gas density variations. However, it does not give quantitative information of gas density. PLIF imaging of supersonic jets has been done using diatomic tracers (Lachney, E. R. and Clemens, N. T. 1998). A major difficulty with the diatomic molecules as tracers is that their absorption wavelength bands that are quite narrow and, hence, lasers of specific wavelengths have to be used as excitation source. Higher gas temperature is necessary for the formation of diatomic molecules or radicals in the flow, which is very difficult in low temperature supersonic flow facilities.

Major problems of supersonic flow visualization using polyatomic tracers are condensation of the tracers, due to low temperatures prevailing in the flow region, and collisional quenching of the fluorescence at high pressures. Handa et al. (2011) showed that acetone PLIF can be used for supersonic jet flow visualization, even though it suffers from low temperature condensation. Oxygen is invariably present in many gas flow experiments and leads to quenching of fluorescence emission, as discussed in chapters 3 and 4. Thus, a quantitative understanding of the effect of

oxygen on LIF intensity is very essential. Fluorescence quenching in organic molecules by oxygen and other quenchers is well studied in liquid and gas phase. In the present study, acetone is used as the tracer and a high speed intensified gated CCD camera is used for supersonic jet flow visualization by the PLIF technique at Mach number 2.5. PLIF image of supersonic jet is compared with the Schlieren image for the same tank pressure conditions. Image averaging and Gaussian filters were used to improve the quality of the recorded PLIF images. Further, in order to study the effect of oxygen in real time flow, air was used as the bath gas and the results are compared with that for nitrogen for three different tank pressures. This methodology can be extended to quantitative flow visualization of supersonic jet and jet mixing studies.

5.2 Supersonic flow from Convergent-divergent (C-D)nozzle

A nozzle is a device used to achieve necessary increase in velocity of fluid flows at the cost of pressure. From the continuity equations, we can write down the well-known area velocity relation (Liepmann, H. W. and Roshko, A.1957)

$$\frac{dA}{A} = (M^2 - 1)\frac{dV}{V} \tag{5.1}$$

where A is the cross section area of the nozzle, V is the velocity of the flow, M is the mach number of the flow, dV and dA are the small increment in the velocity and cross sectional area of the nozzle, respectively. For subsonic flows (M<1) the value of (M^2-1) becomes negative and, hence, for an increase in velocity (dV-positive), flow area has todecrease in the direction of flow (dA-negative). If inlet flow is supersonic (M>1), we have (M^2-1) positive, and so the flow velocity increases (dV -positive) with increasing flow area in the direction of the flow (diverging section).

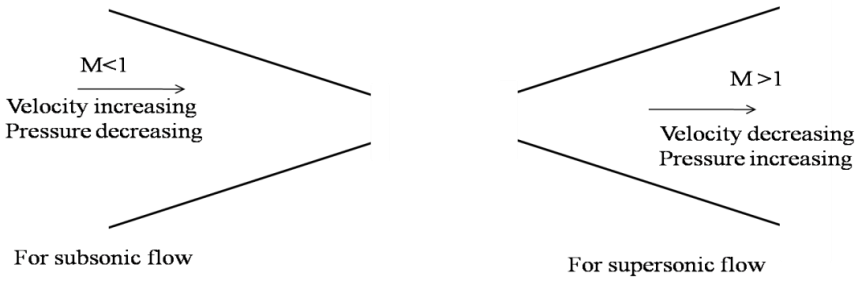

Figure 5.1 Gas flow in a converging and diverging passage.

When the flow is at Mach number unity (M=1), the flow area dA approaches zero as indicated by equation 5.1. These aspects are illustrated in figure 5.1.Thus, to get a transition from subsonic regime to supersonic flow speed, the gas should pass through a converging-diverging passage (nozzle) as shown in figure 5.2.

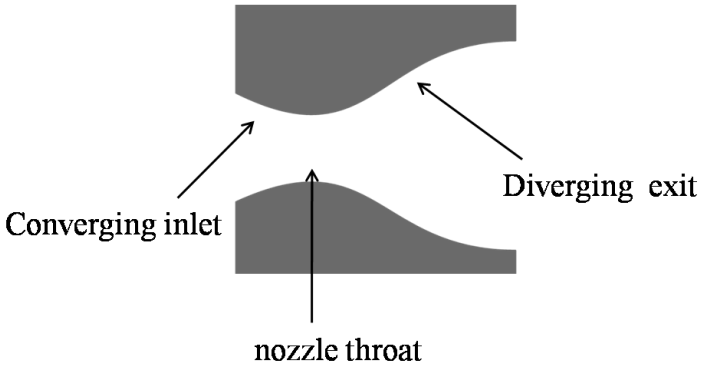

Figure 5.2 Converging and diverging nozzle for obtaining supersonic gas flows.

5.3 Structure of supersonic jet

When free jet from C-D nozzle expands into the ambient atmosphere, an interaction between expansion and compression waves produce a typical structure termed oblique shocks and one or more normal shocks, known as Mach discs. When an external pressure or back pressure is higher than the exit pressure at the nozzle flow compression is in backward direction and separate from the walls of the nozzle. This is called over-expanded jet otherwise, it is called under-expanded. Supersonic over-expanded jet structure is well known in the previous literature and is visualized

by different techniques (Norman, M. L. 1982, Arnette, S. A. 1993, Hadjadj, A. and Onofri, M. 2009).

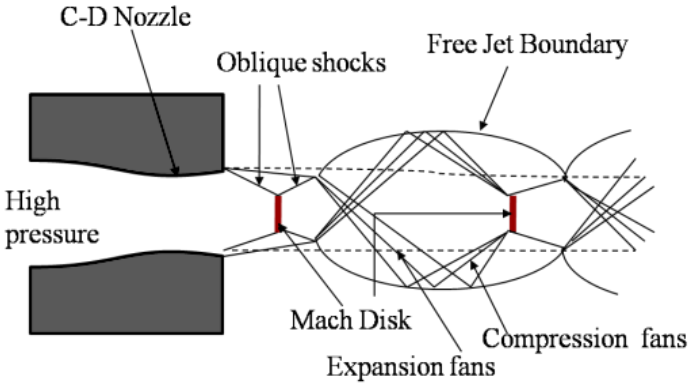

Figure 5.3 Shock cell structure in the plume of an over-expanded jet.

Figure 5.3 shows typical over-expanded steady state shock cell structure in a supersonic jet. Acetone tracer based LIF technique was employed to visualize supersonic nitrogen and air jets.

5.4 Supersonic jet and Schlieren optical setup

Figure 5.4 shows experimental setup for PLIF imaging of supersonic jet employed for the present study. The supersonic jet of nitrogen or air was created in our laboratory using axisymmetric convergent divergent (C-D) nozzle with throat diameter of 2 mm and exit diameter of 5 mm. The bath gases, nitrogen or air contained in high pressure cylinders, was purged through the liquid acetone, taken in a bottle, and then passed through the C-D nozzle into ambient atmosphere.

In the setup, laser beam of 266 nm wavelength from Nd:YAG laser (Model LAB190 from Spectra Physics Inc., USA) was transformed into a planar laser sheet using a cylindrical lens, as described earlier in sec. 4.4.1 of chapter 4. For imaging purpose, a high speed gated ICCD camera from Stanford Computer Optics Inc. (Model-4 Quik E/digital HR) with a minimum gate time of 1.2 ns was employed. The camera was connected to the computer and Nd:YAG laser for external trigger. After each laser pulse, the camera shutter opening delay was set to 50 ns and the optimized

exposure time was fixed to 25 ns throughout the experiment. To filter out other stray light, acetone LIF filter (LaVision GmbH, Goettingen Germany) was placed in front of the camera. ICCD camera and the C-D nozzle are shown in figure 5.5.

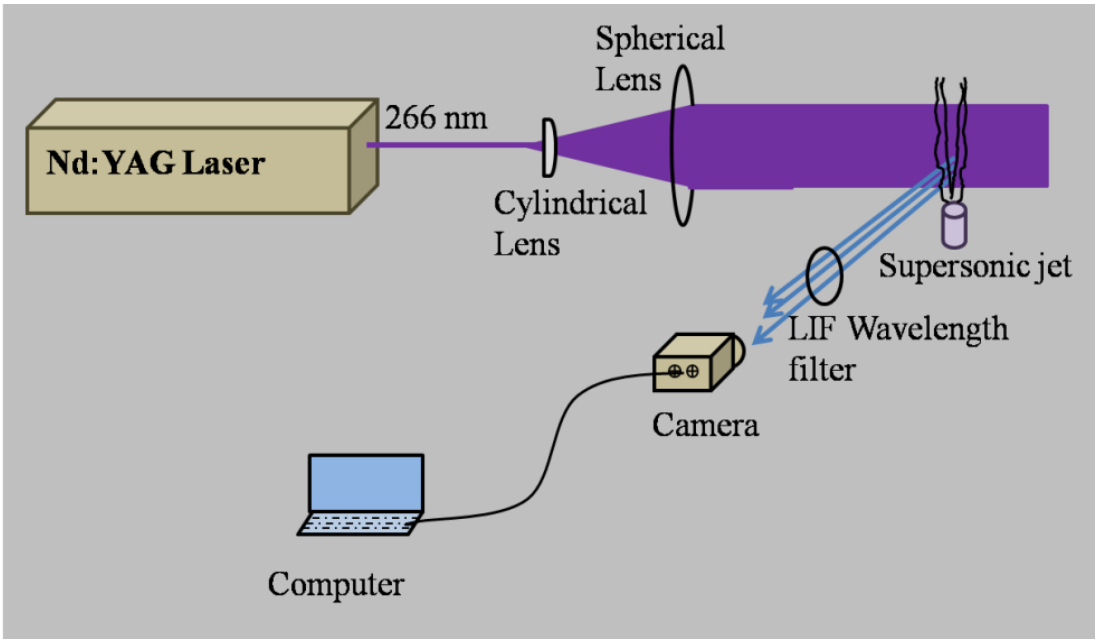

Figure 5.4 Experimental arrangement for PLIF visualization of supersonic gas flows.

Figure 5.5 Intensified gated CCD camera and convergent-divergent (C-D) nozzle.

The linear fluorescence regime was ensured by keeping incident laser energy at 20 mJ/pulse, which is well below the saturation intensity for acetone.

Schlieren imaging technique is frequently used in imaging shock structures in high speed flows. Hence, for comparison purposes, we have used a conventional Schlieren set up with concave mirrors as shown in figure 5.6(Liepmann, H. W. and Roshko, A.1957). Schlieren imaging is based on the principle that light rays deflected due to the variation in refractive index are blocked from reaching the camera or viewing screen. In our experiments we used xenon lamp as the light source and concave mirrors, of diameter 200 mm and focal length 3000 mm, as the imaging elements. A sharp stainless steel sheet was used as the knife edge.

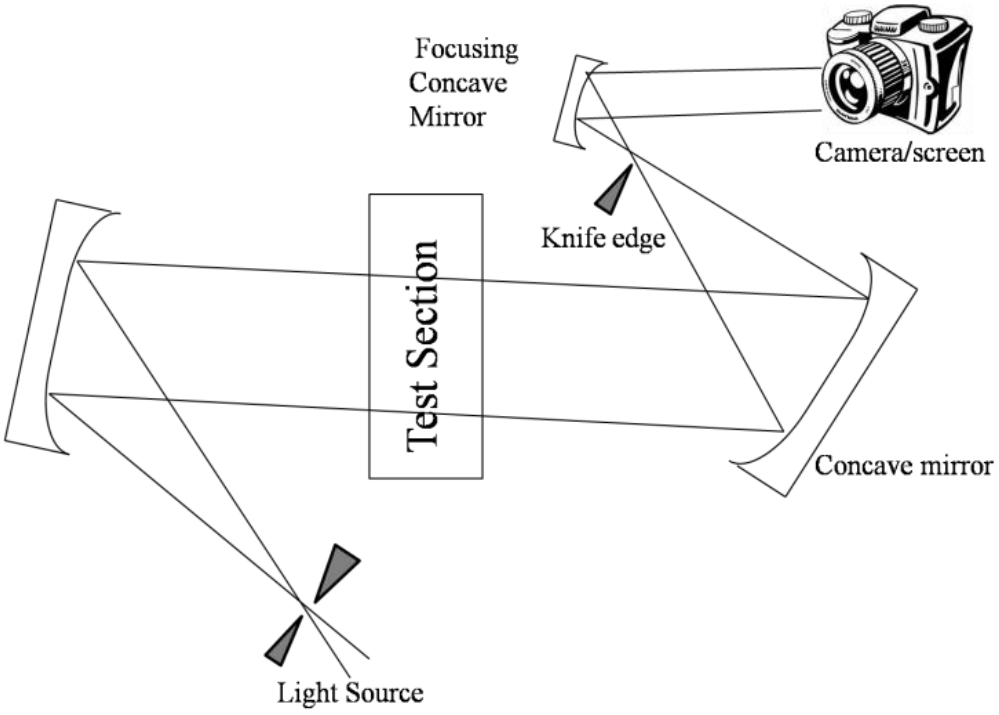

Figure 5.6 Schematic of the Schlieren set up with concave mirrors of diameter 200 mm and focal length of 3000 mm.

Figure 5.7 shows PLIF images of over-expanded nitrogen jet of mach 2.5 for four different tank pressures. The main challenge in implementing acetone PLIF in supersonic jets are condensation of the tracer at the exit of the nozzle and low signal to noise ratio at higher velocities. Intensity in a single shot image was very poor hence several images were obtained at 10 Hz frequency and stored. Each image was obtained by averaging 500 such images.

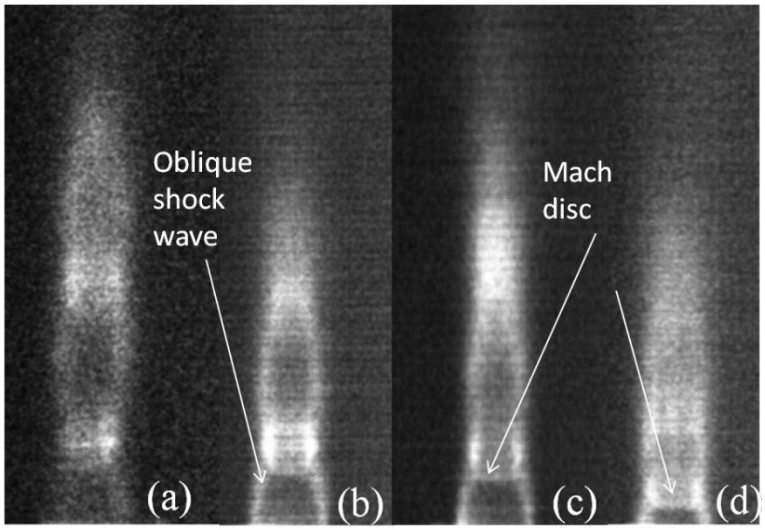

Figure 5.7 PLIF image of over-expanded nitrogen jet for gas tank pressure of a) 18 bar b) 16 bar c) 14 bar d) 12 bar.

Oblique shock waves and Mach disc are clearly observed in these images. Figure 5.8 shows the effect of averaging on the gray scale intensity of the image for 18 bar tank pressure. It is seen that averaging of about 400 images is sufficient for getting reliable data.

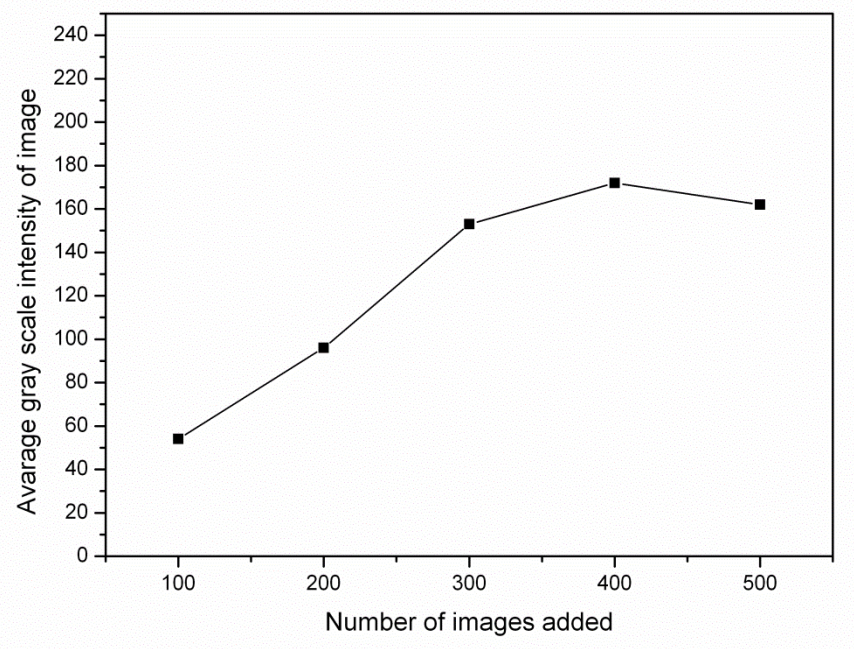

Figure 5.8 Effect of averaging on PLIF imaging of supersonic jet.

The images were further processed using Gaussian filter as described in chapter 4 of this thesis.

5.5 Comparison of PLIF with Schlieren and CFD simulations

For the purpose of validation, acetone PLIF images of supersonic jets were compared with the Schlieren image and simulation results based on Computational Fluid Dynamics (CFD), using FLUENT13.0 commercial software package. For the same conditions, acetone PLIF image for 18 bar tank pressure was compared with the Schlieren image. Figure 5.9 shows the comparison between Schlieren and acetone PLIF images. The brighter regions in PLIF image correspond to the darker parts in Schlieren image and vice versa.

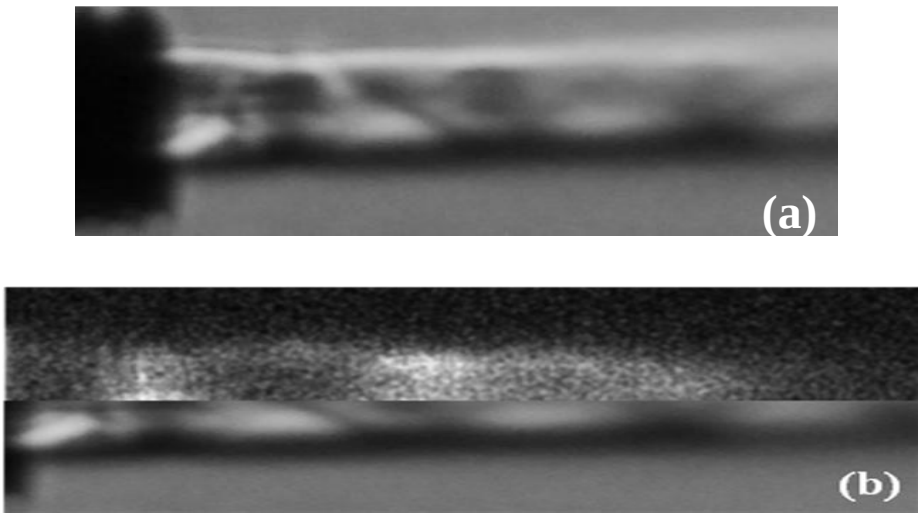

Figure 5.9 a) Schlieren image b) comparison between Schlieren and PLIF images of the supersonic jet at 18 bar stagnation pressure.

The location of the shock cell and the shock cell structure in PLIF image are seen to be matching well with Schlieren image. Further, the brighter regions in PLIF image correspond to large number density of tracer molecules leading to higher intensity. Thus, for steady state jets, in spite of the problem of condensation, it is

possible to get more information on the shock waves and shock cell structure using acetone PLIF.

CFD calculations were carried out by using Finite Volume Method (FVM) implemented in the software package FLUENT (version 13.0). In this work, initially, geometry of the domain was set up using GAMBIT software. Rectangular grid was used to mesh the entire domain. In these calculations equations for conservations of mass, momentum and energy are solved for laminar viscous gas flow.

Conservation of mass

$$\frac{\partial \rho}{\partial t} + \nabla \bullet (\rho V) = 0 \tag{5.2}$$

where ρ is the density of the fluid and V is the velocity.

Conservation of x-component of momentum

$$\frac{\partial (\rho u)}{\partial t} + \nabla \bullet (\rho u V) = -\frac{\partial p}{\partial x} + \rho f_x + (F_x)_{viscous} \tag{5.3}$$

Conservation of y-component of momentum

$$\frac{\partial (\rho v)}{\partial t} + \nabla \bullet (\rho v V) = -\frac{\partial p}{\partial y} + \rho f_y + (F_y)_{viscous} \tag{5.4}$$

Conservation of z-component of momentum

$$\frac{\partial (\rho w)}{\partial t} + \nabla \bullet (\rho w V) = -\frac{\partial p}{\partial z} + \rho f_z + (F_z)_{viscous} \tag{5.5}$$

where f and F denote body and viscous forces. Subscripts x, y and z are the components of momentum along three Cartesian coordinates.

Conservation of energy

$$\frac{\partial}{\partial t}\left[\rho\left(e+\frac{V^2}{2}\right)\right]+\nabla\bullet\left[\rho\left(e+\frac{V^2}{2}\right)V\right]=\rho\dot{q}-\nabla\bullet(\rho V)+\rho(f\bullet V)+\dot{Q}'_{viscous}+\dot{W}'_{viscous} \quad (5.6)$$

where $\dot{q}$ represents rate of heat addition per unit mass, $\dot{Q}'$and $\dot{W}'$are viscous source terms, and *e* is the internal energy of the flow.In these simulations, 2nd order, double precision density based solver for viscous flow in rectangular grid was used and grid independent studies were done for the final verification of the simulated results. The boundary conditions required for the FLUENT software are the values of pressure at inlet and outlet of the nozzle and the gas cell inner-wall, respectively. The actual physical parameters such as the nozzle stagnation pressure and back pressure are included through these boundary conditions.

Figure 5.10 shows the simulated density images of supersonic jet evaluated using FLUENT (ver.13.0).

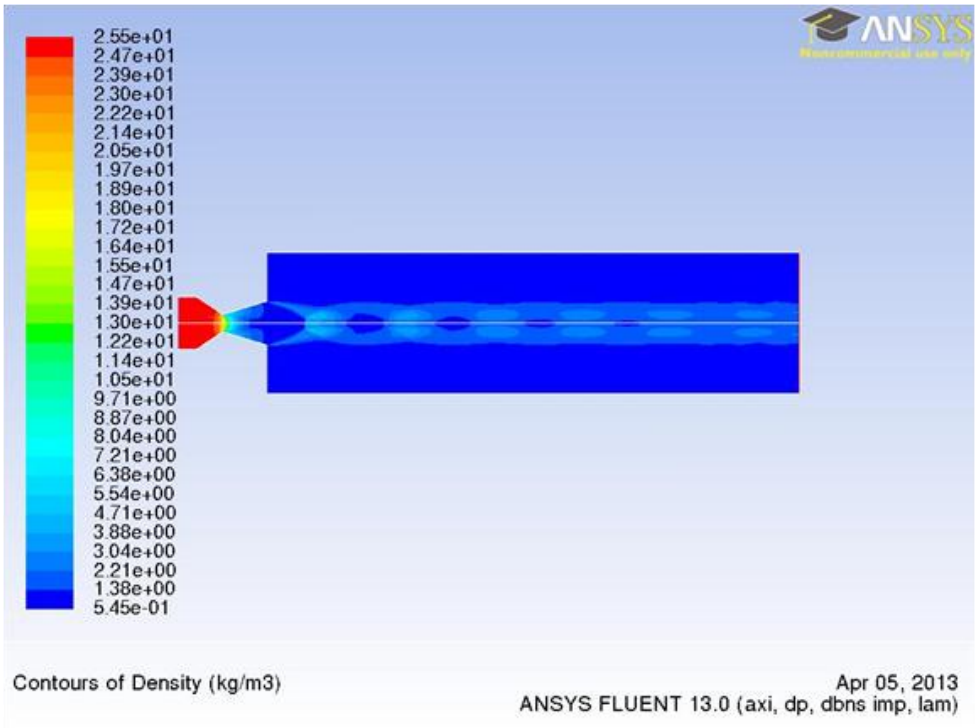

Figure 5.10 Simulated image using CFD for tank pressure of 16 bar.

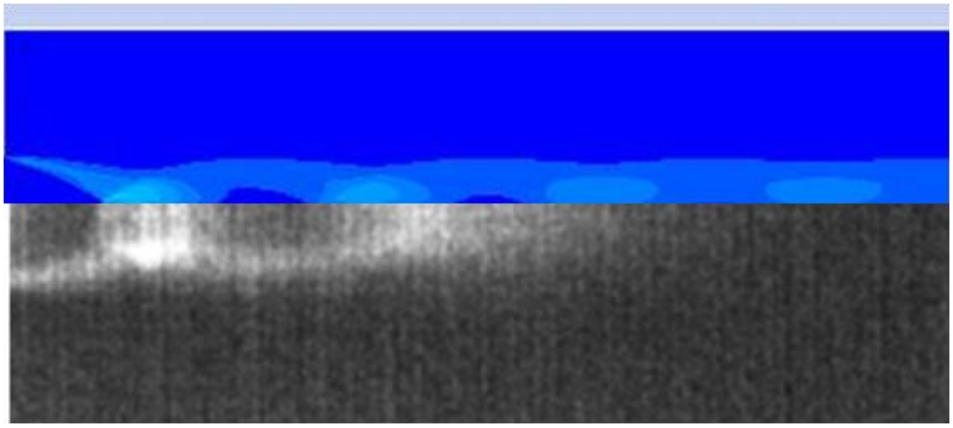

Figure 5.11 Comparison between CFD simulated density image (top) and PLIF density image (bottom) for tank pressure of 16 bar.

5.6 Effect of oxygen in supersonic jets

To study the effect of oxygen on PLIF intensity from supersonic jets, air was used as the bath gas instead of nitrogen. Figure 5.12 shows the processed acetone PLIF images of air at four different tank pressures.

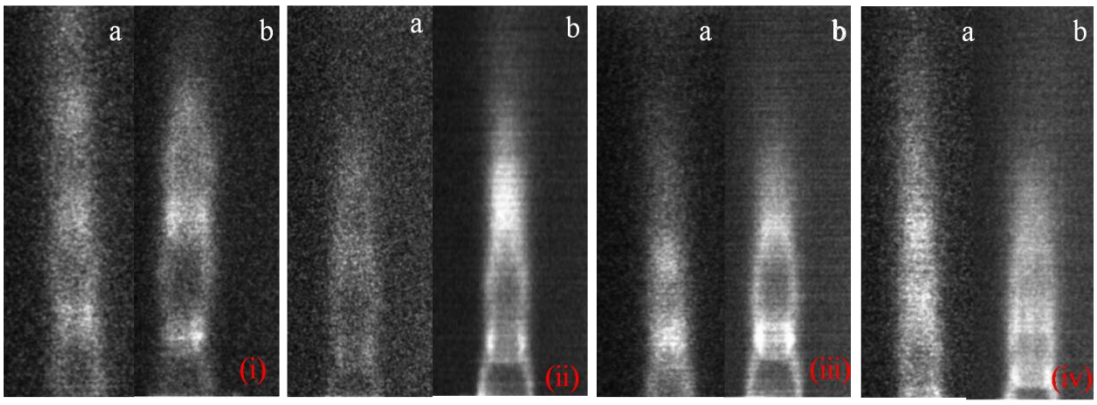

Figure 5.12 Comparison between PLIF images of over-expanded Supersonic jets in a) air and b) nitrogen for tank pressures of i) 18 bar ii) 16 bar iii) 14 bar iv) 12 bar respectively.

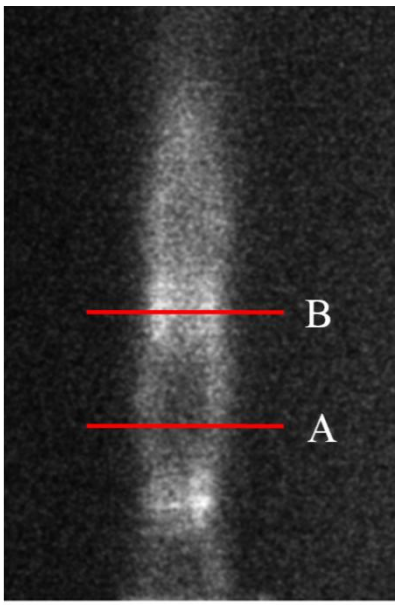

Figure 5.13 Location of cross sections chosen for image intensity observation in nitrogen supersonic jet at 18 bar tank pressure.

Image intensity profiles at two different cross-sections (see Figure 5.13), one at the middle of the shock cell (A) and the other at the centre of the Mach disk (B) is presented in Figures 5.14(a) and 5.14(b).

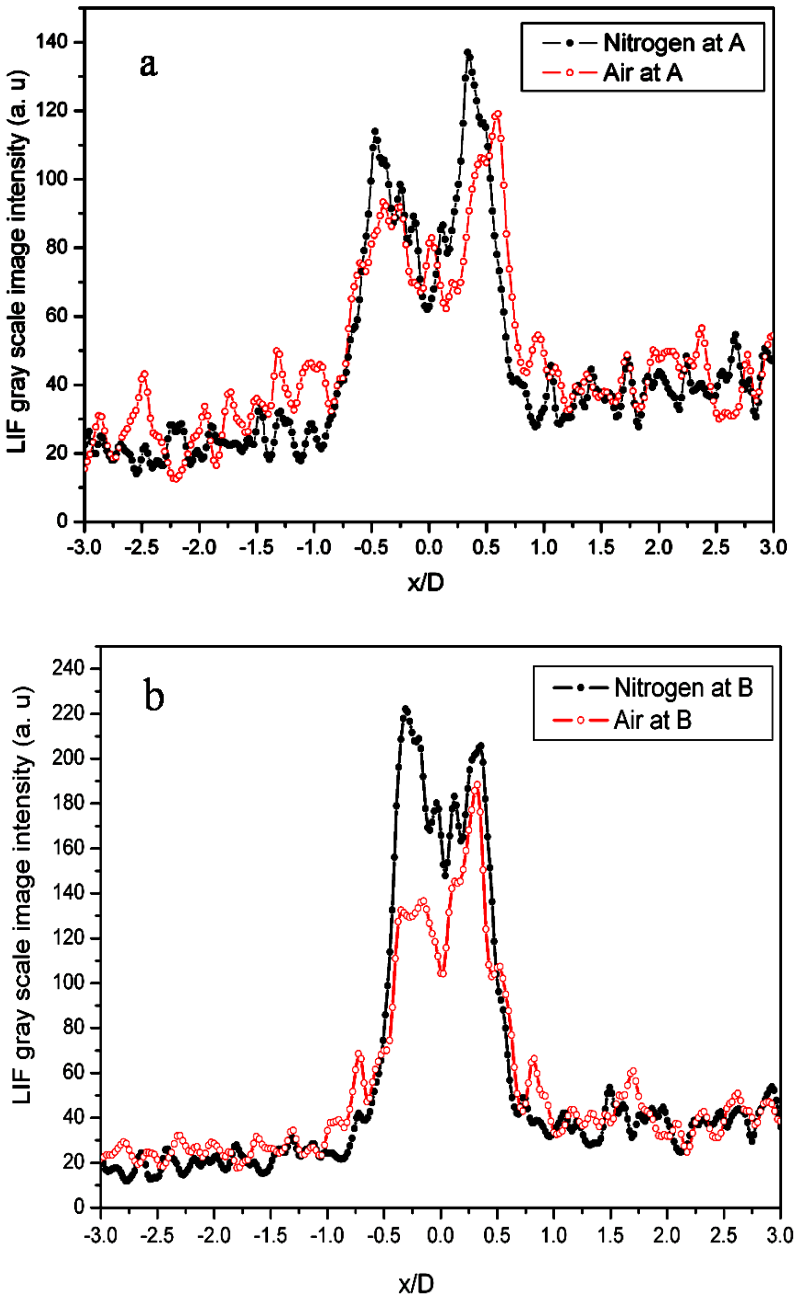

Figure 5.14 Gray scale intensity in nitrogen and air jets at (a) middle of the shock cell and at (b) the center of the mach disk as indicated in figure 5.13.

As can be seen there is drop in the PLIF intensity, well within the jet, in case of air compared with nitrogen. In the middle of the shock cell (at location A) jet

expansion was nearly 1.5 times nozzle exit diameter (D), whereas, it was same as the nozzle diameter in the mach disk (at location B). We also see that the signal noise level, in the region away from shock boundaries, is same for both air and nitrogen. Shock waves could not be observed unambiguously in the case of air jets. The low PLIF intensity is due to the fluorescence quenching effect by molecular oxygen. Oxygen is usually present in its ground triplet state. The energy transfer through non-radiative decay may lead to the reduction in intensity of the images in case of air as explained in chapter 3 of the present thesis. In the previous chapters we have reported the effect of oxygen in static cell and found that fluorescence quenching occurring for ketones is collisional in nature.

Figure 5.15 shows the effect of air pressure on the average gray scale intensity of the image. There is linear drop in the PLIF intensity, which is attributed to collisional transfer from acetone to triplet state of oxygen molecule. As the tank pressure increases collision frequency of bath gas molecules and tracer molecules also increases. This collisional energy transfer diminishes the LIF intensity with increase in pressure. Thus, the technique developed by us provides an elegant method to record, and improve, the acetone PLIF image of supersonic jets, despite the problem of condensation of the tracer in such experiments.

.

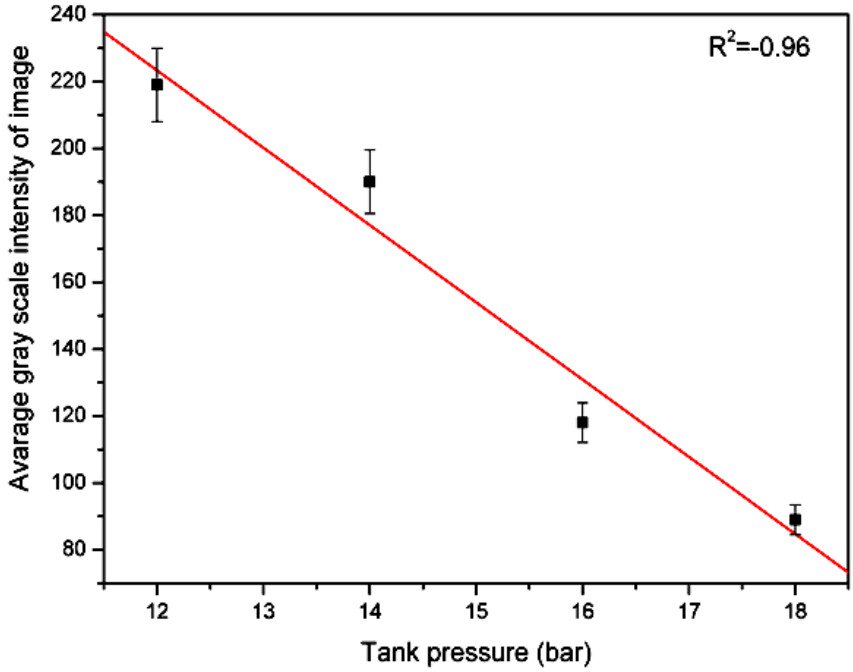

Figure 5.15 Effect of stagnation pressure on PLIF image intensity in air supersonic jets.

5.7 Conclusion

Supersonic nitrogen jet is visualized by employing PLIF technique using acetone as the tracer. Inspite of the serious problem of condensation of acetone, this work demonstrates that acetone can still be used for steady state supersonic jet flow visualization and mixing studies. PLIF images of supersonic flow were compared with the Schlieren images and CFD simulations. Further, the effect of oxygen on fluorescence was clearly observed at supersonic speeds. Drop in fluorescence intensity with increase in pressure shows that oxygen quenching is due to collisions. It is also observed that, there is a decrease in the image intensity with increasing tank pressure for air. This is attributed to collisional energy transfer from acetone to triplet state of oxygen.

CHAPTER 6

CONCLUSIONS AND FUTURE DIRECTIONS

6.1 Summary

Gas flow visualization has several applications in fluid dynamics, such as design of aircrafts and combustion research. There are several flow visualization methods such as Shadowgraphy, Schlieren, Smoke flow visualization, PLIF and Absorption Spectroscopy. Among these various methods, Schlieren and Smoke flow visualization are very popular and frequently used because of experimental simplicity. For quantitative measurements PLIF is widely used in numerous studies in the field of fluid dynamics and combustion research.

The present work focuses on the study of LIF from ketone based tracers for gas flow visualization. For all these studies a frequency quadrupled, Q switched, Nd:YAG laser (266 nm) was used as an excitation source. The quenching effect of oxygen on LIF of acetone, Methyl Ethyl Ketone (MEK) and 3-pentanone was studied quantitatively at low pressures (~700 torr) with oxygen partial pressures upto 450 torr. Nitrogen was used as a bath gas into which these molecular tracers were added in different quantities according to their vapor pressure at room temperature. Further Smoluchowski theory was used to calculate the quenching parameters and compared with the experimental results. The molecular density distribution measurement in turbulent nitrogen jet ($Re \approx 3X10^3$), using acetone and MEK tracers was demonstrated. Emitted fluorescence images of subsonic jet flow field were recorded on CMOS camera. The dependence of PLIF intensity on acetone vapor density was used to convert PLIF image of nitrogen jet into the density image on pixel by pixel basis. Instantaneous quantitative density image of nitrogen jet, seeded with acetone was obtained. Arrow head shaped coherent turbulent structures were observed in our experiments. It was found that coherent structures observed in our experiments were non-overlapping with separate boundaries. Breaking of coherent structures into turbulence was clearly observed. PLIF imaging was used for supersonic jet, using

acetone as molecular tracer. For supersonic jet, the fluorescence images were recorded on ICCD camera. Significant decrease in the PLIF intensity due to the presence of oxygen was clearly observed. The dependence of PLIF intensity on averaging of images and air pressure was studied. It was demonstrated that even with the presence of the condensation of acetone, one can obtain good quality PLIF images. It was also shown that averaging and Gaussian image processing of steady state jet PLIF images can further improve the image quality for quantitative analysis.

6.2 Main conclusions of the thesis

The following conclusions can be drawn from the present thesis work.

1. In the first chapter, brief quantum theoretical formalism has been given for polarization states of fluorescence emitted from an atom excited by the polarized light (laser).
2. Investigation of the quenching of LIF signal from the ketone tracers by molecular oxygen in nitrogen bath gas was carried out. SV coefficients for acetone, MEK and 3-pentanone were found to be 17.104, 18.069 and 34.409 (L mol^{-1}) respectively.From the SV coefficients and quenching rate constants the effect of molecular oxygen was found to be relatively low, for acetone and MEK when compared with that for 3-pentanone. These tracers can be used for the gas flows with trace amount of oxygen at atmospheric pressures despite the lower quantum yield relative to 3-pentanone.
3. It was found that, the estimation of quenching rate using Stokes Einstein diffusion relation deviates from the experimental result. For example quenching rate constant for acetone from experiment was found to be 8.77($10^9 LM^{-1}s^{-1}$) and from the Stokes-Einstein relation 0.614($10^9 LM^{-1}s^{-1}$), whereas from Chapman and Enskog relation 7.66 ($10^9 LM^{-1}s^{-1}$).This is due to the under estimation of diffusion coefficient. The results obtained by using diffusion coefficient from Chapman and Enskog relation were comparable with the experimental quenching rates.

4. MEK has been identified as a tracer for gas flow visualization at ambient temperature. MEK number density dependency on LIF signal shows linear behaviour.

5. Turbulent flow from subsonic jet was imaged using acetone and MEK in the PLIF technique. MATLAB code based on Gaussian function was developed for processing of PLIF images for better gas flow visualization.

6. In a turbulent flow coherent arrowhead shaped structures were observed even at low Reynolds numbers in the order of 10^3.These structures were found to be more axisymmetric than spiral.The high intensity modes were observed to be present for x/D=1, 4, 7 which confirms that coherent structures occurred at definite spatial frequencies present in the flow at 3x/D.

7. Acetone PLIF images of nitrogen and air jet released into ambient atmosphere at subsonic velocities was compared. Oxygen quenching was found to be low, because of the lower collision frequencies at low gas flow velocities. This was also confirmed by investigations at higher velocities.

8. For steady state supersonic jet, it is possible to get considerable amount of information on shock waves and cell structure using acetone PLIF. Image processing and averaging over set of images improves the quality of the image considerably.

9. There was appreciable drop in the intensity of air jet compared to nitrogen both seeded with acetone at supersonic velocities. Shock waves could not be observed unambiguously in the case of air. This clearly shows that, there is fluorescence quenching effect by molecular oxygen.

6.3 Future Directions

After completing the work reported in this thesis, we feel that it is necessary to improve the ketone tracer based technique for low temperature supersonic flow visualization.

There is a need to find out better tracer with low condensation and low toxicity with and high quantum efficiency appropriate for use with commercially available lasers. Pressure and temperature dependent studies for the new tracers are very much essential. In case of subsonic jet flow visualization, transition from coherent structure to fully developed turbulence needs to be understood. For this, there is need to develop fluid dynamic model which can be further compared with the experimental results. Development of PLIF technique using polyatomic molecules to hypersonic flows are to be explored.

Appendix I

The electromagnetic radiation is a transverse electromagnetic wave with the electric and magnetic fields $\vec{E}$and $\vec{H}$ vibrating perpendicular to the direction of propagation. Using Coulomb [1], $\vec{E}(\vec{r},t)$ and $\vec{H}(\vec{r},t)$ may be expressed in terms of the vector potential $\vec{A}(\vec{r},t)$ through

$$\vec{E} = -\frac{\partial \vec{A}}{\partial t}, \vec{H} = \vec{\nabla} \times \vec{A} \qquad \text{(A.1)}$$

The vector field $\vec{A}(\vec{r},t)$ satisfies the Maxwell equations

$$(\nabla^2 - \frac{\partial^2}{\partial t^2})\vec{A} = 0 \qquad \text{(A.2)}$$

$$\vec{\nabla} \cdot \vec{A} = 0 \qquad \text{(A.3)}$$

a) Polarization

Electromagnetic radiation propagating in a direction given by $\vec{k}$ with a polar co-ordinates (k, θ_k, ϕ_k) is characterized by the wave number k=2π/λ and ω=2πν where λ denotes the wavelength and ν denotes the frequency. The geometry for our analysis is shown below

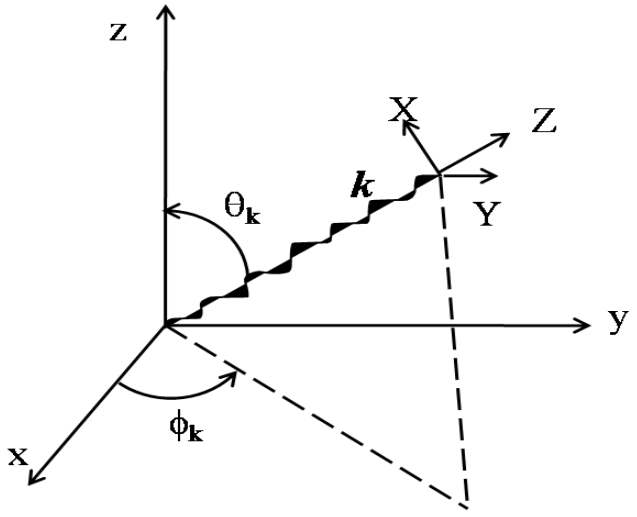

Figure A.1 Co-ordinate system for analysis of light polarization.

Let the dimension-less unit vectors ($\hat{\varepsilon}_X, \hat{\varepsilon}_Y, \hat{\varepsilon}_Z$) definethe x, y, z axes of the laboratory frame and ($\hat{\imath}, \hat{\jmath}, \hat{k}$) define the X, Y, Z axes associated with the radiation propagating along $\vec{k}$ as shown in the figure A.1.

Any state of linear polarization can be written in the form

$$\hat{\varepsilon}(\alpha) = \hat{\imath}\cos\alpha + \hat{\jmath}\sin\alpha \qquad \text{(A.4)}$$

withα ranging from 0 to π with $\hat{\varepsilon}(0) = \hat{\imath}$, $\hat{\varepsilon}(\pi/2) = \hat{\jmath}$

Since $\vec{E}(\vec{r}, t)$ and $\vec{H}(\vec{r}, t)$ given by equation (1) are real valued, $\vec{A}(\vec{r}, t)$ must be real valued and satisfy Maxwell's equations (A.2) and (A.3). Clearly $\cos(\omega t - \vec{k}\cdot\vec{r})$ and $\sin(\omega t - \vec{k}\cdot\vec{r})$ are linearly independent solutions of (A.2).

Any solution $\vec{A}(\vec{r}, t)$ of equation (A.2) corresponding to an arbitrary linearly polarized light may thus be written as

$$\vec{A}(\vec{r}, t) = \hat{\varepsilon}(\alpha)[\mathrm{a}\cos(\omega t - \vec{k}\cdot\vec{r}) + \mathrm{b}\sin(\omega t - \vec{k}\cdot\vec{r})] \qquad \text{(A.5)}$$

where a and b are arbitrary constants independent of space time co-ordinates. i. e.,

$$\vec{A}(\vec{r}, t) = \hat{\varepsilon}(\alpha)\left[\mathrm{a}\frac{\mathrm{e}^{\mathrm{i}(\omega t - \vec{k}\cdot\vec{r})} + \mathrm{e}^{-\mathrm{i}(\omega t - \vec{k}\cdot\vec{r})}}{2} + \mathrm{b}\frac{\mathrm{e}^{\mathrm{i}(\omega t - \vec{k}\cdot\vec{r})} - \mathrm{e}^{-\mathrm{i}(\omega t - \vec{k}\cdot\vec{r})}}{2\mathrm{i}}\right]$$

$$= \hat{\varepsilon}(\alpha)\left[\frac{\mathrm{a} + \mathrm{ib}}{2}\mathrm{e}^{-\mathrm{i}(\omega t - \vec{k}\cdot\vec{r})} + \frac{\mathrm{a} - \mathrm{ib}}{2}\mathrm{e}^{\mathrm{i}(\omega t - \vec{k}\cdot\vec{r})}\right]$$

$$= \hat{\varepsilon}(\alpha)\mathrm{c}\mathrm{e}^{-\mathrm{i}(\omega t - \vec{k}\cdot\vec{r})} + c.c. \qquad \text{(A.6)}$$

where c= (a+ib)/2 and c.c. stands for the complex conjugate of the first term of RHS.

Although $\vec{A}(\vec{r}, t)$ is real valued, the complex form represented by the first term in (A.6) is often employed (for mathematical convenience) with the understanding that its complex conjugate (c.c.) is to be added. It is obvious immediately that the condition $\vec{\nabla}\cdot\vec{A} = 0$ in equation (A.3) is the same now as$\hat{\varepsilon} \cdot \vec{k} = 0$.

Let $\hat{\varepsilon}_1$ and $\hat{\varepsilon}_2$ denote any two linear polarization states in the X-Y plane which are orthogonal to each other, so that

$$\hat{\varepsilon}_1(\alpha) = \hat{\imath}\cos\alpha + \hat{\jmath}\sin\alpha \qquad \text{(A.7)}$$

$$\hat{\varepsilon}_2(\alpha) = \hat{\imath}\cos\left(\alpha + \frac{\pi}{2}\right) + \hat{\jmath}\sin\left(\alpha + \frac{\pi}{2}\right)$$

$$= -\hat{\imath}\sin\alpha + \hat{\jmath}\cos\alpha \qquad \text{(A.8)}$$

as shown in the figure A.2.

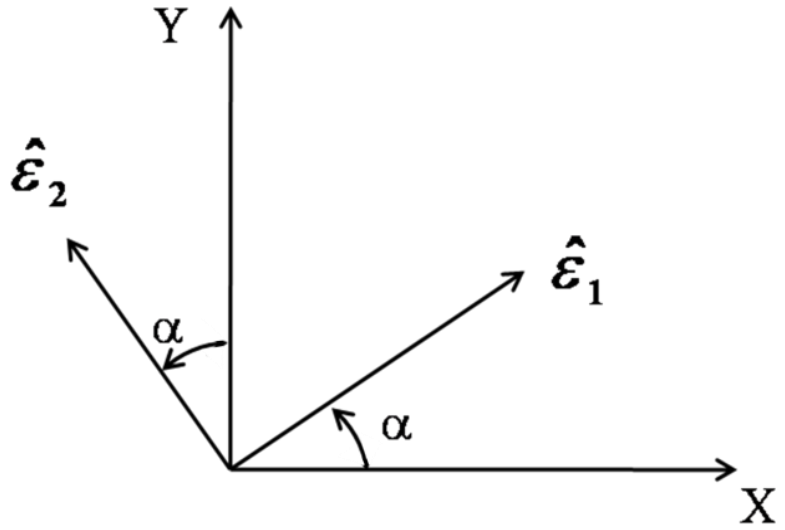

Figure A.2 Representation of linear polarization states in X-Y plane.

It is important to note that one can also write a solution of the Maxwell equations in the form

$$\vec{A}(\vec{r},t) = \mathrm{a}\hat{\varepsilon}_1 \cos\left(\omega t - \vec{k}\cdot\vec{r}\right) + \mathrm{b}\hat{\varepsilon}_2 \sin(\omega t - \vec{k}\cdot\vec{r})] \qquad \text{(A.9)}$$

$\vec{A}$ as shown in the figure A.3. Rewriting (A.9) in the form

$$\vec{A}(\vec{r},t) = A_1\hat{\varepsilon}_1 + A_2\hat{\varepsilon}_2 \qquad \text{(A.10)}$$

the field may be viewed as a vector with components

$$A_1 = \mathrm{a}\cos\left(\omega t - \vec{k}\cdot\vec{r}\right),\ A_2 = \mathrm{b}\sin(\omega t - \vec{k}\cdot\vec{r}) \qquad \text{(A.11)}$$

along $\hat{\varepsilon}_1$ and $\hat{\varepsilon}_2$.

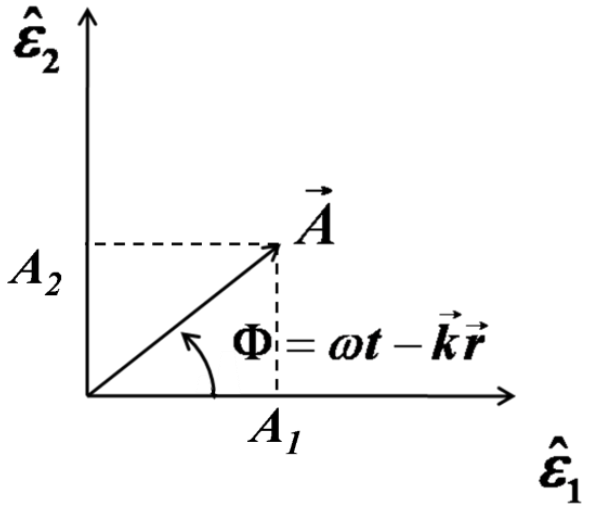

Figure A.3 Vector $\vec{A}(\vec{r},t)$ with its components $A_1$and A_2.

Clearly

$$\frac{{A_1}^2}{a^2} + \frac{{A_2}^2}{b^2} = 1\,, \qquad \text{(A.12)}$$

which is an equation for an ellipse and it reduces to circle if a=b.

As time t evolves at any given$\vec{r}$, $\Phi = \omega t - \vec{k}\cdot\vec{r}$increases with time. Therefore the vector $\vec{A}$ rotates anticlockwise, if both a and b are positive. On the other hand, if a is positive and b is negative, $\vec{A}$ rotates clockwise with respect to time. In other words the rotations correspond to right and left handed rotations when viewed along $\vec{k}$.

Let us now express

$$a=A\cos\beta;\ b=A\sin\beta \qquad \text{(A.13)}$$

with A positive and

$$-\pi/4 \le \beta \le \pi/4 \qquad \text{(A.14)}$$

So that in the range

$0 \le \beta \le \pi/4$ both a and b are positive, whereas in the range$-\pi/4 \le \beta \le 0$, a is positive and b is negative in equation (A.11).

We may now rewrite

$$\vec{A}(\vec{r},t) = A\left[\hat{\varepsilon}_1\cos\beta\,\frac{e^{i(\omega t-\vec{k}\cdot\vec{r})}+e^{-i(\omega t-\vec{k}\cdot\vec{r})}}{2} + \hat{\varepsilon}_2\sin\beta\,\frac{e^{i(\omega t-\vec{k}\cdot\vec{r})}-e^{-i(\omega t-\vec{k}\cdot\vec{r})}}{2i}\right]$$

$$= A\left(\frac{\hat{\varepsilon}_1\cos\beta + i\,\hat{\varepsilon}_2\sin\beta}{2}\right)e^{-i(\omega t-\vec{k}\cdot\vec{r})} + A\left(\frac{\hat{\varepsilon}_1\cos\beta - i\,\hat{\varepsilon}_2\sin\beta}{2}\right)e^{i(\omega t-\vec{k}\cdot\vec{r})}$$

$$= A\hat{\varepsilon}(\alpha,\beta)e^{-i(\omega t-\vec{k}\cdot\vec{r})} + c.c.\,, \qquad \text{(A.15)}$$

where

$$\hat{\varepsilon}(\alpha,\beta) = \hat{\varepsilon}_1(\alpha)\cos\beta + i\,\hat{\varepsilon}_2(\alpha)\sin\beta \qquad \text{(A.16)}$$

Note that $\hat{\varepsilon}(\alpha,\beta)$is a function of both α and β since $\hat{\varepsilon}_1$ and $\hat{\varepsilon}_2$ are the functions of $0 \le \alpha \le \pi$.

The above form of $\vec{A}(\vec{r},t)$ given by equation (A.15) is most general, since the earlier form given by equation (A.6) is obtained as special case of (A.15) by setting β=0, in which case $\hat{\varepsilon}(\alpha,0)$ defines all the states of linear polarization. The range $0 < \alpha \le \pi$, $0 \le \beta < \pi/4$ represents right circularly elliptic states, while $0 \le \alpha \le \pi$, $-\pi/4 <$

$\beta \leq 0$ represents left elliptic states of polarization. $\beta = {}^{\pi}/_{4}$ corresponds to right circular and $\beta = -{}^{\pi}/_{4}$ corresponds to left circular polarization.

$$\hat{\varepsilon}_{RC} = \hat{\varepsilon}\left(\alpha, {}^{\pi}/_{4}\right) = \frac{1}{\sqrt{2}}(\hat{\varepsilon}_1 + i\hat{\varepsilon}_2) \quad \text{(A.17)}$$

$$\hat{\varepsilon}_{LC} = \hat{\varepsilon}\left(\alpha, -{}^{\pi}/_{4}\right) = \frac{1}{\sqrt{2}}(\hat{\varepsilon}_1 - i\hat{\varepsilon}_2) \quad \text{(A.18)}$$

We use the complex form

$$\vec{A}(\vec{r}, t) = A\hat{\varepsilon}(\alpha, \beta)\mathrm{e}^{-\mathrm{i}(\omega t - \vec{k}\cdot\vec{r})} \quad \text{(A.19)}$$

with the understanding that c. c is added to ensure that $\vec{A}(\vec{r}, t)$ is real valued. The form $\hat{\varepsilon}(\alpha, \beta)$ given by (A.16) is thus the most general one for the polarization.

b) Orthogonal states of polarization

By definition $\hat{\varepsilon}_1 \cdot \hat{\varepsilon}_1 = 1$; $\hat{\varepsilon}_2 \cdot \hat{\varepsilon}_2 = 1$; and it is clear that $\hat{\varepsilon}_1 \cdot \hat{\varepsilon}_2 = 0$; using (A.7) and (A.8).In contrast to $\hat{\varepsilon}_1$ and $\hat{\varepsilon}_2$ which are real $\hat{\varepsilon}(\alpha, \beta)$ defined by (A.16) is complex vector as such the scalar product between such vectors has to be defined through

$$\langle\hat{\varepsilon}(\alpha', \beta')|\hat{\varepsilon}(\alpha, \beta)\rangle = \hat{\varepsilon}(\alpha, \beta)^* \cdot \hat{\varepsilon}(\alpha, \beta)$$

so that in particular, we have

$$\langle\hat{\varepsilon}(\alpha, \beta)|\hat{\varepsilon}(\alpha, \beta)\rangle = \hat{\varepsilon}(\alpha, \beta)^* \cdot \hat{\varepsilon}(\alpha, \beta) = 1$$

If $\langle\hat{\varepsilon}(\alpha', \beta')|\hat{\varepsilon}(\alpha, \beta)\rangle = 0$, the two complex vectors $\hat{\varepsilon}(\alpha, \beta)$ and $\hat{\varepsilon}(\alpha, \beta)$ are said to be orthogonal. It is clearly seen that $\hat{\varepsilon}_{RC}$ and $\hat{\varepsilon}_{LC}$ are orthogonal to each other.

c) Representation of polarization on Poincare's Sphere

A geometric way of looking at the states of polarization is presented by Poincare's sphere. Let us now define polar angles (Θ_p, Φ_p) on the Poincare sphere as shown in the figure A4 through the angles

$$0 \leq \Theta_p = {}^{\pi}/_{2} - 2\beta \leq \pi \quad \text{(A.20)}$$

$$0 \leq \Phi_p = 2\alpha < 2\pi \quad \text{(A.21)}$$

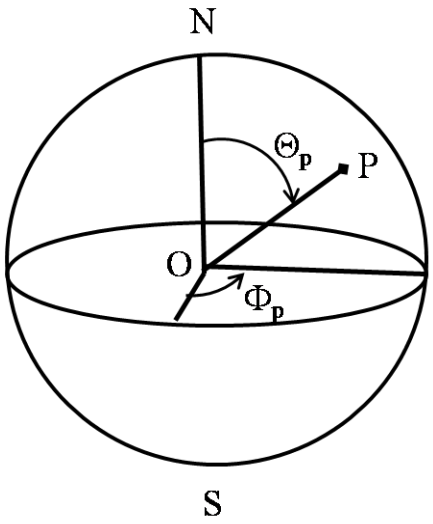

Figure A.4 Polarization representation on the Poincare's sphere.

$\hat{\varepsilon}(\alpha,\beta)$given by equation (A.16) is a complex and is a unit vector in a complex 2 dimensional linear vector space $P(\Theta_p, \Phi_p)$ and $P'(\Pi - \Theta_p, \Pi + \Phi_p)$.

For $\beta = 0$we have $\Theta_p = {}^{\pi}/_{2}$, and therefore all linear polarized states are represented on the equatorial line in the Poincare sphere and $\beta = {}^{\pi}/_{4}\,\Theta_p = 0$ which corresponds to North Pole represents right circular polarization $\beta = -{}^{\pi}/_{4}\,\Theta_p = \pi$ which correspond to South Pole represents left circular polarization. Points lying in the northern hemisphere correspond to right elliptic polarized states. Points on the southern hemisphere represent left elliptic polarized states. Thus there is one to one correspondence between the states of polarization and points on the Poincare sphere.

Note that right circular and left circular polarized states are represented by north and south poles respectively which are diametrically opposite to each other or orthogonal to each other as we have seen already. In fact any two states which are diametrically opposite to each other on the Poincare sphere are orthogonal to each other. A point Θ_p, Φ_p on the Poincare sphere corresponds to $\hat{\varepsilon}\left({}^{\Phi_p}/_{2}\,, {}^{\pi}/_{4} - {}^{\Theta_p}/_{2}\right)$

$$|\Theta_p, \Phi_p\rangle = \left|\hat{\varepsilon}\left({}^{\Phi_p}/_{2}\,, {}^{\pi}/_{4} - {}^{\Theta_p}/_{2}\right)\right\rangle \qquad \text{(A.22)}$$

using (A.20) and (A.21).

Similarly, a diametrically opposite point on the Poincare sphere corresponds to

$$|\pi - \Theta_p, \pi + \Phi_p\rangle = \left|\hat{\varepsilon}\left(\pi/2 - \Phi_p/2\ ,\ \Theta_p/2 - \pi/4\right)\right\rangle \qquad \text{(A.23)}$$

This applies to linear polarized states $|\pi/2\ , \Phi_p\rangle$as well$\langle \pi/2\ , \Phi_p |\ \pi/2\ , \Phi_p + \pi\rangle = 0$.

d) Stokes parameters

The vector potential $\vec{A}\ (\vec{r}, t\ )$ given by equation (A.19) represents an electromagnetic wave with amplitude *A* and polarization $\hat{\varepsilon}(\alpha, \beta)$. Choosing a pair of orthogonal states, $\hat{\varepsilon}_a$ and $\hat{\varepsilon}_b$ which may be referred to as basis states, we may in general write

$$\vec{A}(\vec{r}, t) = [a\hat{\varepsilon}_a + b\hat{\varepsilon}_b]e^{-i(\omega t - \vec{k}\cdot\vec{r})} \qquad \text{(A.24)}$$

where a and b denote the amplitudes associated with $\hat{\varepsilon}_a$ and $\hat{\varepsilon}_b$ respectively. We may then define the intensities $I(\hat{\varepsilon}_a) = |a|^2$ and $I(\hat{\varepsilon}_b) = |b|^2$.

Electromagnetic radiation is said to be unpolarized, if the two intensities $I(\hat{\varepsilon}_a)$ and $I(\hat{\varepsilon}_b)$ associated with any pair of orthogonal states $\hat{\varepsilon}_a$ and $\hat{\varepsilon}_b$ are equal otherwise it is polarized. They may either be linearly polarized states like $\hat{\varepsilon}_1$ and $\hat{\varepsilon}_2$ or circularly polarized states like $\hat{\varepsilon}_{RC}$ and $\hat{\varepsilon}_{LC}$ or even elliptically polarized states. Quite often, one employs either a pair of linearly polarized states or right circular and left circular polarized states as a basis in a two dimensional complex linear vector space $\{\hat{\varepsilon}(\alpha, \beta)\}$ to which all the $\hat{\varepsilon}(\alpha, \beta)$ belong.

For example, $\hat{\varepsilon}(\alpha, \beta)$ is written in terms of the basis states $\hat{\varepsilon}_1$ and $\hat{\varepsilon}_2$ in (A.16). Inverting equation (A.17) and (A.18) we may also write

$$\hat{\varepsilon}(\alpha, \beta) = \frac{1}{\sqrt{2}}\left[\hat{\varepsilon}_{RC}e^{-i\beta} + \hat{\varepsilon}_{LC}e^{-i\beta}\right] \qquad \text{(A.25)}$$

if right and left circularly polarized states are chosen as basis states. Stokes introduced a set of three parameters known as Stokes parameters S_1, S_2, S_3 to characterize polarized radiation. They are defined as follows,

$$S_1 = I\left(\hat{\varepsilon}(0)\right) - I\left(\hat{\varepsilon}(\pi/2)\right) \qquad \text{(A.26a)}$$

$S_2 = I\left(\hat{\varepsilon}(\pi/4)\right) - I\left(\hat{\varepsilon}(3\pi/4)\right)$ (A.26b)

$S_3 = I(\hat{\varepsilon}_{RC}) - I(\hat{\varepsilon}_{LC})$ (A.26c)

The total intensity may also be added as another parameter

$S_0 = I = I\left(\hat{\varepsilon}(0)\right) + I\left(\hat{\varepsilon}(\pi/2)\right)$ (A.27a)

$= I\left(\hat{\varepsilon}(\pi/4)\right) + I\left(\hat{\varepsilon}(3\pi/4)\right)$ (A.27b)

$= I(\hat{\varepsilon}_{RC}) + I(\hat{\varepsilon}_{LC})$ (A.27c)

The set of four parameters S_0, S_1, S_2, S_3 gives complete information about the polarized radiation.

e) Density matrix ρ

We have already pointed out that any general state of polarization may be expressed in terms of a pair of orthonormal basis states $\hat{\varepsilon}_a$ and $\hat{\varepsilon}_b$ as in (A.24) i.e. as a vector in the complex two dimensional vector space $\{\hat{\varepsilon}(\alpha,\beta)\}$. Since the space is complex, we use Dirac notation and write explicitly as

$|\hat{\varepsilon}\rangle = a|\hat{\varepsilon}_a\rangle + b|\hat{\varepsilon}_b\rangle$ (A.28)

where a and b are complex numbers in general, which are given by $a = \langle\hat{\varepsilon}_a|\hat{\varepsilon}\rangle$, $b = \langle\hat{\varepsilon}_b|\hat{\varepsilon}\rangle$. We may then define the density matrix ρ of polarization as the 2×2 Hermitian matrix

$$\rho = \begin{bmatrix} |a|^2 & ab^* \\ ba^* & |b|^2 \end{bmatrix} \quad \text{(A.29)}$$

which may readily be seen to be the matrix representation of what may be referred to as the density operator ρ_{op} given by

$\rho_{op} = |\hat{\varepsilon}\rangle\langle\hat{\varepsilon}|$ (A.30)

in terms of the chosen basis states $|\hat{\varepsilon}\rangle$.

Clearly

$Tr\rho = |a|^2 + |b|^2 = 1,$ (A.31)

when we choose a different basis say $|\hat{\varepsilon}_{a'}\rangle$ and $|\hat{\varepsilon}_{b'}\rangle$ the density matrix changes to

$$\rho' = \begin{bmatrix} |a'|^2 & a'b'^* \\ b'a'^* & |b'|^2 \end{bmatrix} \quad \text{(A.32)}$$

which is nothing but the matrix representation of the same $\rho_{op} = |\hat{\varepsilon}\rangle\langle\hat{\varepsilon}|$ with respect to the new basis.

For example, suppose the given state of polarization is $|\hat{\varepsilon}_1\rangle$. Then the density matrix ρ is given by

$$\rho = \begin{bmatrix} 1 & 0 \\ 0 & 0 \end{bmatrix} \tag{A.33}$$

with respect to the orthonormal basis $|\hat{\varepsilon}_1\rangle$ and $|\hat{\varepsilon}_2\rangle$.

The same state $|\hat{\varepsilon}_1\rangle$ is given by

$$\rho' = \begin{bmatrix} |a'|^2 & a'b'^* \\ b'a'^* & |b'|^2 \end{bmatrix} \tag{A.34}$$

with respect to circular polarization states $|\hat{\varepsilon}_{RC}\rangle$ and $|\hat{\varepsilon}_{LC}\rangle$. Since the density operator for the state $|\hat{\varepsilon}_1\rangle$ is given by

$\rho_{op} = |\hat{\varepsilon}_1\rangle\langle\hat{\varepsilon}_1|$, as follows that

$$a' = \langle\hat{\varepsilon}_{RC}|\hat{\varepsilon}_1\rangle, b' = \langle\hat{\varepsilon}_{LC}|\hat{\varepsilon}_1\rangle. \tag{A.35}$$

Appendix II

(i) A matlab code based on Gaussian function for PLIF image analysis.

```
clear all;
clc;
fname='AcetonePLIF.jpg'; %%%%%% reading the image
I=imread(fname);
im=rgb2gray((I));
iim=im;
%%%%%%%%%%image pixel corrections %%%%%%%%%%%%%
[a,b]=size(im);
A=zeros (a,b);
n=0;
k=0;
m=0;
l=0;
for n=1:1:a,
for m=1:1:b,
if (k>=a)
           k=a;
else
           k=n+1;
end
if (l<=1)
           l=1;
else
          l=n-1;
end
if (im(n,m)<im(k,m))
iim(n,m)=(im(k,m)+im(l,m))/2; % Avaraging and %storing in
an array iim
end
```

```
end
end
%%%%%%%%%%%%%%%%Gaussian%%%%%%%%%%%%%%%%
PSF = fspecial('gaussian',6,1);
convoluted = convn(iim,PSF);
for n=1:1:a
for m=1:1:b
if (convoluted(n,m)<=5)
A(n,m)=0;
else
A(n,m)=convoluted(n,m);
end
end
end
himage = imshow(convoluted,[0 80]);
hpixelinfopanel = impixelinfo(himage);
hdrangepanel = imdisplayrange(himage);
hpixreg = impixelregion(himage);
title('Processed Image');
%%%%%%%%%%%%%%%%End%%%%%%%%%%%%%%%%%%
```

(ii) A matlab code for converting PLIF image into density image.

```
clear all;
clc;
fname='ac_1.jpg';
I=imread(fname);
im=rgb2gray((I));
iim=im;
for n=1:1:a,
for m=1:1:b,
if A(n,m)>6,
B(n,m)=(A(n,m))-15.8985)/.5138;%%constants are taken from
%%%calibration plot
```

```
B(n,m)=(A(n,m)-11.82)/.339;
else
B(n,m)=A(n,m);
end
if B(n,m)<=5.00,
B(n,m)=0;
else
B(n,m)=B(n,m);
end
end
end
for n=1:1:a,
for m=1:1:b,
if (B(n,m)<=6)
B(n,m)=0;
else
B(n,m)=B(n,m);
end
     %Conversion of partial pressure to number density
     Bd(n,m)=((B(n,m)*0.133225*1000)*6.0221)/(8.314*300);
Bd(n,m)=B(n,m)*0.1; %%%%To get the power 24
end
end
% % s = xlswrite('tempdata.xls', A);
% figure;imshow(B, [0,120])
% hiimage = imshow(B,[0,120]);
%%%%%%%%%%%%%%%%partial pressure imaging%%%%%%%%%%%%%%%%
figure;image(B)
hiimage = imshow(B,[]);
colormap(jet)
hpixelinfo = impixelinfo(hiimage);
hdrange = imdisplayrange(hiimage);
```

```
hpixregi = impixelregion(hiimage);
title('Partial pressure(torr) Image');
%%%%%%%%%%%%%%%density imaging%%%%%%%%%%%%%%%%%%%%%
figure;
image(Bd)
higmage = imshow(Bd,[]);
colormap(jet)
hapixelinfo = impixelinfo(higmage);
hadrange = imdisplayrange(higmage);
hapixregi = impixelregion(higmage);
title('Acetone number density(10^2^4/m^-^3)Image');
%%%%%%%%%%%%%%% end%%%%%%%%%%%%
```

References

- Abdel-Rahman A.(2010). "A review of effects of initial and boundary conditions on turbulent jet," WWSEAS Transactions on Fluid Mechanics, 4(5), 257–275.

- Acharya, T. and Ray, A. K. (2005). "Image processing principles and applications." A John Wiley & Sons, Inc., Publication, Hoboken, New Jersey.

- Agrawal, A. and Prasad, A. K.(2002). "Organizational modes of large-scale vortices in and axisymmetric turbulent jet," Flow, Turbulence and Combustion, 68, 359-377.

- Arik, M., Celebi N. and Onganer, Y. (2005). "Fluorescence quenching of fluorescein with molecular oxygen in solution." *J. Photochem. Photobiol. A: Chem.,* 170, 105-111.

- Arnette, S. A., Samimy, M. and Elliott, G. S. (1993). "On streamwise vortices in high Reynolds number supersonic axisymmetric jets" Phys. Fluids A, 5, 187-202.

- Ball, C. G., Fellouah, H. and Pollard, A.(2012)."The flow field in turbulent round free jets," *Progress in Aerospace Sciences*, 50, 1–26.

- Biradar, D. S., Thipperudrappa, J. andHanagodimath, S. M. (2007). "Fluorescence Quenching Studies of 1,3-Diphenyl Benzene."*Spect. Lett.*, 40, 559-571.

- Crimaldi, J. P. (2008). "Planar laser induced fluorescence in aqueous flows." *Exp. Fluids*, 44, 851–863.

- Cruyningen, I. V., Lozano, A. and Hanson, R. K. (1990). "Quantitative imaging of concentration by planar laser-induced fluorescence."*Exp. Fluids*, 10, 41-49.

- Desevaux, P. (2001). "A method for visualizing the mixing zone between two co-axial flows in an ejector" *Optics and Lasers in Engg.*, 35, 317–321.

- Deusch, S. and Dracos, T.(2001). "Time resolved 3D passive scalar concentration-field imaging by laser induced fluorescence (LIF) in moving liquids." *Meas. Sci. Technol*., 12,188-200.

- Dilecce, G., Simek, M., Vigliotti, M. and De Benedictis, S. (2000). "Fast LIF Approach to NO Rotational Temperature and Density Measurement: Application to a Gas-Dynamic Expansion*." Appl. Spectrosc*., 54(6), 824-831.

- Dimotakis, P.E.(1983). "Structure and dynamics of round turbulent jets*" Phy. Fluids, 26(11)*, 3185–3195.

- Dimotakis, P.E.,(2000). "The mixing transition in turbulent flows*" J. Fluid Mech. 409*, 69–98.

- Dimotakis, P.E.,(2005). "Turbulent mixing*" Annu. Rev. Fluid Mech.* 37, 329–356.

- Fiedler H. E. (1998). "Control of free turbulent shear flows." In:Gad-el-Hak Mohamed, Pollard, A., Bonnet J. P., editors. "Flow control: fundamentals and practices." Springer- Verlag; 58, 335–429.

- FazleHussain A. K. M.(1986). "Coherent structures and turbulence," J. Fluid Mech., 173, 303-356.

- Guibert, P. and Perrard, W.(2002). "Concentration measurements in a pressurized and heated gas mixture flow using laser induced fluorescence." *Trans. ASME.*, 124,512-522.

- Gross, J. and Vrabec, J.2006). "An equation-of-state contribution for polar components: dipolar molecules." *AIChE J.*, 52(3), 1194-1204.

- Guibert, P., Modica, V. and Morin, C. (2006). "Influence of pressure, temperature and gas phase composition on biacetyl laser-induced fluorescence." *Exp. Fluids*, 40, 245–256.

- Hadjadj, A. and Onofri, M. (2009). "Nozzle flow separation." *Shock Waves*, 19,163–169.

- Handa, T., Masuda, M., Kashitani, M. and Yamaguchi, Y. (2011) "Measurement of number densities in supersonic flows using a method based on laser-induced acetone fluorescence." *Exp. Fluids*, 50, 1685-1694.

- Hiller, B. and Hanson, R.K. (1988). "Simultaneous planar measurements of velocity and pressure fields in gas flows using laser-induced fluorescence." *Appl. Opt.*, 27(1), 33-48.

- Hsu, A., Srinivasan, R., Bowersox, R. D. W. and North, S. W. (2009)."Application of molecular tagging towards simultaneous vibrational temperature and velocity mapping in an underexpanded jet flowfield." *47th AIAA Aerospace Sciences*, 5-8, January 2009, Orlando, Florida.

- Hu, H. and Koochesfahani, M. M. (2002)."A novel method for instantaneous, quantitative measurement of molecular mixing in gaseous flows." *Exp. Fluids*, 33, 202-209.

- Iida, N. and Ando, A.(1994). "Concentration measurement in a transient gas jet using the laser induced fluorescence method."*JSAE Rev.,* 15, 123-131.

- Jackson, J. D. (1962). "Classical electrodynamics." John Wiley, New York.

- Jackson, J. D. and Okun, L. B.(2001). "Historical roots of gauge invariance." Rev. Mod. Phys., 73, 663-680.

- King, G. F., Lucht, R. P. and Craig Dutton, J.(1997). "Quantitative dual-tracer planar laser-induced fluorescence measurements of molecular mixing."*Opt. Lett.,* 22(9), 633–635.

- Koban, W., Koch, J.D., Hanson, R.K. and Schulz, C.(2005). "Oxygen quenching of Toluene Fluorescence at Elevated temperatures."*Appl. Phys. B,* 80,777–784.

- Koban, W., Koch, J. D., Sick, V., Wermuth, N., Hanson, R. K. and Schulz, C. (2005). "Predicting LIF signal strength for toluene and 3-pentanone under engine related temperature and pressure conditions." *Proc. Of the Comb. Inst.*, 30, 1545–1553.

- Koch, J. D. and Hanson, R.K. (2003)."Temperature and excitation wavelength dependencies of 3-pentanone absorption and fluorescence for PLIF applications." *Appl. Phys. B,* 76, 319–324.

- Koch, J.D. (2005). "Fuel tracer photo physics for quantitative planar laser-induced fluorescence."Ph.D. thesis, Stanford Univ., California, USA.

- Kuznicki, S. M., Bell, V. A., Nair, S., Hillhouse, H. W., Jacubinas, R. M., Braunbarth, C. M., Toby, B. H. and Tsapatsis, M. A 2001). "A titanosilicate molecular sieve with adjustable pores for size-selective adsorption of molecules." Nature, 412, 720-724.

- Lackowicz, J. R. (2006). "Principles of Fluorescence Spectroscopy". 3rd Ed., Springer Verlag: New York.

- Lachney, E. R. and Clemens, N. T. (1998). "PLIF imaging of mean temperature and pressure in a supersonic bluff wake."*Exp. Fluids*, 24, 354-363.

- Lee, M. P., McMillin, B. K. and Hanson, R. K. (1993). **"**Temperature measurements in gases by use of planar laser-induced fluorescence imaging of NO" *Appl. Opt.*,32(27), 5379-5396.

- Liepmann, H.W. and Roshko, A. (1957). **"**Elements of gas dynamics."John wiley and sons inc., New york.

- Löffler, M., Beyrau, F. and Leipertz, A.(2010). **"**Acetone laser-induced fluorescence behavior for the simultaneous quantification of temperature and residual gas distribution in fired spark-ignition engines." *Appl. Opt.*,49(1), 37-49.

- Lozano, A., Yip, B. and Hanson, R. K.(1992). "Acetone: a tracer for concentration measurements in gaseous flows by planar laser-induced fluorescence." *Exp. Fluids*, 13, 369-376.

- Luong, M., Zhang, R., Schulz, C. and Sick, V.(2008)."Toluene laser-induced fluorescence for in-cylinder temperature imaging in internal combustion engines." *Appl. Phys. B*, 91, 669–675.

- Leyko, M., Moreau, S., Nicoud, F. and Poinsot T. (2011). "Numerical and analytical modelling of entropy noise in a supersonic nozzle with a shock." *J. of Sound and Vibr.*,330 , 3944–3958.

- McMillin, B. K., Palmer, J.L. and Hanson, R.K. (1993). "Temporally resolved, two-line fluorescence imaging of NO temperature in a transverse jet in a supersonic cross flow." *Appl. Opt.*,32(36), 7532-7545.

- Mitchell, D., Honnery, D. and Soria, J. (2007) "Study of Underexpanded Supersonic Jets with Optical Techniques." *16th Australasian Fluid Mechanics Conference*, 2-7 December 2007, Crown Plaza, Gold Coast, Australia.

- Modica, V., Morin, C. and Guibert, P.(2007). "3-Pentanone LIF at elevated temperatures and pressures: measurements and modeling."*Appl. Phys. B*, 87, 193–204.

- Moerner, W. E. and Fromm, D.P. (2003). "Methods of single-molecule fluorescence spectroscopy and microscopy." *Rev. Sci. Instrum.*, 74(8), 3597-3619.

- Morris, P. J., McLaughlin, D. K. and Kuo, C. W. (2013). "Noise reduction in supersonic jets by nozzle fluidic inserts." *J. of Sound and Vibr.*,332, 3992–4003.

- Mycek, M. A. and Pogue, B. W. (2003). "Handbook of biomedical fluorescence."Marcel Dekker, Inc., New York.

- Nau, W. M. and Scaiano, J.C.(1996). "Oxygen quenching of excited aliphatic ketones and diketones." *J. Phy. Chem.*, 100, 11360–11367.

- Norman, M. L., Smarr, L., Winkler, K. H. A. and Smith, M. D. (1982). "Structure and Dynamics of supersonic jets." *Astron. Astrophy.*, 113, 285-302.

- O'Sullivan, M. and Testa A. C. (1970). "Fluorescence of aliphatic ketones" *J. Am..Che..Soc.*, 92(20), 1542-1544.

- Oo, Y. Y., Nagendra, K. N., Ananthamurthy, S., Vijayashankar, R. and Ramachandran, G.(2004) "Polarization of line radiation in the presence of external electric quadrupole and uniform magnetic fields." *J. Quant. Spectrosc. Radiat. Transfer*, 84(1), 35–64.

- Oo, Y. Y. (2004). "Studies in astrophysical line formation theory." Ph.D. Thesis Bangalore University, Bengaluru, India.

- Oo, Y. Y., Nagendra, K. N., Ananthamurthy, S., Swarnamala, S.,Vijayashankar, R. and Ramachandran, G.(2005) "Polarization of line radiation in the presence of external electric quadrupole and uniform magnetic fields: II. Arbitrary orientation of magnetic field." *J. Quant. Spectrosc. Radiat. Transfer*, 90(3-4), 343-366.

- Oo, Y. Y., Sampoorna, M., Nagendra, K. N., Ananthamurthy, S. and Ramachandran, G.(2007) "Scattering polarization in the presence of magnetic and electric fields." *J. Quant. Spectrosc. Radiat. Transfer*, 108(2), 161-179.

- Patil, N. R., Melvanki, R. M., Kapatkar, S. B., Chandrasekhar, K., Ayachit, N. H. and Umapathy, S. (2012). "Solvent effect on the fluorescence quenching of biologically active carboxamide by aniline and carbon tetrachloride in different solvents using S–V plots." *J. of Lumin.*, 132, 558-565.

- Pitz, R.W. (2008). "Hydroxyl tagging velocimetry."38th Fluid Dynamics Conference and Exhibition, 23 – 26, June 2008, Seattle, Washington.

- Reid, R. C., Prausnitz, J. M. and Poling, B. E. (1987). "The Properties of Gases and Liquids." McGraw-Hill, Inc. New York.

- Restic, S. (2006). "Optical methods in wind tunnel flow visualization." *FME Transactions*, 34, 7–13.

- Rose, M. E. (1957). "Elementary Theory of Angular Momentum." Jhon Wiley, New York.

- Rossmann, T., Mungal, M. G. and Hanson, R. K.(2001). **"**Nitric-oxide planar laser-induced fluorescence applied to low-pressure hypersonic flow fields for the imaging of mixture fraction." *Appl. Opt.*,42(33), 6682-6695.

- Schulz, C. and Sick, V. (2005). "Tracer-LIF diagnostics: quantitative measurement of fuel concentration, temperature and fuel/air ratio in practical combustion systems." *Prog. Energy Combust. Sci*., 31, 75–121.

- Sick, V. and Wermuth, N. (2004). "Single-shot imaging of OH radicals and simultaneous OH radical/acetone imaging with a tunable Nd :YAG laser." *Appl. Phys. B*, 79, 139–143.

- Siddhartha S. S., Narasimha R., Basu A. J., and Kailas S.V. (2000). "Coherent structures in numerically simulated jets with and without off-source heating" *Fluid Dynamics Research*, 26, 105–117.

- Smith, J. D. and Sick, V.(2007). "Quantitative, dynamic fuel distribution measurements in combustion-related devices using laser-induced fluorescence imaging of biacetyl in iso-octane." *Proc. Combust. Inst.*, 31,747-755.

- Solomon, C. and Breckon, T. (2011). "Fundamentals of image processing a practical approach with examples in matlab" A John Wiley & Sons, Ltd.,UK.

- Stenflo, J. O.(1998). "Hanle-Zeeman scattering matrix." *Astron. Astrophys.*, 338, 301–310.

- Stern, O. and Volmer, M. (1919). "On the quenching-time of fluorescence." *Physik. Zeitschr*., 20, 183.

- Stevens, R. E., Ma, H., Stone, C. R., Walmsley, H. L. and Cracknell, R. (2007). "On planar laser-induced fluorescence with multi-component fuel and tracer design for quantitative determination of fuel concentration in internal combustion engines." *Proc. IMechE Part D: J. Automobile Engineering*, 221,713-724.

- Sutton, J. A., Fisher, B. T. and Fleming, J. W. (2008). "A laser-induced fluorescence measurement for aqueous fluid flows with improved temperature sensitivity." *Exp. Fluids*, 45, 869–881.

- Tani, T., Oda, M., Mashimo, K., Tachibanab, F. and Horiuchi, H. (2006). "Single- molecule imaging towards precise detection of individual photophysics." *J. Lumin.*, 119–120, 173–177.

- Thipperudrappa, J. Biradar, D. S., Lagare, M. T., Hanagodimath, S. M., Inamdara, S. R. and Kadadevaramath, J. S. (2004). "Fluorescence quenching of bis-msb by carbon tetrachloride in different solvents." *J. of Photosc.* 11(1), 11-17.

- Thurber, M.C., Grisch, F. and Hanson, R.K. (1997). "Temperature imaging with single- and dual-wavelength acetone planar laser-induced fluorescence."*Opt. Lett.*, 22(4), 251–253.

- Thurber, M.C., Grisch, F., Kirby, B.J., Votsmeier, M. and Hanson, R.K. (1998)."Measurements and modeling of acetone laser-induced fluorescence with implications for temperature-imaging diagnostics." *Appl. Opt.*,37(21), 4963-4978.

- Thurber, M. C.(1999). "Acetone laser-induced fluorescence for temperature and multi parameter imaging in gaseous flows" Ph.D. thesis, Stanford Univ., California, USA.

- Thurber, M.C. and Hanson, R.K. (1999). "Pressure and composition dependences of acetone laser-induced fluorescence with excitation at 248, 266, and 308 nm." *Appl. Phy. B*, 69, 229–240.

- Thurber, M. C. and Hanson, R. K. (2001). "Simultaneous imaging of temperature and mole fraction using acetone planar laser-induced fluorescence." *Exp. Fluids*, 30, 93-101.

- Tian, X. and Roberts, P. J. W. (2003). "A 3D LIF system for turbulent buoyant jet flows." *Exp. Fluids*, 35, 636-647.

- Tseng, C. C., Voytovych, D. M., Kulatilak, D., Bhuiyan A. H., Lucht, R. P., Merkle, C. L., Hulka, J. R. and Jones, G.W.(2009). "Structure and mixing of a transient flow of helium injected into an established flow of nitrogen: two dimensional measurement and simulation."*Exp. Fluids*, 46, 559-575.

- Unger, D. R. and Muzzio, F.J. (1999). "Laser-induced fluorescence technique for the quantification of mixing in impinging jets." *AIChE Journal*, 45(12), 2477-2486.

- Valuer, B(2002). "Molecular Fluorescence Principles and Applications."WILEY-VCH Verlag GmbH, Germany.

- Yuen, L. S., Peters, J. E. and Lucht, R. P. (1997). "Pressure dependence of laser-induced fluorescence from acetone." *App. Opt.*,36(15), 3271-3277.

- Young, I. T. and van Vliet, L. J. (1995). "Recursive implementations of the Gaussian filter" *Sig. Process.,* 44,139–151.

- Zangi, R. and Kaufman, L. J.(2007). "Frequency-dependent Stokes-Einstein relation in supercooled liquids." *Phys. Rev. E*, 75, 051501-04.

Publications

(A) Research papers in International Journals

1) **V. M. Shelar,** G. M. Hegde, G. Umesh, G. Jagadeesh and Reddy K. P. J. (2013), "Gas Phase Oxygen Quenching Studies of Ketone Tracers for Laser Induced Fluorescence Applications in Nitrogen Bath Gas", ***Spect. Lett.***,47(1), 12-18.

2) **Shelar Vikas M.,** Umesh G., Hegde G. M., Jagadeesh G. and Reddy K. P. J.(2012), "Quantitative Density Imaging of Subsonic Jet Using Planar Laser Induced Fluorescence of MEK", ***IEEE Conf. Proc.*** (DOI 10.1109/ICOE.2012.6409583**)**.

3) **Vikas M. Shelar,** Gopalkrishna M. Hegde, Govindarao Umesh, Gopalan Jagadeesh and K.P.J. Reddy (2013), "Visualization of Coherent Structures in Turbulent Subsonic Jet Using Planar Laser Induced Fluorescence of Acetone", ***Eur. Phys. J. of Appl. Phys.***, 62, 31102-07.

4) **Shelar Vikas. M.,** Shrisha Rao M.,Hegde G. M., Umesh G., Jagadeesh G., Reddy K. P. J. (2013), "Acetone Planar Laser Induced Fluorescence for Supersonic Flow Visualization in Air and Nitrogen Jet", ***Meas. Sc. Tech. Elsvier***(under review)

(B) Research Papers presented in Conferences

5) **Shelar Vikas M.**, Sharath N., Umesh G., Hegde G., Jagadeesh G., Reddy K. P. J., Ramachandran G. (2011), "*Oxygen quenching studies of laser induced fluorescence from Acetone and Methyl Ethyl Ketone in argon bath gas"*, ***2nd DAE-BRNS Symposium on Atomic Molecular and Optical Physics, 22-25, February, Karnatak University Dharwad, Dharwad, India.***

6) **Shelar Vikas M.,** Hegde G. M., Jagadeesh G., Reddy K. P. J., G. Umesh (2011), "Planar Laser Induced Fluorescence of Acetone for Turbulent Gas Flow Visualization from Subsonic Ejector". 3nd International Conference on "Current Developments In Atomic, Molecular, Optical & Nano Physics" ***CDAMOP 2011, 14-16, December, University of Delhi, Delhi, India.***

7) **Shelar Vikas M.**, Umesh G., Hegde G. M., Jagadeesh G. and Reddy K. P. J.(2012), "*Quantitative Density Imaging of Subsonic Jet Using Planar Laser Induced Fluorescence of MEK",**ICOE-2012,International Conference on Optical Engineering, 26-28, July, VTU, Belgavi, India.***

BRIEF BIO-DATA

Contact address

Vikas M. Shelar,
S/o M. G. Shelar,
Hattargi Post,
Belgavi, Karnataka-591 243
Email: vikasms2007@gmail.com
Mobile +919986450983.

Qualification: Master of Science (Physics)
Bachelor of Science (Physics, Chemistry, Mathematics),

Research experience:

Worked as **Junior Research Fellow (JRF)** on **Doppler Weather Radar** development in **ISRO (Indian Space Research Organization) Radar Development unit (ISRAD**) Bangalore, India, from Aug-2006 to Aug-2007.

Teaching experience:

Worked in **K.N.S Institute of Technology Bangalore** as faculty in Department of Physics from Aug-2007 to july-2008.

List of publications

Publications in journals/peer reviewed conference proceedings:

1. **V. M. Shelar**, G. M. Hegde, G. Umesh, G. Jagadeeshand K. P. J.Reddy, G*as phase oxygen quenching studies of ketone tracers for laser induced fluorescence applications in nitrogen bath gas,* ***Spect. Lett.***, (2013). 47(1), 12-18.
2. **Vikas M. Shelar,** Gopalkrishna M. Hegde, Govindarao Umesh, Gopalan Jagadeesh and Reddy K. P. J., *Visualization of coherent structures in turbulent subsonic jet using planar laser induced fluorescence of acetone,* ***Eur. Phys. J. of Appl. Phys***(2013) 62, 31102.
3. **Shelar Vikas. M.,** Shrisha Rao M., Hegde G. M., Umesh G., Jagadeesh G., Reddy K. P. J., *Acetone Planar Laser Induced Fluorescence for Supersonic Flow Visualization in Air and Nitrogen Jet*, ***Meas. Sc. Tech. Elsvier,*** (2013) (Under review)
4. **Vikas M. S.**, Umesh G., Hegde G. M., Jagadeesh G. and Reddy K. P. J., *Quantitative density imaging of subsonic jet using Planar Laser Induced Fluorescence of MEK,* ***IEEE Conference Proceedings*** (2012) (doi:10.1109/ICOE.2012.6409583**)**

5. Manjunatha K.B., Dileep R., **Shelar Vikas M**., G. Umesh, M. N. Satyanarayan and B. Ramachandra Bhat, *Third-Order nonlinear optical properties and optical switching of Palladium (I) Complex*, ***AIP Conf. Proc.*** 1391, 706-708 (2011).
6. DirekKhajonrat, Chandrasekar V, Viswanathan G, **Shelar V**,, *Simultaneous radar observations of tropical cyclones by space-based and ground-based radar*,***IEEE Int. Proc.,*** 23-28 July 2007, 3899 – 3902.
7. K. B. Manjunatha, **Vikas M**. **Shelar,** R. Dileep, G. Umesh, M. N. Satyanarayan and B. RamachandraBhat, *Third-Order nonlinear optical, optical power limitingand all-optical switching studies of Palladium Complexes,* ***Synthesis and Reactivity in Inorganic, Metal-Organic, and Nano-Metal Chemistry***(2013), 44:2, 282-290.

Publications in conferences/symposia:

1 Rajkumar Y., **Vikas S.**, Ankush Nayak ,Neeta Magaji, Ramesh Kumar B., Udupa K. R., Umesh G., Udaya Bhat K., *A study on laser shock peening of 316 stainless steel weldments,*11thInternational Conference on High Nitrogen Steels and Interstitial Alloys (HNS 2012) GRT Grand Hotel, Chennai, India September 27-29, 2012.

2 **Shelar Vikas M.**, Umesh G., Hegde G. M., Jagadeesh G. and Reddy K. P. J., *Quantitative density imaging of subsonic jet using Planar Laser Induced Fluorescence of MEK,*International Conference on Optical Engineering (ICOE 2012) VTU,Belgavi, July 26-28, 2012.

3 **Shelar Vikas M**., Hegde G. M., Jagadeesh G., Reddy K. P. J., G. Umesh, *Planar laser induced fluorescence of acetone for turbulent gas flow visualization from subsonic ejector*, 3nd International Conference On "Current Developments In Atomic, Molecular, Optical & Nano Physics" CDAMOP 2011, University of Delhi, Delhi.December 14-16, 2011.

4 Manjunatha K.B., Dileep R., **Shelar Vikas M**, G. Umesh, M. N. Satyanarayan and B. Ramachandra Bhat, *Third-Order nonlinear optical properties and optical switching of Palladium (I) Complex*, International Conference on Light, 23 -25 May 2011, National Institute of Technology Calicut, Kerala, India.

5 **Shelar Vikas M.,** Sharath N., Umesh G., Hegde G, Jagadeesh G., Reddy K. P. J., Ramachandran G., *Oxygen quenching studies of laser induced fluorescence from Acetone and Methyl Ethyl Ketone in argon bath gas*, 2nd DAE-BRNS Symposium on Atomic Molecular and Optical Physics, Karnatak University Dharwad, Dharwad, Feb. 22-25, 2011.

6 K. B. Manjunatha, Dileep R., **Shelar Vikas M.**, G. Umesh, M. N. Satyanarayan and B. RamachandraBhat, *Third-Order nonlinear optical*

properties of Palladium (I) complex Photonics – 2010, International Conference on Fiber Optics and Photonics, Indian Institute of Technology Guwahati, Guwahati, India, December 11-15, 2010.

7 K. B. Manjunatha, Dileep R., **Shelar Vikas M.**, G. Umesh, M. N. Satyanarayan and B. Ramachandra Bhat, *Nonlinear optical properties of Thiolato complex of Ruthenium in solution and PMMA matrix using single beam Z-scan technique,* NLS-19, RRCAT, Indore, Dec. 1-4, 2010.

8 K. B. Manjunatha, Dileep R., **Shelar Vikas M**, Hidayath Ulla, G. Umesh, M. N. Satyanarayan and B. RamachandraBhat, *Nonlinear refractive index and reverse saturable absorption of Thiolato complexes of Ruthenium* , Photonics – 2010 , International Conference on Fiber Optics and Photonics, Indian Institute of Technology Guwahati, Guwahati, India, December 11-15, 2010.

9 Sujaya C, H. D. Shashikala, **Shelar Vikas M.**, G. Umesh, Yogesha S., A.C. Hedge, *Microhardness and corrosion behaviour of pulsed laser deposited Al_2O_3 coatings onTi-6Al-4V, Titanium and Inconel,* International Conference on Recent Trends in Materials and Characterization - RETMAC 2010, NITK, Surathkal, India, February 14-15, 2010.

10 K. B. Manjunatha, **Shelar Vikas Manohar**, Seetharam Shettigar, G. Umesh, M. N. Sathyanarayan, *Third-Order Nonlinear optical and optical power limiting studies on Amino Substituted Chalcones,* International Conference on Recent Trends in Materials and Characterization - RETMAC 2010, NITK, Surathkal, India, February 14-15, 2010.

11 K. B. Manjunatha, Dileep R., **Shelar Vikas M.**, G. Umesh, M. N. Satyanarayan and B. Ramachandra Bhat, *Third-Order nonlinear optical properties and optical switching of Palladium (I) Complex,* Optics'11. NIT Calicut, May 23-25, 2011.

12 G.Viswanathan& **Vikas Shelar**, *Precipitation measurements in Tropical Southern India-Case studies using Doppler weather radar* Geophysical Research Abstracts, Vol. 9, 07443, 2007.